

Process Simulation of a 1 MW_{th} Chemical Looping Pilot Plant with Coal and Biomass as Fuel

*Master of Science Thesis in the Master Degree Programme,
Innovative and Sustainable Chemical Engineering*

Adrian Gunnarsson

Department of Chemical and Biological Engineering

Division of Energy and Materials

CHALMERS UNIVERSITY OF TECHNOLOGY

Gothenburg, Sweden 2014

MASTER OF SCIENCE THESIS

Process Simulation of a 1 MW_{th} Chemical Looping Pilot Plant with Coal and Biomass as Fuel

ADRIAN GUNNARSSON

Supervisors: Dr.-Ing. Jochen Ströhle
M.Sc. Peter Ohlemüller
Dipl.-Ing. Markus Junk
Examiner: Assoc. Prof. Henrik Leion

Department of Chemical and Biological Engineering
CHALMERS UNIVERSITY OF TECHNOLOGY
Gothenburg, Sweden 2014

Process Simulation of a 1 MW_{th} Chemical Looping Pilot Plant with Coal and Biomass as Fuel

ADRIAN GUNNARSSON

© ADRIAN GUNNARSSON, 2014.

Technical Report No. T2014-XXX
Department of Chemical and Biological Engineering
CHALMERS UNIVERSITY OF TECHNOLOGY
SE-412 96 Gothenburg
Sweden
Telephone +46 (0)31 772 1000

Cover: Illustration of the 1 MW_{th} chemical looping pilot plant.

Reposervice
Gothenburg, Sweden 2014

Acknowledgements

The author acknowledges Technische Universität Darmstadt and the Energy Systems & Technology department for the technical support and guidance in this master thesis project.

A special thanks goes out to examiner Henrik Leion for showing the opportunity to perform the master thesis project abroad and guidance. To the supervisors Jochen Ströhle, Peter Ohlemüller and Markus Junk for always being so helpful and to ÅForsk for the financial support.

Abstract

The purpose of this work is to develop fluidized bed reactor models for the air and fuel reactors in a chemical looping pilot plant. The models are elaborated to consider fluid dynamics and chemical reactions in the reactors as well as a particle distribution with the reactor heights.

The modelled reactors are parts of the worlds largest chemical looping pilot plant located at Technische Universität Darmstadt with a thermal effect of 1 MW_{th}. The pilot plant is built to be used with solid fuels of coal and biomass and for this reason a model considering the solid pyrolysis is also elaborated in this work. To better predict future test campaigns with the plant a setup for the process model is performed in Aspen Plus considering the whole plant. Implementing the reactor models using Fortran code, simulations can be performed while operating parameters easily can be varied.

Experimental data from a 100 kW unit located at Chalmers University of Technology was used for validation of the reactor models showing good model predictions. Simulations for three planned test campaigns have been performed for the 1 MW_{th} pilot plant considering two different oxygen carriers and two different solid fuels and mixtures. The results from the simulations were tested with sensitive analyses of different drift parameters to determine and give a recommendation of process conditions for the planned test campaigns. Comparisons between the different oxygen carriers and solid fuel compositions are also performed in this work from the simulation results.

It was shown from the simulations that high pressure drops in both reactors are desirable to achieve high fuel conversions. A higher fuel reactor temperature is also beneficial to reach high fuel conversions but a higher mass flow circulation of oxygen carrier is then required. In a comparison between ilmenite and iron ore as oxygen carriers it was shown that slightly higher conversions as well as a smaller mass circulation of oxygen carrier could be expected when using iron ore. When adding biomass to the fuel a lower overall char conversion can be expected.

Keywords: CO₂ capture, CLC modelling, Aspen Plus, process simulation

Contents

1	Introduction	1
1.1	Background	1
1.2	Project objectives	2
2	Carbon capture and storage	4
2.1	Post-combustion CO ₂ capture	4
2.2	Pre-combustion CO ₂ capture	4
2.3	Oxy-fuel combustion	5
2.4	Chemical looping combustion	6
2.5	Transport of CO ₂	6
2.6	Storage of CO ₂	6
3	Chemical looping combustion of solid fuels	8
3.1	CLC plants around the world	9
4	The 1 MW_{th} CLC pilot plant	11
4.1	Plant description	11
4.2	Oxygen carriers	13
4.2.1	Ilmenite ore	14
4.2.2	Iron ore	16
4.3	Solid fuels	17
4.3.1	Coal as fuel	18
4.3.2	Biomass as fuel	19
4.4	Reactions	19
4.4.1	Fuel pyrolysis	20
4.4.2	Char gasification	20
5	Process model description	22
5.1	Unit operations	22
5.1.1	Air and fuel reactor	22
5.1.2	Decomposers	23
5.1.3	Post Oxidation Chamber	24
5.1.4	Cyclones	24
5.1.5	Carbon stripper	24
5.1.6	Loop seals	25
5.1.7	Mixers	25
5.2	Streams	26
5.3	Calculators	27
5.4	Boundary conditions	27
5.4.1	Design Specifications	28
5.5	The fluidized bed model	28
5.5.1	Overall particle distribution	29

5.5.2	Bottom bed particle distribution	33
5.5.3	Reaction kinetics	33
5.5.4	Results evaluation	38
5.6	Pyrolysis model	38
5.7	Model Validation	41
6	Results and discussion	44
6.1	Fuel reactor entrainment	44
6.2	Ilmenite as oxygen carrier	45
6.3	Comparison of ilmenite and iron ore as oxygen carriers	47
6.4	Comparison of coal and coal with biomass as fuels	49
6.5	Excess of air	51
6.6	Planned test campaigns recommendations	52
6.7	Particle distribution	53
7	Conclusions	54
8	Further work	55
8.1	Validation work	55
8.2	Model update	55
8.3	Large coal particles	55
	Bibliography	57
A	Extra results	61
B	Fortran code	72
B.1	Air reactor	72
B.2	Fuel reactor	81
B.3	Pyrolysis	99

List of Figures

1	Illustration of a chemical looping combustion unit with the two fluidized bed reactors and the circulating oxygen carrier.	8
2	A flowsheet of the 1 MW _{th} chemical looping plant at Technische Universität Darmstadt.	12
3	A flowsheet of the 1 MW _{th} chemical looping plant at Technische Universität Darmstadt, new configuration.	13
4	Particle size distribution for the dried ilmenite particles. The average particle diameter was calculated to 127 μm	16
5	Particle size distribution for the dried Taldinsky coal. The average particle diameter was calculated to 3108 μm	19
6	Illustration of the reaction steps for the solid fuel. In this Figure the drying is excluded.	20
7	A flowsheet of the components and streams at the 1 MW _{th} chemical looping plant at Technische Universität Darmstadt as built in Aspen Plus for simulations.	23
8	A typical solid particle entrainment with height in the fluidized bed reactor.	29
9	Bottom bed zone with bubbles and lean zone above the bottom bed zone.	29
10	Comparison between experimental data, simulation results and Abads model for the dry gas composition.	43
11	Comparison between experimental data, simulation results and Abads model for the CO ₂ capture efficiency (η_{OO}) and the oxygen demand (Ω_{OD}).	43
12	Sensitive analysis of the mass entrainment in the fuel reactor for a variation of the steam feed.	44
13	Gas conversions in the fuel reactor and the reactor heat demands together with the required circulating mass of oxygen carrier for ilmenite, varying the reactor pressure drops.	45
14	Gas conversions in the fuel reactor and the reactor heat demands together with the required circulating mass of oxygen carrier for ilmenite, varying the fuel reactor temperature.	46
15	Comparison of the gaseous conversions of two char gasification approaches. Gasification of 100 % and a modelled char gasification.	46
16	Comparison of the air reactor heat demands and the required mass circulation of oxygen carrier of two char gasification approaches. Gasification of 100 % and a modelled char gasification.	47
17	Comparison of the gaseous fuel conversions using ilmenite and iron ore varying the pressure drop.	48
18	Comparison of the air reactor heat demands and required mass circulation of oxygen carrier using ilmenite and iron ore varying the pressure drop.	48

19	Comparison of the gaseous fuel conversions using ilmenite and iron ore, varying the fuel reactor temperature.	49
20	Comparison of the gaseous fuel conversions using coal and coal with biomass.	50
21	Comparison of the air reactor heat demands and required mass circulation of oxygen carrier using coal and coal with biomass varying the pressure drop.	50
22	Comparison of the gaseous fuel conversions using coal and coal with biomass varying the fuel reactor temperature.	51
23	How the char and gas conversions are affected by a air feed variation and how the air heat demand and excess air ratio varies with the air feed using ilmenite.	51
24	How the pressure changes with the reactor height.	53
25	The gas and char conversions and the reactor heat demands and required mass circulation of oxygen carrier, varying the pressure drop for ilmenite.	61
26	The gas and char conversions and the reactor heat demands and required mass circulation of oxygen carrier, varying the fuel reactor temperature for ilmenite.	61
27	The gas conversions and the reactor heat demands and required mass circulation of oxygen carrier, varying the pressure drop for iron ore.	62
28	The gas conversions and the reactor heat demands and required mass circulation of oxygen carrier, varying the fuel reactor temperature for iron ore.	62
29	The gas conversions and the reactor heat demands and required mass circulation of oxygen carrier, varying the pressure drop for iron ore and biomass.	63
30	The gas conversions and the reactor heat demands and required mass circulation of oxygen carrier, varying the fuel reactor temperature for iron ore and biomass.	63
31	The gas and char conversions and the reactor heat demands and required mass circulation of oxygen carrier, varying the pressure drop for iron ore.	64
32	The gas and char conversions and the reactor heat demands and required mass circulation of oxygen carrier, varying the fuel reactor temperature for iron ore.	64
33	The gas and char conversions and the reactor heat demands and required mass circulation of oxygen carrier, varying the pressure drop for iron ore with biomass.	65
34	The gas and char conversions and the reactor heat demands and required mass circulation of oxygen carrier, varying the fuel reactor temperature for iron ore with biomass.	65

35	A 500 kW feed of coal and a circulating mass flow of 10, 15 and 20 ton/h of ilmenite while varying the pressure drops in the two reactors.	66
36	A 750 kW feed of coal and a circulating mass flow of 10, 15 and 20 ton/h of ilmenite while varying the pressure drops in the two reactors.	66
37	A 1000 kW feed of coal and a circulating mass flow of 10, 15 and 20 ton/h of ilmenite while varying the pressure drops in the two reactors.	67
38	A 500 kW feed of coal, a circulating mass flow of 10 ton/h of ilmenite and a pressure drop of 140 mbar. The temperature in the fuel reactor is varied for a steam feed off 200, 300 and 400 kg/h.	67
39	A 750 kW feed of coal, a circulating mass flow of 10 ton/h of ilmenite and a pressure drop of 140 mbar. The temperature in the fuel reactor is varied for a steam feed off 200, 300 and 400 kg/h.	68
40	A 1000 kW feed of coal, a circulating mass flow of 15 ton/h of ilmenite and a pressure drop of 140 mbar. The temperature in the fuel reactor is varied for a steam feed off 200, 300 and 400 kg/h.	68
41	Coal feeds of 500, 750 and 1000 kW and a circulating mass flow of 10, 15 and 20 ton/h of iron ore while varying the pressure drops in the two reactors.	69
42	Coal feeds of 500, 750 and 1000 kW and a circulating mass flow of 10, 15 and 20 ton/h of ilmenite while varying the pressure drops in the two reactors.	70
43	Variation of the ratio of solid particles of char and oxygen carrier, y_{koks} , in the fuel reactor.	70
44	Variation of the decay constant, a_0 , in the fuel reactor.	70
45	Variation of the solids concentration in the bottom bed zone, ε_{sd} , in the fuel reactor.	71
46	Variation of the stoichiometric coefficient, α , in the gasification reaction, see reaction 22.	71
47	Variation of the tar pyrolysis fraction for the produced amount of CO and CH_4 , see section B.3.	71

List of Tables

1	Reactor dimensions for the 1 MW _{th} chemical looping pilot plant. . . .	12
2	Physical properties of pre-oxidized and activated ilmenite	16
3	Physical properties of iron ore.	17
4	Taldinsky coal and torrefied biomass composition from analyses. . . .	26
5	Design specifications used in Aspen Plus.	28
6	Kinetic parameters for coal char gasification (Abad, Gayán et al., 2013). .	36
7	Kinetic parameters for ilmenite.	37
8	Kinetic parameters for Iron ore.	37
9	Solid fuel products after pyrolysis.	40
10	Operational points for the 100 kW chemical looping pilot plant at Chalmers University of Technology.	41
11	Proximate and ultimate analyses together with the pyrolysis products for the El Cerrejón coal.	42
12	Recommendation for the three planned test campaigns with perfect char gasification (1) and modelled char gasification (2).	52

Abbreviations and symbols

Chemical substances

C	Carbon
CH_4	Methane
C_2H_6	Ethane
CO	Carbon monoxide
CO_2	Carbon dioxide
Fe_2O_3	Hematite
Fe_3O_4	Magnetite
$FeTiO_3$	Ilmenite
Fe_2TiO_5	Pseudobrookite
H_2	Hydrogen
H_2O	Water
H_2S	Hydrogen sulfide
Me_xO_y	Oxidized oxygen carrier
Me_xO_{y-1}	Reduced oxygen carrier
N_2	Nitrogen
NH_3	Ammonia
O_2	Oxygen
SO_2	Sulfur dioxide
TiO_2	Rutile

Abbreviations

AR	Air reactor
$CIPSD$	Conventional substream with particle size distribution for solids
CLC	Chemical looping combustion
$CLOU$	Chemical looping with oxygen uncoupling
CS	Carbon stripper
$DECOMP$	Decomposer
EST	Energy Systems and Energy Technology
$Fortran$	Formula Translating system
FR	Fuel reactor
$iG - CLC$	In situ gasification chemical looping combustion
LS	Loop seal
$MIXED$	Conventional substream for liquids and gases
$NCPSD$	Nonconventional substream with particle size distribution for solids
POC	Post oxidation chamber
PSD	Particle size distribution
VM	Volatile matter

Symbols

Variables and constants

a	Decay constant for solid fraction in lean zone	$[m^{-1}]$
a'	Decay constant of clusters in the freeboard	$[m^{-1}]$
Ar	Archimedes number	-
A_t	Cross sectional reactor area	$[m^2]$
A_0	Gas-distributor area per nozzle	$[m^2]$
\bar{b}	Stoichiometric coefficient	-
C	Gas concentration	$[mol/m^3]$
C_d	Oxygen concentration out from dense zone	$[mol/m^3]$
C_l	Oxygen concentration out from lean zone	$[mol/m^3]$
C_0	Oxygen concentration in to air reactor	$[mol/m^3]$
$char$	Solid ratio of char and ash	-
d_b	Bubble diameter	$[m]$
d_p	Particle diameter	$[m]$
d_p^*	Dimensionless particle diameter	-
dm_c	Mass change of char	$[kg]$
E	Activation energy	$[kJ/mol]$
E_{SG}	Kinetic parameter in biomass gasification	$[K]$
\bar{f}_l	Average volume of solids in lean reactor zone	-
g	Gravitational constant	$[m/s^2]$
G_{sat}	Total mass flux of solids	$[kg/m^2 \cdot s]$
G_{sat}^*	Saturated mass flux of solids	$[kg/m^2 \cdot s]$
H_d	Dense zone reactor height	$[m]$
H_l	Lean zone reactor height	$[m]$
H_r	Total reactor height	$[m]$
K_{be}	Gas-interchange coefficient between bubble and emulsion phase	$[s^{-1}]$
k_{bio}	Gasification reaction constant for biomass	$[s^{-1} \cdot atm^{-1}]$
K_{CO,CO_2}	Gasification parameters for coal with carbon dioxide	$[atm^{-1}]$
K_{H_2,H_2O}	Gasification parameters for coal with steam	$[atm^{-1}]$
k_{CO_2}	Gasification parameter for coal with carbon dioxide	$[s^{-1} \cdot atm^{-1}]$
k_{H_2O}	Gasification parameter for coal with steam	$[s^{-1} \cdot atm^{-1}]$
K_{ff}	Overall rate constant in bottom bed zone	$[s^{-1}]$
K_r	Overall oxidation rate of particles in emulsion zone	$[s^{-1}]$
k_s	Reaction constant	$[m/s]$
k_{s0}	Preexponential reaction coefficient	$[m/s]$
M	Molar mass	$[kg/kmol]$
m_d	Mass inventory in dense reactor zone	$[kg]$
m_l	Mass inventory in lean reactor zone	$[kg]$

m_o	Fully oxidized form of oxygen carrier	[kg]
m_{OC}	Mass inventory of oxygen carrier	[kg]
m_r	Fully reduced form of oxygen carrier	[kg]
n	Reaction order	-
n_i	Molar flow of specie i	[mol/s]
P_i	Partial gas pressure	[atm]
Q_{AR}	Heat demand at the air reactor	[kW]
Q_{FR}	Heat demand at the fuel reactor	[kW]
R	Ideal gas constant	[J/mol · K]
$Re_{p,mf}$	Particle Reynolds number at minimum fluidization conditions	-
r_g	Grain radius	[m]
R_O	Oxygen transport capacity	-
S_{BET}	Specific surface area	[m ²]
u_{mf}	Gas velocity at minimum fluidization conditions	[m/s]
u_t^*	Dimensionless terminal gas velocity	-
u_t	Terminal velocity	[m/s]
u_{vis}	Visible bubble flow velocity	[m/s]
$u_{b\infty}$	Single bubble velocity	[m/s]
u_0	Superficial gas velocity	[m/s]
W	Total mass inventory in reactor	[kg]
W_d	Mass inventory in dense zone	[kg]
W_l	Mass inventory in lean zone	[kg]
X_C	Char conversion	-
X_{OC}	Oxygen carrier conversion	-
X_{O_2}	Oxygen conversion	-
y_{koks}	Solid ratio of char and oxygen carrier	-
z	Bed height	[m]

Greek letters

α	Gasification coefficient	-
γ_{core}	Solids fraction at reactor core	-
γ_{wall}	Solids fraction at reactor wall	-
ΔP	Reactor pressure drop	[Pa]
ΔH	Enthalpy change	[kJ/mol]
δ_b	Bubble fraction in bottom bed	-
δ_d	Volume fraction between core and wall zone in dense zone	-
$\bar{\delta}_l$	Average volume fraction between core and wall zone in lean zone	-
ε_f	Void fraction at the top of the bottom bed	-
ε_s	Void fraction in the lean zone	-
ε_{sd}	Solids fraction in dense zone	-

ε_{se}	Solids fraction at reactor exit	-
$\bar{\varepsilon}_{se}$	Mean solids fraction in lean reactor zone	-
ε^*	Carrying capacity of the gas	-
η_{bed}	Contact efficiency at the top of the bottom bed	-
η_{OO}	Carbon dioxide capture efficiency	-
λ	Excess air ratio	-
μ_g	Dynamic gas viscosity	$[Pa \cdot s]$
ρ_g	Gas density	$[kg/m^3]$
ρ_m	Molar density of oxygen carrier	$[mol/m^3]$
ρ_s	Solid particle density	$[kg/m^3]$
$\rho_{skeletal}$	Skeletal density	$[kg/m^3]$
ν	Stoichiometric coefficient	-
τ	Time for complete solid conversion	$[s]$
ϕ	Particle sphericity	-
Φ	Oxygen-carbon ratio	-
χ	Molar fraction	-
Ψ	Ratio of the visible bubble flow and the gas flow through the bubbles	-
Ω_{OD}	Oxygen demand	-

1 Introduction

One of the largest environmental challenges today is the global warming caused by human activity. Large amounts of the greenhouse gas carbon dioxide from fossil fuels are emitted to the atmosphere every day, increasing the global warming effect. The greenhouse gas effect appears due to the ability of some gases to absorb infrared radiation that is directed out from the earth. The energy direction can then be altered by the gas molecules and infrared radiation, that is heat, can be directed back to the earth with the effect of an increasing global temperature. Another greenhouse gas than carbon dioxide is water vapour and the effect is completely natural and even necessary for life to exist on the earth. However, the human increase of the greenhouse gas effect may result in an average temperature increase of several degrees which most likely will lead to more extreme weathers and new season patterns (Britannica, 2014). It is therefore of great importance to reduce these emissions in one way or another. A final solution would be to only use renewable energy sources for all types of energy transformations resulting in a non-increasing carbon dioxide portion in the atmosphere. Renewable sources such as solar power, wind power, wave power and the use of biofuel among others should replace the fossil power sources, reducing the human impact. However, this is not the situation yet since a large part of the electric energy usage world-wide originates from coal power plants producing enormous amounts of carbon dioxide. In the future fossil fuels will most probably still be a necessary and dominating source for energy production (Cho et al., 2004). Since the development in alternative energy sources takes time, and with a concurrent globally increased energy demand (IEA, 2012), temporary solutions are necessary in the mean time.

Another approach is to prevent the produced carbon dioxide to be emitted to the atmosphere, that is to capture the greenhouse gas. There are several such techniques already available and others that are under development. One very promising such technique is *chemical looping combustion* since the gas capturing is inherent in the system and the energy losses are small. However, the technique is not yet used commercially but still under development.

The worlds largest pilot plant for chemical looping combustion is located at Technische Universität Darmstadt, Germany (Ströhle et al., 2013). This project aims to build a model for the chemical looping pilot plant in Darmstadt and use it to simulate the process for three different planned test campaigns in Aspen Plus.

1.1 Background

After the nuclear accident in Fukushima, Japan 2011, Germany decided to remove all their nuclear energy plants before 2022 (Nicola, 2013). To replace the reduced energy production Germany aims to use renewable energy sources but it is probable that fossil coal will be used as well, since it is widely available. Even though the nuclear power is not a renewable energy source, the carbon dioxide emissions are

small compared to coal produced energy (World Nuclear Association, 2011). For this reason there is a risk that the carbon dioxide emissions will increase in Germany in the future.

To lower the carbon dioxide emissions the usage of fossil energy sources has to be reduced. Either by a lower usage of the products from the consumers or by changing the fuel used to renewable sources such as solar power, wind power, wave power and biofuel among others. Another option to reduce the carbon dioxide emissions could be to capture the gas after combustion, preventing it to diffuse into the atmosphere. Different technical solutions are available to capture the carbon dioxide and are gathered under the name *carbon capture and storage (CCS)* techniques. (Intergovernmental Panel on Climate Change, 2005)

To increase the understanding and develop the “second generation” of carbon capturing techniques the worlds largest chemical looping pilot plant was planned and erected at Technische Universität Darmstadt, Germany. The plant has since it was erected been tested in two test campaigns (Orth, 2013) and new test campaigns have been planned. To better understand and estimate how the plant should be operated during these test campaigns it is desirable to model the pilot plant and simulate the process in advance. Aspen Plus is a widely used software for process simulations in the chemical industry and it was chosen to be used for the simulations of the planned test campaigns.

1.2 Project objectives

The project objectives of this master thesis includes:

- Setup a process model of the 1 MW_{th} chemical looping pilot plant for coal and biomass in the software Aspen Plus
- Integration and development of existing fluidized bed models for the air and fuel reactor into the process model
- Elaboration and integration of a pyrolysis model for solid fuels
- Integration of a model for calculating the particle distribution with the height of the reactor
- Perform process simulations to determine process conditions for three planned test campaigns

Where the model should account for the characteristics of the fluidized bed reactors such as the fluid dynamics and chemical reactions. The elaborated models will be implemented to Aspen Plus using Fortran code and Microsoft Excel.

Three different test campaigns for the 1 MW_{th} chemical looping pilot plant at Technische Universität Darmstadt have been planned. These three test campaigns considers the usage of either ilmenite or iron ore as oxygen carrier with either pure coal or coal with biomass as a solid fuel as:

- Ilmenite with coal
- Iron ore with coal
- Iron ore with 90 % coal and 10 % torrefied biomass

2 Carbon capture and storage

Carbon capture and storage has been suggested as a temporary solution to decrease the carbon dioxide emissions to the atmosphere. Different techniques has been developed over the years and the general idea is to *capture* the carbon dioxide at the energy plants where it is produced in large amounts. Well captured the greenhouse gas can be treated and *transported* to a final *storage* location (Intergovernmental Panel on Climate Change, 2005). Some different techniques, transport and storage options are presented in the sections below.

2.1 Post-combustion CO₂ capture

In the post-combustion system the carbon dioxide is separated from the flue gases after the fuel has been combusted. To separate the carbon dioxide from the remaining flue gases a liquid solvent is commonly used in these systems to absorb the greenhouse gas. The use of monoethanolamine (MEA) is one such solvent. However, the solvent has to be regenerated after a certain time since it will be saturated. This requires further extra separation units and energy demanding steps. The oxidising agent used with the combustion is usually oxygen and is acquired directly by combustion with air. Due to the high ratio of nitrogen in the air there will be only a small fraction of carbon dioxide in the flue gases. This fraction is usually in the range of 3-15 % by volume and the presence of nitrogen is aggravating the separation as well as increasing the size of the equipment.(Intergovernmental Panel on Climate Change, 2005)

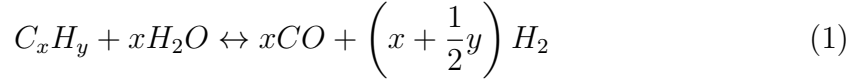
For the gas separation of the flue gases it is also possible to use solid absorbent agents. Calcium oxide can for example be used as it reacts with the carbon dioxide to form calcium carbonate. The regenerating process can be performed by calcining the calcium carbonate at high temperatures back to calcium oxide and pure carbon dioxide which is then captured. To move the solid absorbent between the absorption reactor and the reactor for the regeneration fluidization of the solids has been used. A weakness for the process is that the absorbent is deactivated rapidly and large make-up streams are necessary. However, the method has a high efficiency and a low cost compared to the MEA process. (Lasheras et al., 2011)

Post-combustion systems based on absorption processes are available and commercially used today. These current plants has the potential to capture 85-95 % of the process produced carbon dioxide. (Intergovernmental Panel on Climate Change, 2005)

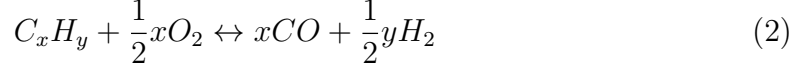
2.2 Pre-combustion CO₂ capture

In the pre-combustion system the fuel is treated before combustion to produce a mixture of hydrogen and carbon monoxide, also known as syngas. The common ways to do this is by either adding steam or oxygen to the fuel. The former option

is called *steam reforming* and the latter for *partial oxidation*. The reaction for the steam reforming can be written as:



and the partial oxidation can be written as:



If more steam is added the carbon monoxide will continue converting to carbon dioxide by the *water gas shift reaction* as:



The carbon dioxide can then finally be separated from the hydrogen, usually by a chemical or physical absorption, whereafter it can be stored. The hydrogen can be used as a carbon free fuel for later combustion. Comparing the pre-combustion techniques to the post-combustion technique, the fuel conversion step requires more elaborated techniques and are more costly. However, the concentration of carbon dioxide is large after the water-gas-shift reaction and the pressure is usually high in these applications resulting in a more favourable carbon dioxide separation.

Pre-combustion systems are as the post-combustion systems available and commercially used with a potential to capture 85-95 % of the process produced carbon dioxide. (Intergovernmental Panel on Climate Change, 2005).

2.3 Oxy-fuel combustion

The carbon dioxide capture is usually complicated due to the large volumetric flows of nitrogen when using air for the combustions. If the flue gases were to be stored directly the volumes would be undesirable large due to the nitrogen present. To avoid this an oxy-fuel process can be used where nearly pure oxygen is used instead of air. In the ideal case the only products would be carbon dioxide and steam where the steam can easily be separated by condensation. However, this requires separation of oxygen from air before combustion. Classically the separation is performed by differences in bubble points by cooling the gases to very low temperatures. Substitutional separation methods using membranes or chemical looping cycles are under development.

A problem that occurs when performing combustion in nearly pure oxygen is the high temperature in the flame and flue gases. For the most typically used power plant materials the flame temperature is far too high and the flue gas temperature has to be controlled and cooled.

Oxy-fuel systems are not yet used on a commercial scale but comparing to the post- and pre-combustion systems the oxy-fuel system has a potential to capture nearly 100 % of the process produced carbon dioxide. Depending on the oxygen separation stage the process might be very costly. (Intergovernmental Panel on Climate Change, 2005).

2.4 Chemical looping combustion

The chemical looping combustion technology is still under development but it is a carbon dioxide capturing method that has shown on a high capturing efficiency without the need of any extra gas separation step of the flue gases. As in the oxy-fuel combustion methods the fuel is never in direct contact with air and the products for an ideal case are just carbon dioxide and steam. This is possible when small particles of metal oxides, so called oxygen carriers, are introduced to the system. By oxidation of these oxygen carriers with air in a first step where oxygen will be chemically bound to the solid particles. The oxidized particles can then be used in a second step where they will be reduced while under reaction with a fuel. Both the oxidation and reduction of these particles are performed in fluidized bed reactors where a good contact between the solids and gases are formed. By connecting these two reactors the oxygen carrier can be circulated and reused many times and the carbon dioxide capturing will be inherent in the method. (Ströhle et al., 2013), (Intergovernmental Panel on Climate Change, 2005). The chemical looping combustion process is described in more detail under section 3.

2.5 Transport of CO₂

After the capturing of the carbon dioxide has been performed it is supposed to be stored at a final storage location. A transport of the greenhouse gas is necessary between the capturing and storage. The transport can occur in either of the three phases of gas, liquid or solid. Since gases occupies large volumes they are usually pressurised when they are to be transported. The most common way to transport carbon dioxide gas is in a pressurised state with pipelines. The carbon dioxide can also be transported with ships but then it is usually liquefied to reduce the required volumes even further. Carbon dioxide in solid state is not a usual way to transport the specie since the solidification process requires large amounts of energy, even though it is possible.

Elaborated transport systems are necessary for a functional and effective carbon dioxide transport. The development of such systems cost a lot of money and takes time to complete. However, long-distance pipelines for carbon dioxide transport already exists in the world. The pipeline with the largest capacity in the USA 2005 had a capacity of 19.3 Mton/year. Only small amounts of carbon dioxide have been transported with ships. (Intergovernmental Panel on Climate Change, 2005)

2.6 Storage of CO₂

There are some options for how and where the carbon dioxide can be stored. One option is to use *geological storage* where the gas is compressed and injected into the earth crust. There it is to be stored in old oil reservoirs, depleted gas fields, saline formations etc. either at an onshore or offshore location. Norway has as an

example successfully captured and stored carbon dioxide since 1996 at their offshore oil reservoir *Sleipner* in the North sea (Global CCS Institute, 2014).

Another storage option could be *ocean storage* where the carbon dioxide could either be injected and solved directly into the ocean or deposited on the seabed. At a depth larger than 3 km, the carbon dioxide will be in a liquid state with a density larger than water. The deposited gas would then stay in a carbon dioxide lake on the seabed. However, the experience of handling carbon dioxide in the deep-sea is limited as well as the understanding in the deep-sea ecosystems and how they would be affected.

A third storage option for the carbon dioxide is *mineal carbonation*. The idea in this storing method is to get the carbon dioxide with metal oxides bearing materials to form insoluble carbonates. This reaction could either be performed in an additional operation unit to the separation plant or by injection of the gas into geologically rich metal oxide sources. In difference from the other storage options the carbonised material could fill a function as a construction material as an example. (Intergovernmental Panel on Climate Change, 2005).

3 Chemical looping combustion of solid fuels

A technique used to separate the oxygen from the air without costly separation by cooling is *chemical looping combustion* (CLC), as shortly described in section 2.4. The method includes two connected fluidized bed reactors and a circulating oxygen carrier, see Figure 1. The oxygen carrier forms a bed of solid particles at the bottom of the reactor and by blowing a fluidizing gas from beneath, the small particles will be affected from the drag from the surrounding gas. If the gas velocity becomes large enough the drag force will be as large as the gravitational force of the particles and the bed starts to act like a fluid. The particle bed is then said to be fluidized at minimum fluidization conditions. This condition ensures good mass and heat transfer between the fluidizing gas and the particles (Kunii & Levenspiel, 1991).

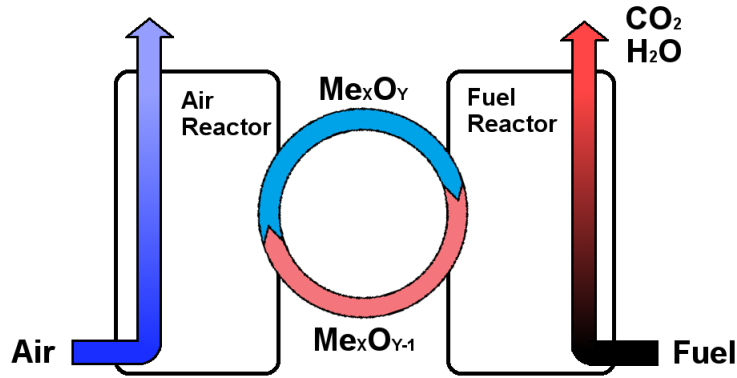
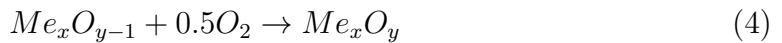


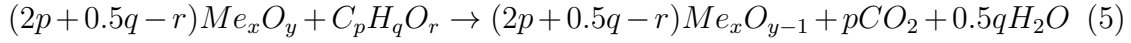
Figure 1: Illustration of a chemical looping combustion unit with the two fluidized bed reactors and the circulating oxygen carrier.

The oxygen carriers are in a first step present in the *air reactor*, which is fluidized with air, in a reduced state. The reduced oxygen carrier can react with the oxygen in the surrounding gas flow and the reaction can be described with the following general formula (Abad, Adánez et al., 2013):



Where Me_xO_y represents a suitable oxygen carrier in its oxidized stage. The oxidized particles are then transported from the air reactor to the *fuel reactor*. This transport can be made possible by increasing the fluidizing gas velocity so that it exceeds the minimum fluidization velocity. This results in a larger drag acting on the particles and a *carryover* can take place when the velocity is increased enough. The gases out from the air reactor are separated from the solid particles before the particles enter the fuel reactor. The fuel reactor is as the air reactor also fluidized, but not with air. The fluidizing gas should be easy to separate from the produced carbon dioxide and commonly used fluidizing gases in the fuel reactor are gaseous fuels, recirculated flue gases or steam. The oxygen carrier is reduced by reaction with the fuel and a simplified reduction reaction for most organic fuels can be expressed as

(Abad, Adánez et al., 2013):



The reduced oxygen carriers are then transported back to the air reactor once again, circulating between the two fluidized bed reactors. With this process the fuel will have no direct contact with the air, the amount of flue gases is reduced and for an ideal combustion the only products will be carbon dioxide and steam. The water can easily be separated through condensation and then the carbon dioxide can be transferred and stored at another location. The oxygen carbon dioxide separation is therefore inherent in the chemical looping process. (Abad, Gayán et al., 2013), (Cuadrat, Abad, García-Labiano et al., 2012)

It is possible to use gaseous, liquid or solid fuels in a chemical looping combustion plant (Markström et al., 2013). An advantage using gaseous or liquid fuels is that they can be introduced as the fluidizing gas to the fuel reactor. However, solid fuels such as coal are widely available and will most certainly be used for energy production in the nearest future (Ströhle et al., 2013). Solid fuels are converted in a number of steps when used as a fuel in a chemical looping plant. Different gases leaves the fuel as volatile matter and solid particles of char and ash will be present and fluidized in the reactor as well (Matthesius et al., 1987). That is, the reaction scheme in the fuel reactor will be considered to be more complicated when using a solid fuel.

It should be noted that while reaction (4) is always an exothermic reaction (5) can be either exothermic or endothermic, depending on the oxygen carrier and the fuel (Zafar et al., 2007). However, the total amount of heat that is released in the two reactors is equal to the heat that would be released in a normal combustion case (Cho et al., 2004). The reactor temperatures and the overall heat balance can be controlled by the mass circulation rate of oxygen carrier and the average residence time of solids in each reactor (Intergovernmental Panel on Climate Change, 2005).

3.1 CLC plants around the world

The chemical looping combustion technique is still under development and not used commercially but a number of test facilities have been built and tested. A short description of a few selected CLC plants are presented below.

Darmstadt, Germany - A 1 MW_{th} chemical looping pilot plant has been erected at Technische Universität Darmstadt. Both the air and the fuel reactor are circulating fluidized beds and the plant has been tested without electrical heating. The plant is today the largest chemical looping pilot plant in the world. (Ströhle et al., 2013)

Gothenburg, Sweden - A 100 kW chemical looping plant has been erected at

Chalmers University of Technology. Both the interconnected reactors are circulating fluidized beds. For a separation of char and oxygen carrier particles the system includes a four chambered carbon stripper. An oven is enclosing the reactor system and electrical heating can be applied to reach the required temperatures (Markström et al., 2013). A smaller CLC facility of 10 kW is also located at Chalmers and have been used in many tests for solid fuels (Lyngfelt, 2014).

Hamburg, Germany - A 25 kW chemical looping combustion plant is located at Hamburg University of Technology. This plant consists of a circulating fluidized bed reactor, the air reactor, coupled with a two-stage bubbling fluidized bed, the fuel reactor. Electrical heating is possible on both the reactors and fluidizing gas to the fuel reactor can either be steam or carbon dioxide or a mixture of both. The largest difference from the 1 MW_{th} plant at Darmstadt is the fuel reactor since the bed is a bubbling bed and not a high velocity bed, that is the fluidizing gas velocity is lower. (Thon et al., 2012)

Nanjing, China - A 1 kW CLC prototype for solid fuels has been tested in South-east University Nanjing. The air reactor is a fast fluidized bed while the fuel reactor is a spout-fluid bed reactor and both reactors are heated electrically (Song et al., 2013). A larger plant of 10 kW has also been built in Nanjing (Lyngfelt, 2014).

Ohio, USA - At Ohio State University two CLC units of 2.5 and 25 kW have been built and tested (Lyngfelt, 2014). The fuel reactor has been replaced with a *reducer* and a *oxidizer* where the fuel is oxidized in the reducer. The oxygen carrier is oxidized in a first step in the oxidizer with steam and then with air in the combustor (Tong et al., 2014).

Stuttgart, Germany - A 10 kW dual fluidized bed facility is located at University of Stuttgart. The air reactor is a circulating fluidized bed and the fuel reactor is a single stage bubbling fluidized bed reactor. Both of the reactors are electrically heated. The fuel reactor bed has been fluidized with a mixture of nitrogen and steam. (Mayer et al., 2012)

Zaragosa, Spain - A smaller unit of 0.5 kW has been built and tested at University of Zaragosa. The unit was the first to demonstrate a total gas fuel conversion when using a oxygen carrier with oxygen uncoupling (CLOU) properties (Lyngfelt, 2014). The difference between CLC and CLOU is that oxygen gas is released from the CLOU oxygen carrier in the fuel reactor and the fuel will react with a gas rather than a solid (Mattisson, 2013).

4 The 1 MW_{th} CLC pilot plant

The 1 MW_{th} chemical looping pilot plant that has been erected at Technische Universität Darmstadt is today the worlds largest CLC plant in the world designed to be used for solid fuels such as coal and biomass (Ströhle et al., 2013). Below will follow a short description of the plant itself, test campaigns performed and planned test campaigns.

4.1 Plant description

Both the air and the fuel reactor are circulating fluidized bed reactors which are interconnected to each other. The oxygen carrier is oxidized in the air reactor with air and entrained with the gas flow out from the reactor. The particles are then separated from the gases by the usage of a cyclone from where the particles falls down to a loop seal. Previously the particles were then transported to the fuel reactor by a screw conveyor but this was replaced after a first test campaign with a L-valve due to condensation problems of steam that caused a plugging of the screw conveyor. In the fuel reactor the oxygen carrier will be reduced by reaction with the gaseous fuels and will eventually leave the fuel reactor with the fluidizing gases. The solid fuel will be gasified in the fuel reactor but since the reaction time for a total gasification is longer than the normal residence time for the particles in the fuel reactor unreacted char particles will also be entrained together with the oxygen carrier. To increase the fuel conversion it is necessary to separate the char and oxygen carrier particles and transfer the char particles back to the fuel reactor once again. This separation has been performed in two steps at the 1 MW_{th} pilot plant. The first step is the usage of a so called “low-efficiency cyclone” which is attached to the fuel reactor. The low efficiency of the cyclone means that it has a low efficiency in the separation of fines and lighter particles, that is the char particles, will leave with the gases which then enter a “high-efficiency cyclone”. In this cyclone the char particles will be separated from the gases and transported back to the fuel reactor via a loop seal. The heavier oxygen carriers together with some char particles leaves the low-efficiency cyclone in the bottom from where it reaches the second separation step, the carbon stripper. The carbon stripper is a bubbling fluidized bed and a separation between the two kinds of particles will occur due to a density difference. The char particles will be transferred back to the fuel reactor and the oxygen carrier is introduced once again to the air reactor from the carbon stripper (Orth, 2013). Gases leaving the high-efficiency cyclone may contain gases that were not oxidized in the fuel reactor. For this reason they will pass a post oxidation chamber (POC) where they are fully oxidized by the addition of pure oxygen to the flue gases (Ströhle et al., 2013). A simplified flowsheet of the chemical looping plant as described above can be seen in Figure 2 below. The reactor dimensions can be seen in Table 1 (Ströhle et al., 2013).

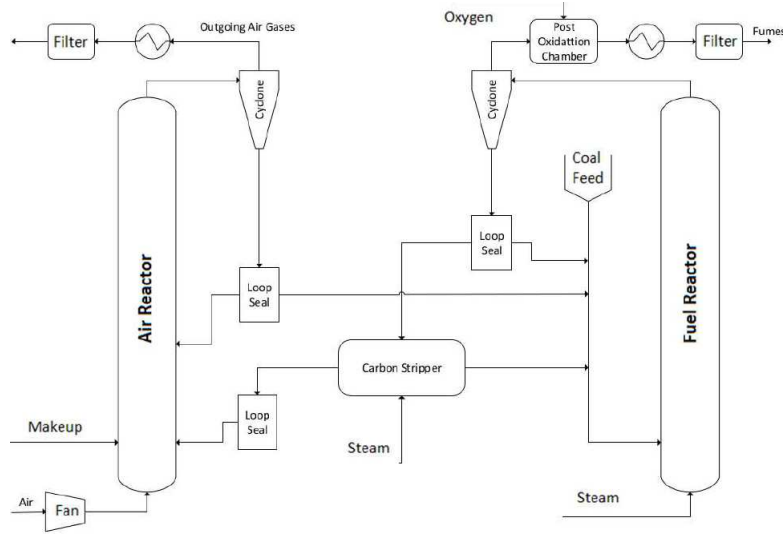


Figure 2: A flowsheet of the 1 MW_{th} chemical looping plant at Technische Universität Darmstadt.

Table 1: Reactor dimensions for the 1 MW_{th} chemical looping pilot plant.

Parameter	Value [m]
Fuel reactor height	11.4
Fuel reactor diameter	0.40
Air reactor height	8.7
Air reactor diameter	0.59

For minimizing the heat losses in the plant the whole reactor system has been refractory lined which allows an autothermal operation, that is without using any electrical heating of the reactors (Ströhle et al., 2013). The reaction occurring in the air reactor is exothermic and there is a need to remove heat from the reactor. This is possible at the plant by using five cooling tubes that have been attached at the top of the air reactor. The cooling tubes are movable and can be moved up and down in the bed to meet the required heat demand (Orth, 2013).

A second test campaign was performed in November to December 2012 with the plant configuration as described above. The testing period was performed during about 480 hours and several tests were performed. The fuel used was coal and the fuel reactor was fluidized using mixtures of steam, carbon dioxide and air. The oxygen carrier used in this test campaign was ilmenite. The coal particles used were pulverised and had hence a very small average particle diameter of 50 μm . This caused a major issue since much of the coal was entrained with a small residence time in the fuel reactor. It has therefore been considered to use larger coal particles in further test campaigns (Orth, 2013).

Since the second test campaign the 1 MW_{th} plant configuration has been changed for the new planned test campaigns as mentioned in section 1.2. It has been decided that coarser coal particles will be used in the plant and that a simplification of

the configuration will be performed by excluding the low-efficiency cyclone and the carbon stripper. The particles leaving the fuel reactor will instead be separated from the gases in a high-efficiency cyclone and transported to the air reactor. That is, no separation stage between char and oxygen carrier is present and the char particles that leaves the fuel reactor will be oxidized in the air reactor. However, the larger coal particles are assumed to have a longer residence time in the fuel reactor. Also the biomass that is planned to use has a large particle diameter. A simplified flowsheet of the chemical looping plant with these modifications can be seen in Figure 3 below.

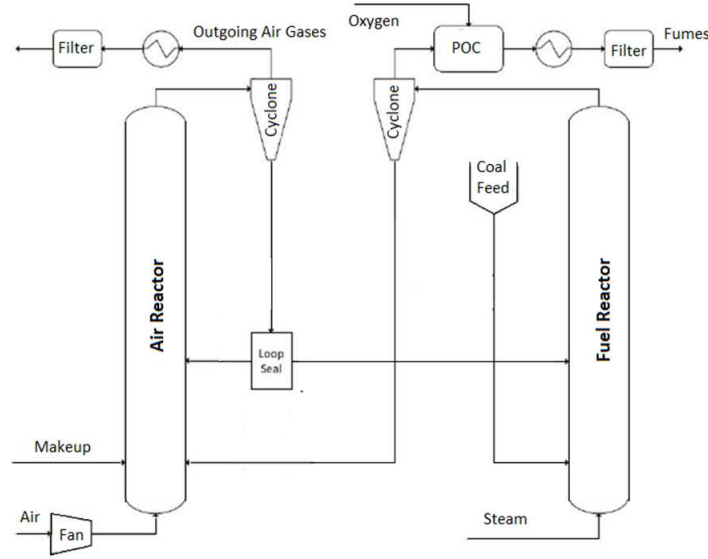


Figure 3: A flowsheet of the 1 MW_{th} chemical looping plant at Technische Universität Darmstadt, new configuration.

4.2 Oxygen carriers

It is of great importance to select an oxygen carrier with desirable properties to achieve an efficient process. The fact that the oxygen carrier is a solid simplifies the separation between oxygen and remaining air gases since only oxygen is reacting with the particles. The separation is then performed by gravitational and rotational forces using cyclones. In the fuel reactor the particles should be reduced since the purpose of the oxygen carriers is to oxidise the fuel. It is therefore of large importance that the oxygen carrier fulfils some desired properties such as a high reactivity in both the oxidation and reduction reaction. To fully convert the fuel it is also of great importance that the oxygen carrier has a large enough oxygen transport capacity, that is as large fraction of oxygen in the oxygen carrier as possible. To get the desired final products from the combustion, which are carbon dioxide and steam, the oxygen carrier should have a high selectivity toward these products (Cuadrat, Abad, García-Labiano et al., 2012).

Since the particles has to be transported between two different reactors in chemical looping combustion it is necessary to have an operating solution for this. With a large enough fluidization velocity the particles will be able to be transported but it will also result in frequent contact between particles as well as between particle and equipment. This contact will further result in attrition of both the oxygen carriers and the equipment. After a certain degree of attrition the particle size will be so small that the particles will start leaving with the gas in the cyclones and a loss of oxygen carrier from the system appears. A desired property for an oxygen carrier is therefore for it to be mechanically resistant with a low attrition rate. An opposite problem would be if the particles were to agglomerate, preventing the oxygen carrier to leave the reactors or even to be fluidized. A good oxygen carrier should therefore show no agglomeration problems (Cuadrat, Abad, García-Labiano et al., 2012).

From these specifications some possible oxygen carriers have turned out to be different metal oxides of common transition state metals. Some suggested oxidized metals are iron, nickel, copper and manganese (Zafar et al., 2007). It has been shown that the cost for oxygen carriers based on iron are less expensive (Research Fund for Coal & Steel, 2013). And due to the desire of a low cost for the oxygen carrier particles as well as a low environmental effect natural ores are considered to be a good option. (Abad et al., 2011), (Intergovernmental Panel on Climate Change, 2005).

Within the fuel reactor the oxygen that is bound to the oxygen carriers has to react with the fuel in some way. There are two alternatives in how the oxygen can react with the fuel. The first alternative is that the oxygen leaves the solid particles as a gas and the reaction will be a gas phase-gas phase reaction. This is usually referred to as *chemical-looping with oxygen uncoupling*, or shortly *CLOU* (Leion et al., 2009). The second reaction alternative is a heterogeneous reaction where the gaseous fuel react directly at the solid oxygen carrier particles, under so called *in situ gasification CLC* or *iG-CLC* (Abad, Adánez et al., 2013). If solid fuels are used with the second type of oxygen carrier a gasification is required in a first step since the otherwise solid-solid reaction rate is far too slow (Cuadrat, Abad, Gayán et al., 2012).

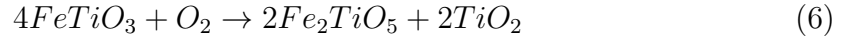
In the planned test campaign three different oxygen carriers have been of interest. These are ilmenite, iron ore and manganese ore. Both ilmenite and iron ore will react heterogeneously with the fuel while the manganese ore has shown of CLOU properties. The manganese ore has shown to generate large amounts of fines due to poor mechanical stability and it was decided to not use this oxygen carrier in the nearest test campaigns. Though it has been shown that the manganese ore can improve the overall process performance (Linderholm et al., 2012).

4.2.1 Ilmenite ore

An oxygen carrier that has been used in a number of studies and also is a common mineral is ilmenite which has shown good oxygen carrier properties ((Abad et

al., 2011), (Abad, Gayán et al., 2013), (Ströhle et al., 2013), (Leion et al., 2008)). The mineral consists of a number of different metal oxides including $FeTiO_3$, Fe_2O_3 , TiO_2 , Fe_2TiO_5 and Fe_3O_4 . The oxidized states working as oxygen carriers are for ilmenite Fe_2O_3 and Fe_2TiO_5 . However, the ilmenite has been shown to mainly consist of Fe_2TiO_5 and TiO_2 (Cuadrat, Abad, García-Labiano et al., 2012).

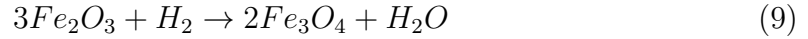
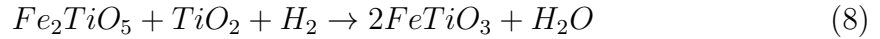
When the ilmenite particles enter the hot air reactor they starts to convert from their reduced to their oxidized form. The oxidation reactions of ilmenite with the oxygen in air can be written as:



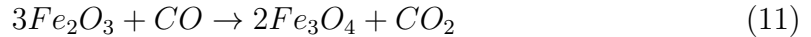
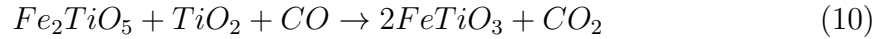
and



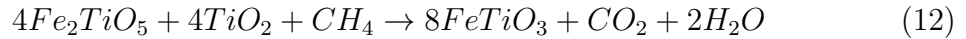
In the fuel reactor the ilmenite will be reduced once again while reacting with the fuel. The number of reduction reactions is two for every reducing agent in the fuel reactor since there are two oxidized stages of ilmenite. The most relevant reducing agents are hydrogen, carbon monoxide and methane and these are the ones considered in this work, even though other reducing agents may appear. The oxygen carrier reductions are alike for the different substances and can be written as the following reaction for hydrogen:



The reduction reactions with carbon monoxide can be written as:



And the reduction reactions with methane can be written as:



A total of two oxidizing and six reduction reactions of the oxygen carriers can therefore occur in the two reactors (Abad et al., 2011).

While using natural ilmenite as an oxygen carrier it has been noticed that the ilmenite undergoes an activation process during the first redox-cycles. During the activation the oxygen transport capacity will decrease and with it the activation energies for the reactions where it is reduced. The change is assumed to occur due to a loss of porosity within the particles as oxidation proceeds (Abad et al., 2011). After a number of reduction-oxidation cycles the ilmenite will be activated and the oxygen transport capacity will reach a constant value (Cuadrat, Abad, García-Labiano et al., 2012). For a plant running for a long time, with a only a small inlet

of fresh material, the ilmenite inventory can be considered activated. This since the activation process more or less diminish after about 20 cycles. As well as the oxygen transport capacity changes with activation also some other properties changes. This is illustrated in Table 2 below (Abad et al., 2011).

Table 2: Physical properties of pre-oxidized and activated ilmenite

		Pre-oxidized	Activated
True density	[kg/m ³]	4100	4250
R _o	[%]	4.0	3.3
r _g	[μm]	1.2	1.25
Porosity	[%]	1.2	12.7

A particle distribution was measured of the ilmenite to be used during the planned test campaigns at the 1 MW_{th} plant. The particles were dried before the particle diameter was measured by sieving. The average particle diameter was calculated to 127 μm, see Figure 4 for the particle size distribution.

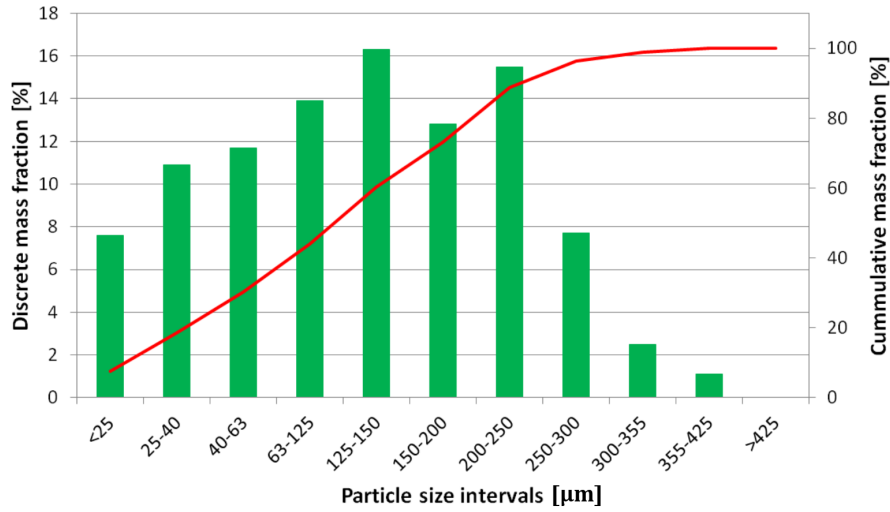


Figure 4: Particle size distribution for the dried ilmenite particles. The average particle diameter was calculated to 127 μm.

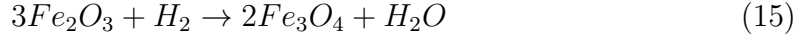
4.2.2 Iron ore

There is an interest to use hematite as an oxygen carrier, partly due to the fact that it is a very common iron ore with a presence of 60 % of the iron ore reserve in the world. Hematite (Fe_2O_3) is the oxidized form of the oxygen carrier and the reduced form is magnetite (Fe_3O_4) (Song et al., 2013).

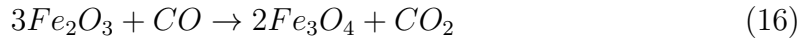
The oxidizing and reducing reactions taking place in the reactors are similar to the reactions with ilmenite (Abad et al., 2011),(Xiao et al., 2012). The reaction in the air reactor can be written as (Song et al., 2013):



In the fuel reactor the oxygen carrier is reduced by reaction with the products from the gasification such as:



and



The iron ore has not shown the same activation process as the ilmenite as can be seen in Table 3 (Research Fund for Coal & Steel, 2013). Comparing to ilmenite the oxygen transport capacity is lower for the iron ore. This means that the molar circulation of the iron ore between the two reactors should be larger compared to the circulation of ilmenite to transfer the same amount of oxygen (Zafar et al., 2007).

Table 3: Physical properties of iron ore.

Parameter		Value
True density	[kg/m ³]	4426
R _o	[%]	2.5
r _g	[μm]	0.916
Porosity	[%]	33.3

4.3 Solid fuels

When using a gaseous fuel in CLC the fuel itself can be used as the fluidizing gas in the fuel reactor. A solid fuel can also be used in CLC but then it is necessary to apply a fluidizing gas. However, using any fuel it is still desired to reach as high fuel conversion as possible. Solid fuels that can be considered to be used in a chemical looping plant are for example coal and biomass. To achieve a high conversion of the solid fuel particles in the fuel reactor they are required to be kept in the fuel reactor. This could either be performed by using large entering particles too heavy to be entrained or using some kind of recycling system for the particles leaving the reactor. What also has to be considered when a solid fuel is used is the production of ashes. The ashes has to be removed from the plant since it otherwise will accumulate within the system. Together with the ash removal there will usually also appear a loss of oxygen carrier. Ashes can also have a fouling effect on the oxygen carriers used in a chemical looping plant. Resulting in a lowered reactivity of the oxygen

carrier due to deactivation. How fast the ash fouling affect is, is not known and is assumed to be dependent on the fuel used. (Linderholm et al., 2012)

To calculate for the mass and heat balances in chemical looping combustion using a solid fuel it is of importance to know the fuel composition. This can be analysed using proximate, ultimate and sulfonate analyses.

The proximate analysis was developed in means of determining the products distribution when a sample of coal is heated under specific conditions. The analysis will give information of the coal composition in the four groups of *moisture*, *ash*, *volatile matter* and *fixed carbon*. The volatile matter consists of gases and vapours taking off during pyrolysis. The fixed carbon is the non-volatile matter of the coal and the ash is the inorganic residue that remains after combustion. In the ultimate analysis it is determined how large the proportions of each of the elements *carbon*, *hydrogen*, *nitrogen*, *sulfur*, *oxygen*, *chlorine* but also *ash* is. Sulfur is present in coal in one of either three forms *organically bound sulfur*, *inorganic sulfur* or *inorganic sulfates*. However, mass fraction of the sulfur compounds is often very small and a sulfonate analysis is not always performed on the fuels. (Speight, 2005)

4.3.1 Coal as fuel

Coal is a fossil solid material that can be used as a fuel with large carbon dioxide emissions. The energy rich material is however widely available and will most certainly be used in the nearest future (Ströhle et al., 2013). It is for these reasons of interest to use a carbon capturing method when using coal for energy production.

The coal char will be oxidized in the fuel reactor and it has been shown that the required time for a total char gasification is usually longer than the normal residence time for solid particles within the reactor. It is therefore desirable to transfer the unreacted char particles that leaves with the oxygen carrier back to the fuel reactor. This is possible by the introduction of a so called carbon stripper as described in section 4.1 (Ströhle et al., 2013). However, it has been decided to not use such a separation step in the planned test campaigns.

Another way to reach a longer residence time for the char particles in the fuel reactor could be to introduce them as larger particles from the start. Since large particles will not be entrained out from the reactor from the surrounding gas but stay in the bottom bed. The particle size used for the coal is therefore large and rough compared to the oxygen carrier size. Though, the coal will be reduced in size with time and breakage and attrition may occur.

The coal used in this work and to be used in the planned test campaigns is a Russian coal called *Taldinsky*. The data collected from the proximate and ultimate analysis can be seen in Table 4 below. The sulfur is distributed between the three sub categories as equal parts to add up to the sulfur measured in the ultimate analysis. The particle size distribution for the Taldinsky coal is shown in Figure 5. The average particle diameter was calculated to 3108 μm .

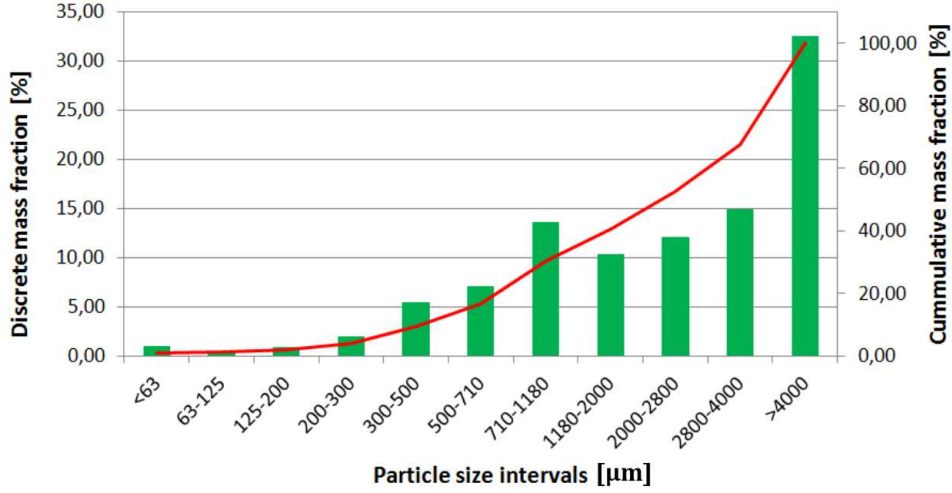


Figure 5: Particle size distribution for the dried Taldinsky coal. The average particle diameter was calculated to 3108 μm .

4.3.2 Biomass as fuel

Another solid fuel that could be used in a chemical looping plant is biomass. Renewable organic matter, such as wood or plants, can be used to derive biomass fuel. Considering biomass as a fuel that does not contribute to the greenhouse effect, capturing the produced carbon dioxide in a chemical looping plant could be considered to result in negative CO_2 emissions (Mendiara et al., 2013). It is for this reason desirable to use biomass instead of fossil fuels such as coal.

The biomass to be used as a fuel may be of a non consistent quality and can aggravate the control of the oxidation. It is however possible to pretreat the biomass before letting it enter the plant to achieve a more uniform feedstock. This pretreatment is called torrefaction, which is a mild pyrolysis process under anaerobic conditions at temperatures of 200-300 °C. It has been shown that by using torrefaction the properties of the biomass has come closer to the properties of coal and co-gasification of torrefied biomass and coal could therefore be a promising option (Kuo et al., 2014).

The biomass consists of large polymers of cellulose and lignin and the kinetics can be expected to differ from the coal kinetics. The biomass will as well as the coal have a longer reaction time for a total gasification than the particle residence time for the oxygen carrier. Also the biomass particles that will be used in the planned test campaigns are for that reason large in comparison to the oxygen carrier.

4.4 Reactions

When the solid fuel enters the fuel reactor it will be converted to different products in three steps. The first step to occur is however not a converting step but a very rapid drying of the fuel in the hot reactor. The first conversion step is when the

fuel is pyrolysed, or devolatilized, and the solid fuel breaks down to solid char and ash particles together with different volatile gases. The pyrolysis step is also very fast and can be considered to occur immediately as the fuels enters the fuel reactor. The second step is the gasification of the solid char particles, where they are gasified with either steam or carbon dioxide. The gasification is comparably a much slower reaction step and the gasification has been identified as a limiting step of the solid fuel conversion (Mendiara et al., 2013). The released and produced gases can then react with the solid oxygen carriers present in the fuel reactor, see Figure 6. (Linderholm et al., 2012)

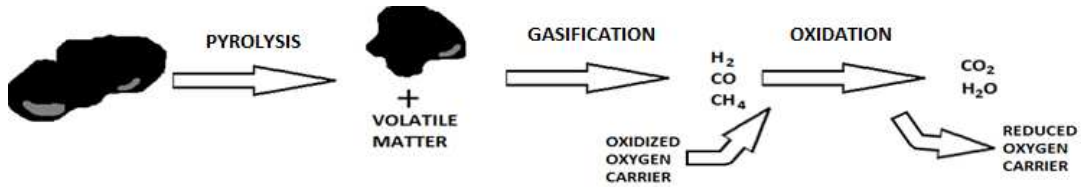
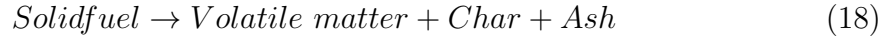


Figure 6: Illustration of the reaction steps for the solid fuel. In this Figure the drying is excluded.

4.4.1 Fuel pyrolysis

The pyrolysis is a very fast reaction step where the solid fuel is converted to char, ash and volatile gases. Since the reaction is fast it can be assumed to be instantaneous at the feeding point to the fuel reactor (Abad, Adánez et al., 2013). The pyrolysis may be expressed with the following reaction (Cuadrat, Abad, García-Labiano et al., 2012):



Since every solid fuel composition is different it is important to consider the proximate, ultimate and sulfonate analyses when modelling the pyrolysis step (Lee Coal gasification kinetics). Larger molecules of tar might also appear from the pyrolysis but they are assumed to undergo a cracking process to non-condensable gases and light hydrocarbons (Kaushal et al., 2010). Assuming that the pyrolysis occurs instantaneously and that the tar compositions are alike for coal and biomass, the same pyrolysis model could be used for both fuels.

4.4.2 Char gasification

Once the fuel enters the fuel reactor it becomes a subject for gasification. The carbon in the char particles starts to react with the hot fluidizing gases of either steam or carbon dioxide. The reactions that takes place during the gasification can be explained using the following expressions (Cuadrat, Abad, Gayán et al., 2012). With carbon dioxide the gasification occurs as:



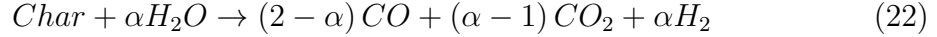
And with steam as:



The produced carbon monoxide could react further with the steam as:

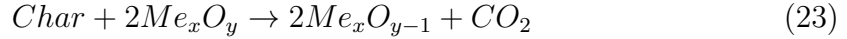


Equations (20) and (21) can be combined to a single expression as:



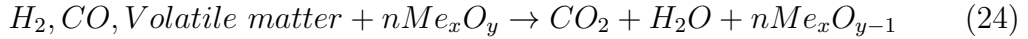
Where α has been experimentally determined to be in the range of 1.5 to 1.1 at 750-900 °C (Lee et al., 1998). Since the fuel reactor temperature will be in the upper region of this interval the value of α is set to 1.1.

The solid char particles could also be considered to react directly with the oxygen carriers that are also present in the fuel reactor.



However, this reaction would be a homogeneous reaction of two solids and it has been experimentally shown to have a very low occurrence and is therefore neglected in this work (Cuadrat, Abad, Gayán et al., 2012).

The products from the gasification reacts further with the oxygen carriers in the fuel reactor as described in the subsections above. Summarized in one expression the reduction of oxygen carrier can be written as:



5 Process model description

To simulate the process model for the 1 MW_{th} chemical looping pilot plant Aspen Plus V8.2 software is used. The software is a powerful tool for simulations of chemical processes where a flow-sheet with different unit operations, materials, heat and work streams easily can be specified. The user has the possibility to set the most parameters such as temperature, pressure, material flows, reactions and particle size distribution among others.

The software has the ability to handle fluids and solids which is of great importance when working with chemical looping combustion. But to make this possible with Aspen an appropriate template has to be chosen. The template used in this project is the “MCINPSD” which includes the three substreams of “MIXED”, “CIPSD” and “NCPSPD” and the possibility of setting a particle size distribution. The MIXED substream consists of all species that are either liquids or gases, that is no solids. The CIPSD substream consists of all conventional homogeneous solids with a defined molecular weight. Finally the NCPSPD substream consists of nonconventional heterogeneous solids without a defined molecular weight, such as coal, ash or biomass.

The software has the possibility to include user defined calculators, design specifications to reach any boundary condition as well as sensitive analyses of the process. Any parameter can be varied and it is possible for the user to set the interval boundaries, step size and what parameters to investigate in such an analysis of the process.

5.1 Unit operations

Most of the unit operations present in the chemical looping combustion process are possible options directly from the Aspen Plus toolbox. The chemical looping pilot plant includes a number of connected different unit operators as well as in- and outgoing streams. Every unit operation requires its own specifications to operate as close to the real pilot plant as possible. The flow-sheet for the process with individual streams and unit operators can be seen in Figure 7 below. The unit operators are presented and described in the following subsections.

5.1.1 Air and fuel reactor

Both the reactors present in the chemical looping plant are fluidized beds with complicated hydrodynamics, particle distributions and chemical reactions as will be described in more details under section 5.5. In older versions of Aspen Plus no fluidized bed unit operation has been an option and therefore the Energy Systems and Energy Technology institution at Technische Universität Darmstadt has performed modelling work of the reactors using implemented Fortran code to Aspen Plus. Conversions and properties of the fluidized beds are calculated within the Fortran code of the model for each reactor. The reactions in the air reactor are exothermic and

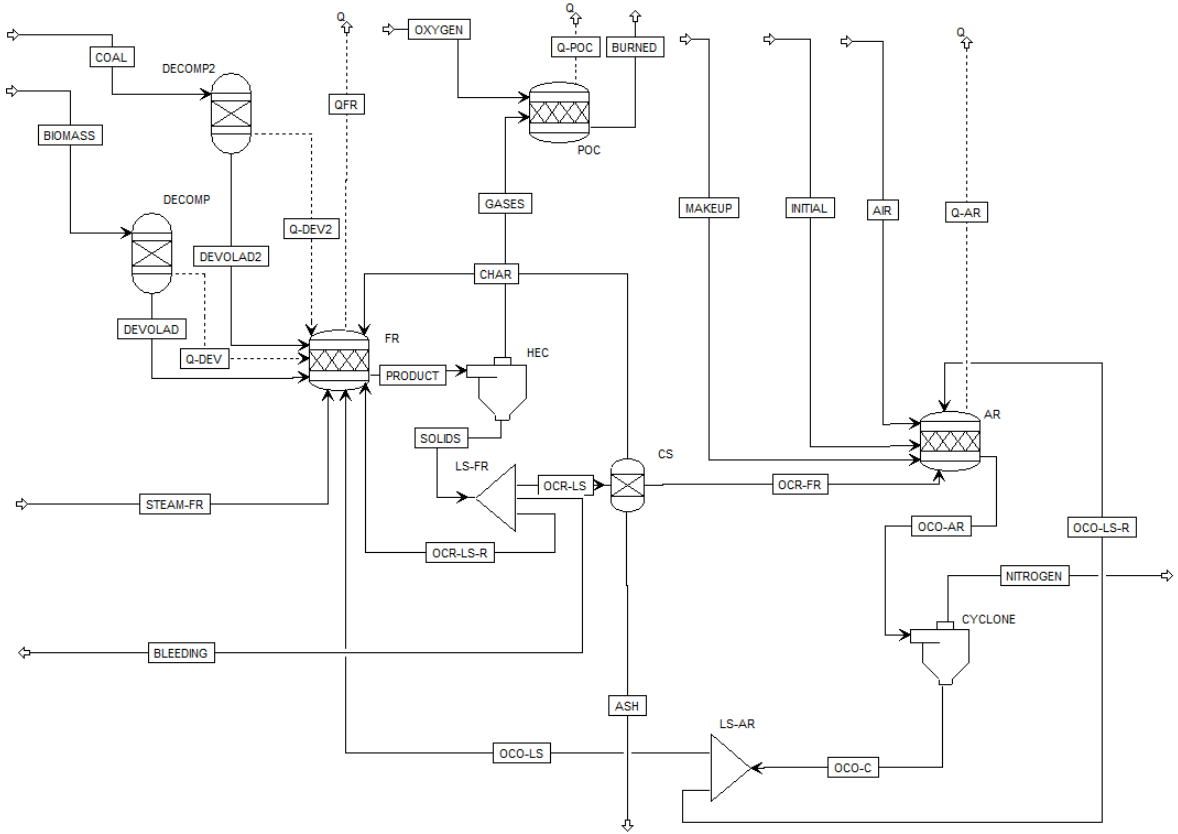


Figure 7: A flowsheet of the components and streams at the 1 MW_{th} chemical looping plant at Technische Universität Darmstadt as built in Aspen Plus for simulations.

heat has to be removed. The reactor is not adiabatic meaning that the heat can be removed to reach the desired outlet temperature. In the fuel reactor the reactions are either exothermic or endothermic and the reactor itself is adiabatic.

In Aspen Plus the two fluidized bed reactors are presented as stoichiometric reactors with a *calculator* where the model is implemented using Fortran code. The air reactor temperature is set to 1050 °C and the reactor pressure to 1 atm. The oxygen carrier conversion is calculated while eventual char particles are considered to be fully oxidized. The fuel reactor pressure is set to 1 atm while the reactor temperature can be varied. All conversions in the fuel reactor are calculated from the model.

5.1.2 Decomposers

The solid fuel entering the fuel reactor is transferred to the final products via three different chemical steps in the fuel reactor. The first step is the pyrolysis of the fuel where it is converted to solid char and ash particles and volatile gases. Due to the very rapid pyrolysis reaction of the fuel it is assumed to occur immediately and therefore it is performed in an earlier unit operator than the fuel reactor in the

simulations, the decomposer. Two decomposers are used, one for each solid fuel, since the pyrolysis products differs for the different fuels. The outlet stream from the decomposers goes directly to the fuel reactor.

Since the products and yields can be calculated from the pyrolysis process from experimental measurements and modelling a RYield reactor can be used in Aspen Plus. The input to such a reactor is the product yield without any information of chemical reactions.

5.1.3 Post Oxidation Chamber

The conversion of the gaseous fuels in the fuel reactor are not complete and some of the fuel gases are leaving with the outgoing flue gases. To prevent this energy loss and to achieve complete combustion a post oxidation chamber is used. The gases are oxidized using pure oxygen to not include any nitrogen from the air to the flue gases. A stoichiometric reactor with total conversion of the combustible gases is used in Aspen Plus. The oxygen that enters the combustion chamber is set as pure oxygen.

5.1.4 Cyclones

There are two cyclones present in the chemical looping plant, one connected to each fluidized bed reactor. The outlet streams from the reactors consists of fluidizing gases, solid particles and from the fuel reactor also combustion gases. The gases are to be separated out from the chemical looping system while it is desirable to keep the oxygen carriers and char particles. Therefore cyclones are used for this separation between gases and solids. The cyclones are highly efficient with an efficiency larger than 99 % at the plant and in the simulation they were simplified and set to have an efficiency of 100 % considering the solids conservation.

In Aspen Plus the cyclones are modelled as *SSplits*, splitting up the incoming stream depending on the substreams, that is gaseous and solids. The settings are that 100 % of the gases and nothing of the solids are leaving with the outgoing stream from the system. The remaining solids enter the loop seals.

5.1.5 Carbon stripper

The particle stream leaving the loop seal at the fuel reactor contains both oxygen carrier and char particles. It is not desirable to transport the char particles to the air reactor since they would react within the hot air reactor and leave with the outgoing air. Therefore a separation of solids is desirable of this stream, and a bubbling fluidized bed is used with steam as fluidizing gas. This unit operator is called a carbon stripper and is separating due to density difference of the particles. The lighter char particles are transported back to the fuel reactor and the heavier oxygen carrier particles are transported to the air reactor. The carbon stripper operates as a low-velocity bubbling bed or a turbulent fluidized bed (Research Fund

for Coal & Steel, 2013). Since the separation will not be perfect some unreacted char particles will however be transported to the air reactor where it is assumed to be fully oxidized.

As a simulation of the carbon stripper a separation unit is used in Aspen Plus. The species are separated as fractions but with the possibility to set a fraction for a single specie. However, in the planned test campaigns the carbon stripper is not present as a simplification of the plant configuration. That is, all char particles will pass on to the air reactor. The carbon stripper will instead be used as a separation unit of ash in the simulations preventing an accumulation with an additional loss of the circulating oxygen carrier. 20 % of the ashes are considered to be separated and the loss of oxygen carrier can be varied.

5.1.6 Loop seals

To prevent backflows in the reactor system loop seals are used. These works in the same manner as a water seal in a water basin, preventing gas to pass. A certain amount of oxygen carrier from the cyclones is trapped in the loop seals temporarily. The loop seals are designed as small fluidized beds, making it possible for the oxygen carriers to transport further in the system. Even though the main function of a loop seal is to prevent backflows they can also be designed to work as splits. In the process the particles continues in either two directions from the loop seals as present in the flowsheet. From the loop seal at the air reactor the particles goes either back to the air reactor or to the fuel reactor. From the loop seal at the fuel reactor the oxygen carriers and char particles either goes back to the fuel reactor or to the carbon stripper.

The loop seals are modelled as simple *splits* in Aspen Plus with a fractional separation to each outgoing stream. That is no specie properties are of importance in these unit operators. For the planned test campaigns the loop seal after the fuel reactor will not be present and the split is specified so that no material is returned to the fuel reactor. The split at the air reactor is specified so that 20 % of the material is recirculated to the air reactor. The split at the fuel reactor is not present as a split in the new configuration for the planned test campaigns and all material passes on to the air reactor.

5.1.7 Mixers

Since loops are present in the chemical looping plant, as well as a number of ingoing streams, mixers can be used to combine a number of streams to one. The mixer is a simple unit operator that only summarise the ingoing streams to one outgoing stream. Two mixers are used in the process model combining the streams. The mixers are set as *Mixers* in Aspen Plus without any further specification.

5.2 Streams

There are both ingoing and outgoing streams to the chemical looping plant. Necessary inlet streams are the fluidizing gases, the injection of the fuels and the oxygen to the post combustion chamber but also a makeup stream for the loss of oxygen carrier in the system. The inventory of oxygen carrier in the system is decreasing due to partly attrition of the solid particles but also due to the required system bleeding to prevent accumulation of ash in the system. The outgoing streams are used fluidized gases, flue gases and the bleeding of the system. In the simulations in Aspen Plus there is also an *initial inlet stream* which is used to reduce the number of iterations. If the only inlet of oxygen carrier was to be the makeup stream a number of iterations would be needed to reach the inventory at a steady state. Instead an initial stream is used with an inflow of oxygen carrier that is close to the steady state inventory and is only calculated for in the first process loop, reducing the number of iterations.

When introducing the fuels to Aspen Plus the proximate, ultimate and sulfonate analysis are used. The analyses of the two solid fuels to be used in the planned test campaigns are shown in Table 4 below. An approximation considering the mass fraction of sulfur from the ultimate analysis to appear as one third of each of the three sulfur compounds is used.

Table 4: Taldinsky coal and torrefied biomass composition from analyses.

Analysis	Component	Portion [%wt]	
		Coal	Biomass
Proximate	Ash _{dry}	9.87	0.63
	Volatile matter _{dry}	37.5	73.6
	Fixed carbon _{dry}	52.7	25.8
	Moisture	12.1	5.43
Ultimate	Ash _{dry}	9.87	0.63
	Carbon _{dry}	72.2	57.2
	Hydrogen _{dry}	5.45	7.28
	Nitrogen _{dry}	2.06	0.07
	Oxygen _{dry}	10.07	34.8
	Chlorine _{dry}	0.00	0.00
	Sulfur _{dry}	0.34	0.03
Sulfonate	Pyritic _{dry}	0.113	0.01
	Sulfate _{dry}	0.114	0.01
	Organic _{dry}	0.113	0.01

How much coal and biomass that should be fed to the fuel reactor to achieve a certain heat power can be calculated from the heating value of the coal. The heating value for the Taldinsky coal is 25.02 MJ/kg, that is a coal feed of 143.9 kg/h to

achieve a 1 MW_{th} plant. The heating value for the torrefied biomass is 19.38 MJ/kg, that is a biomass feed of 185.8 kg/h to achieve a 1 MW_{th} plant. However, biomass is not planned to be used as the only fuel but as a fraction of the fuel inlet. About 10 % of the heat should come from the biomass and the rest from the coal.

5.3 Calculators

Since the fluidized beds can not be expressed in Aspen Plus directly with the Aspen toolbox in a satisfactory way, there is a need of models from the user. The user has the opportunity to use *calculators* within which it is possible to implement Fortran code directly into the Aspen Plus software. Fortran code and statements are easy to use and understand and the code is read from top to bottom. However, the user has to be careful and considering when typing in the code since not all types of eventual errors will be displayed. To solve many of the equations present in the reactor models it is necessary to use iterative methods. This can be implemented in the Fortran code easily using so called *do while*-loops. Certain process values such as mass flow of reactants and operation temperatures can easily be imported from the streams and the final values can in the same manner be exported as desired by the user. In Aspen Plus it has to be defined when the Fortran code is to be executed and since the results wanted are the outlets from the reactors it is executed before the reactor blocks and with the input values, that is before the calculation block is executed. The exported values are in the end the conversions of reactants which are imported to the reactor blocks giving the outlet values.

It is also possible to connect Microsoft Excel to Aspen Plus for the calculations. This is another option to the Fortran code and it was considered to use this option when performing matrix calculations. The model for the pyrolysis step was therefore implemented using Excel rather than Fortran.

5.4 Boundary conditions

There are some boundary conditions for the chemical looping pilot plant considering the mass and heat flows in the system. There is a maximum feed of solid fuel to the plant of about 150 kg/h (Ströhle et al., 2013) which corresponds to about 1 MW_{th} as can be seen under section 5.2. A maximum steam flow of about 400 kg/h to the fuel reactor of superheated steam at 400 °C and a maximum flow of nearly 2500 kg/h of air to the air reactor. The air temperature to the reactor can be heated using heat from separate burning of propane, which is not included in the model.

The fuel reactor is as already mentioned adiabatic and the reactor temperature is therefore a boundary condition that has to be adjusted in some way. The air reactor has to be kept at about 1050 °C and the fuel reactor at about 970 °C, that is, heat could be transferred from the hot exothermic air reactor to the possible cold and endothermic fuel reactor. This heat transfer can be enabled by control of the circulating mass flow of oxygen carrier between the reactors. The larger the solid

mass flow, the larger the heat transfer between the reactors.

5.4.1 Design Specifications

The properties for the inlet and outlet streams has to be set by the user but the boundary conditions within the process also have to be met. In Aspen Plus it is possible to use *design specifications* for this purpose. To reach the desired outlet temperature from the fuel reactor a design specification can be used that changes the circulating mass of oxygen carrier between the reactors. This is done by varying the size of the makeup feed to the system, considering a constant loss from the system. To make sure everything is oxidized and fully combusted out from the post combustion chamber a design specification regulating the oxygen inlet flow depending on the inlet of unreacted fuel to the post combustion chamber is used. A design specification is also used for the air feed which is varied to reach a reasonable excess air ratio. The fuel composition in to the fuel reactor is used to vary the air feed to the air reactor and then as an effect the excess air ratio. The design specifications used can be seen in Table 5.

Table 5: Design specifications used in Aspen Plus.

Parameter	Boundary value	Variated parameter
Q_{FR}	10 kW	Makeup feed of oxygen carrier
POC	Total fuel oxidation	Oxygen feed to POC
λ	1.1-1.3	Air feed to air reactor

5.5 The fluidized bed model

The chemical looping combustion process consists of two fluidized beds where the reactions occurs. To make good predictions of the process conditions it is of great importance that the reactor models are as adequate as possible. Understanding of the hydrodynamics and reactions in the reactors are therefore necessary. Depending on the fluidizing gas velocity and the particle type the fluidizing bed can adapt different properties. A low gas velocity will just fluidize particles and increasing the gas velocity will arise a presence of bubbles and particles are blown up from the bed, a *bubbling bed*. Increasing the gas velocity even further will cause a mass entrainment of particles that will eventually even leave the plant. For this kind of beds the carryover is large and recirculation will be necessary to not risk a complete emptying of the bed, a *circulating fluidized bed* (Kunii & Levenspiel, 1991).

The fluidized beds in the plant are circulating fluidized beds since they are operated at high velocity regimes. The circulating fluidized bed can be divided into two different zones, a *bottom bed* zone and a *lean* zone, with respect to axial concentration and backmixing of solids. The dense zone is located in the bottom of the bed and consists of a high, roughly constant concentration of solid particles. The

lean zone is located above the dense zone and has a considerable lower concentration of solid particles, which is decayed with the height of the reactor (Abad, Gayán et al., 2013). A typical figure of the particle distribution in the reactor can be seen in Figure 8. The typical zones and bubbles in the bottom bed can be seen in Figure 9.

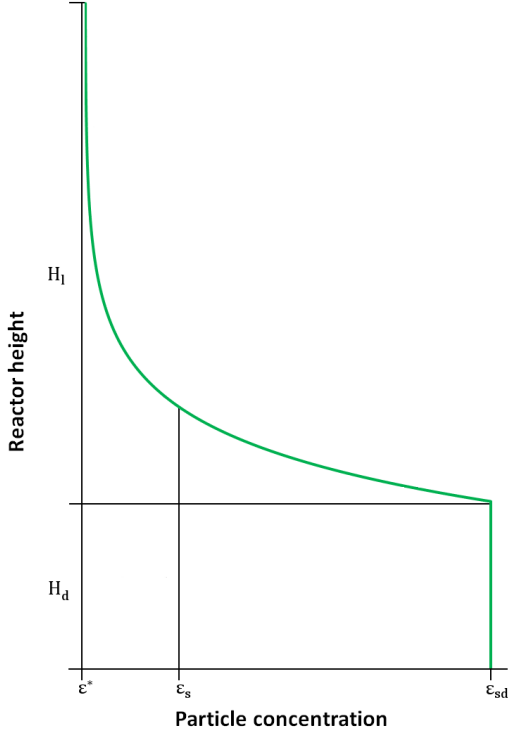


Figure 8: A typical solid particle entrainment with height in the fluidized bed reactor.



Figure 9: Bottom bed zone with bubbles and lean zone above the bottom bed zone.

To achieve a good model it is therefore necessary to understand the two present zones in the reactors as well as how the particles are distributed between the two zones. Then it has to follow how the reactions shall be introduced to the model.

5.5.1 Overall particle distribution

Depending on the inventory in the reactor and the gas velocity to the fluidized bed the particles will partly stay in the bottom bed zone and partly in the lean zone. It is desirable to calculate for this particle distribution with the height of the fluidized bed reactor to achieve an accurate model.

For the bed to be fluidized the fluidization gas velocity has to exceed the minimum fluidization gas velocity, u_{mf} . There are different correlations in the literature to calculate this velocity. One such correlation that is widely used is the correlation

by Wen and Yu:

$$Re_{p,mf} = \frac{u_{mf} \cdot \rho_g \cdot d_p}{\mu_g} = \sqrt{C_1^2 + C_2 Ar} - C_1 \quad (25)$$

Values for C_1 and C_2 can be found in the literature and were proposed to be set to 27.2 and 0.0408 respectively by Grace (Abad, Gayán et al., 2013). Where the dimensionless Archimedes number is calculated as:

$$Ar = \frac{d_p^3 \cdot \rho_g \cdot (\rho_s - \rho_g) \cdot g}{\mu_g^2} \quad (26)$$

When the fluidizing gas velocity is increased above the required velocity to reach minimum fluidization particles will start to follow the surrounding gas and eventually leave the reactor when the gas velocity is fast enough. This velocity is called the terminal particle velocity, u_t and can be calculated as described by Kunii & Levenspiel (1991). A dimensionless particle size, d^* , and a dimensionless gas velocity, u_t^* , are first calculated.

$$d_p^* = d_p \cdot \left[\frac{\rho_g \cdot (\rho_s - \rho_g) \cdot g}{\mu^2} \right]^{1/3} \quad (27)$$

$$u_t^* = \left[\frac{18}{(d_p^*)^2} + \frac{2.335 - 1.744 \cdot \phi}{(d_p^*)^{0.5}} \right]^{-1} \quad (28)$$

And then the actual terminal particle velocity can be found from the following equation:

$$u_t = u_t^* \left[\frac{\mu (\rho_s - \rho_g) \cdot g}{\rho_g^2} \right]^{1/3} \quad (29)$$

When the terminal velocity is known a saturated flux of solids out from the reactor can be estimated as from a correlation by Geldart et al (Kunii & Levenspiel, 1991):

$$G_{sat}^* = 23.7 \cdot \rho_g \cdot u_0 \cdot \exp \left(-5.4 \cdot \frac{u_t}{u_0} \right) \quad (30)$$

Where u_0 is the superficial rise velocity of gas in the reactor and may be calculated as the average gas velocity in the reactor through both reactor zones. These calculations requires the dynamic viscosities for the gases which are gathered from (Welty et al., 2008). However, equation (30) above is considering all particles to be equally large. For a number of particle sizes the total flux of solids can be calculated as:

$$G_{sat} = \sum_i^n (x_i \cdot G_{sat,i}^*) \quad (31)$$

Where x_i is the fraction of a certain size (Kunii & Levenspiel, 1991).

The decaying concentration of solids in the lean zone can be described using a decay constant, a . The decay constant has been shown to adapt a value in an interval

of about 4-12 divided by the superficial gas velocity, u_0 (Kunii & Levenspiel, 1991). A sensitive analysis was performed to find a good fixed value for this parameter, see Figure 44, and a value of 6.0 divided by the superficial gas velocity was chosen. From the appearance of Figure 8 the fraction of solids at the exit, ε_{se} , or at any point in the lean zone, can be estimated as:

$$\varepsilon_{se} = \varepsilon_s^* + (\varepsilon_{sd} - \varepsilon_s^*) \cdot e^{-a \cdot H_l} \quad (32)$$

Where ε_{sd} is the fraction of solids in the dense zone. It has been found to adapt a value in an interval of 0.16-0.22 for a fast fluidized bed (Kunii & Levenspiel, 1991). A mean solids fraction in the lean zone can be calculated by integrating equation (32) and divide by the lean zone height as:

$$\bar{\varepsilon}_{se} = \varepsilon_s^* + \frac{\varepsilon_{sd} - \varepsilon_{se}}{a \cdot H_l} \quad (33)$$

The carrying capacity of the gas, ε_s^* , can be calculated from the saturated flux in equation (30) with the following expression (Kunii & Levenspiel, 1991):

$$\varepsilon_s^* = \frac{G^*}{u_0 - u_T \cdot \rho_s} \quad (34)$$

The total inventory of solids in the reactor is the sum of solids in the bottom bed zone and the lean zone. The solid inventory in each zone can be calculated from the following equations. (Lasheras et al., 2011):

$$W_d = A_t \cdot \rho_s \cdot H_d \cdot \varepsilon_{sd} \quad (35)$$

and

$$W_l = A_t \cdot \rho_s \cdot H_l \cdot \bar{f}_l \quad (36)$$

Expressing the average volume value of solids in the lean zone as:

$$\bar{f}_l = \varepsilon_s^* + \frac{\varepsilon_{sd} - \varepsilon_{se}}{H_l \cdot a} \quad (37)$$

The total inventory of solids in both the lower dense zone and the upper lean zone can then be calculated as:

$$\frac{W}{A_t \cdot \rho_s} = \frac{\varepsilon_{sd} - \varepsilon_{se}}{a} + H_r \cdot \varepsilon_{sd} - H_l \cdot (\varepsilon_{sd} - \varepsilon_s^*) \quad (38)$$

Where W is the total mass inventory in both zones and H_r the total reactor height. This total inventory can be estimated from the pressure drop in the reactors at minimum fluidizing conditions as:

$$m_{OC} = \frac{\Delta p \cdot A_t}{g} \quad (39)$$

Where A_t is the cross sectional area of the reactor and g is the gravitational constant. For a turbulent or fast fluidization bed the total mass inventory can be calculated as (Kunii & Levenspiel, 1991):

$$W = m_{OC} = \frac{0.85 \cdot \Delta p \cdot A_t}{g} \quad (40)$$

From equations (32) and (38) the following expression can be derived:

$$-e^{(-a \cdot H_l)} - a \cdot H_l = \left(\frac{W \cdot a}{A_t \cdot \rho_s} - \varepsilon_{sd} - H_t \cdot \varepsilon_{sd} \cdot a + \varepsilon_s^* \right) / (\varepsilon_{sd} - \varepsilon_s^*) \quad (41)$$

The height of the lean zone, H_l , is still unknown but it can be calculated using iterations. The iteration method chosen is the Newton-Raphson method. The method is implemented by usage of the following (Wedemeier, 2012) equation:

$$x_{n+1} = x_n - \frac{f(x_n)}{f'(x_n)} \quad (42)$$

Since everything is assumed to be known on the right side of equation (41), this value is calculated and assumed to be constant. In the first iteration x_n is set to be the negative value of this constant and the function of x_i is set to be:

$$f(x_n) = -Constant - e^{-x_n} - x_n \quad (43)$$

A value of x_{n+1} may then be calculated and the next iteration can start. When converged, the height of the lean zone is calculated as the final value of x_{n+1} divided with the decay constant a . The height of the bottom bed zone is then simply calculated as the total reactor height subtracted with the height of the lean zone.

$$H_d = H_r - H_l \quad (44)$$

When the reactor zone heights are known the mass inventory in each zone may be calculated from equations 35 and 36. There will also arise a particle distribution in the horizontal plane of the reactor. It has been shown that gases passes to a higher extent in the core of the reactor compared to closer to the wall. By assuming a void fraction at the wall, ε_w , the volume fraction between the core and the zone close to the wall can be expressed as for both the dense and the lean zone of the reactor.

$$\delta_d = \frac{\varepsilon_w - \varepsilon_{sd}}{\varepsilon_w - \varepsilon_s^*} \quad (45)$$

$$\bar{\delta}_l = \frac{\varepsilon_w - \varepsilon_{se}^-}{\varepsilon_w - \varepsilon_s^*} \quad (46)$$

5.5.2 Bottom bed particle distribution

It is assumed to be two phases present in the bottom bed zone. The first one is the *dense* phase consisting of the solid bed particles with the interstitial gas flow. This phase is also referred to as the *emulsion phase*. The second phase is the *bubble* phase consisting of uprising gas bubbles developed in the bed. The bubbles are considered to be free from any solid particles and therefore can no reactions take place between solids and gases in these bubbles. It is for this reason important to calculate the volume fraction of bubbles in the bottom bed. This fraction can be expressed as (Abad, Gayán et al., 2013):

$$\delta_b = \frac{u_{vis}}{u_{vis} + u_{b\infty}} \quad (47)$$

Where u_{vis} is the visible bubble flow and $u_{b\infty}$ is the single bubble velocity to be calculated as:

$$u_{vis} = \psi \cdot (u_0 - u_{mf} (1 - \delta_b)) \quad (48)$$

and

$$u_{b\infty} = 0.71 \cdot \sqrt{g \cdot d_b} \quad (49)$$

ψ is the ratio of the visible flow and the total flow through the bubbles and d_b is the bubble diameter as function of the bed height, z .

$$\psi = f_b \cdot \left(z + 4 \cdot \sqrt{A_0} \right)^{0.4} \quad (50)$$

Where f_b is a function depending on particle diameter, superficial and minimum fluidization velocity.

$$f_b = \frac{0.26 + 0.70 \cdot e^{-3300 \cdot d_p}}{(0.15 + u_0 - u_{mf})^{1/3}} \quad (51)$$

Due to coalescence of the rising bubbles the bubbles will grow in size as they rise in the bed. A correlation by Darton is used to calculate the bubble diameter with the height as:

$$d_b = 0.54 (u_0 - u_{mf})^{0.4} \left(z + 4 \cdot \sqrt{A_0} \right)^{0.8} \cdot g^{-0.2} \quad (52)$$

The fraction in equation (47) can be calculated by iteration of the equations above.

5.5.3 Reaction kinetics

The kinetics in the reactors depends both on the oxygen carrier and the fuel that is used. What is of importance is the transport of the reactants and the reaction kinetics present. Since ilmenite has been used to a much larger extent than iron ore the kinetics has been researched to a larger extent and are more well known.

The oxygen transport capacity for an oxygen carrier is calculated as the fraction of oxygen in the oxidized particle as the following equation indicates (Abad et al., 2011):

$$R_O = \frac{m_o - m_r}{m_o} \quad (53)$$

Where the index o and r represents the fully oxidized and fully reduced form of the oxygen carrier respectively.

Abad et al. (2011) claims that the reaction rate of ilmenite is independent of the particle size and uses a *changing grain size model* to determine the kinetic parameters. Within this model the solid particles are assumed to consist of nonporous spherical grains with uniform initial radius, r_g . The grain radius can be calculated from the skeletal density, the porosity and a specific surface area as (Abad et al., 2007):

$$r_g = \frac{3}{\rho_{skeletal} \cdot (1 - porosity) \cdot S_{BET}} \quad (54)$$

It has been shown by Abad et al. (2011) that a reaction rate for the oxygen carrier can be described by the following expression for both the oxidization and reduction with the grain radius model as:

$$\frac{dX_{OCi}}{dt} = \left[\frac{3}{\tau_i} (1 - X_{OCi})^{2/3} \right] \quad (55)$$

where

$$\tau_i = \frac{\rho_m \cdot r_g}{b_i \cdot k_s \cdot C_{p,i}^{n_i}} \quad (56)$$

and

$$k_s = k_{s0} \cdot e^{-E/(R \cdot T)} \quad (57)$$

Where the values of k_{s0} and E are determined experimentally and k_s is assumed to be a function of the temperature in an Arrhenius type of expression (Abad et al., 2011).

The reduction reactions of the oxygen carrier considered were of methane, carbon monoxide and hydrogen, and an oxidation with oxygen, with a change of parameters.

The number of reactions taking place in the fuel reactor is one for each fuel oxidation simultaneously with the reactions considering the gasification while there is only one reaction taking place in the air reactor. For this reason two different approaches has been considered for the two reactors. Starting with the air reactor, it is important to know that there are some differences between the bottom bed zone and the lean zone. Considering the bottom bed zone an overall rate constant can be expressed as (Lasheras et al., 2011):

$$K_{ff} = \gamma_{core} \cdot K_r + \frac{1}{1/K_{be} + 1/(\gamma_{wall} \cdot K_r)} \quad (58)$$

Where K_{be} is the gas-interchange coefficient between the bubble and emulsion phases in the bottom bed zone and can be calculated from the following expression (Abanades et al., 2004):

$$K_{be} = 4.5 \cdot \frac{u_{mf}}{d_b} \quad (59)$$

The parameter K_r in equation (58) is the reaction term and is equal to the expression of the reaction rate in equation (55). The solid fractions at the core and at the reactor

wall, γ_{core} and γ_{wall} , are set to 0.01 and 0.15 and are derived from experimental data (Lasheras et al., 2011). A fractional expression of the oxygen concentration at the reactor inlet and at the top of the bottom bed can be derived as:

$$\ln \left(\frac{C_0}{C_d} \right) = \frac{K_{ff} \cdot \delta_d \cdot H_d}{u_0} \quad (60)$$

The fractional value of oxygen concentration at the bottom bed zone and the reactor outlet can be calculated from the following expression (Lasheras et al., 2011):

$$\ln \left(\frac{C_d}{C_l} \right) = \frac{(1 - \varepsilon_f)_{bed} \cdot K_r}{u_0 \cdot a} \cdot \left[(1 - e^{-a \cdot H_l}) - \frac{1 - \eta_{bed}}{1 + (a'/a)} \cdot (1 - e^{-(a+a') \cdot H_l}) \right] \quad (61)$$

Where a' is a model parameter set to 6.62/m (Lasheras et al., 2011). The parameter ε_f is the void fraction at the top of the bottom bed and η_{bed} is the contact efficiency at the top of the bottom bed and they are calculated as:

$$\varepsilon_f = \frac{1 - \delta_l}{1 - \varepsilon_{mf}} \quad (62)$$

and

$$\eta_{bed} = \left(\gamma_{core} + \frac{1}{K_r/K_{be} + 1/\gamma_{wall}} \right) \cdot \frac{\delta_d}{1 - \varepsilon_f} \quad (63)$$

From equations (60) and (61) the conversion in the lean zone can be calculated if the inlet concentration is known:

$$X_{O_2} = 1 - \frac{C_l}{C_0} \quad (64)$$

Once the conversion of the oxygen is known the conversion of oxygen carrier can be calculated since the stoichiometric expression for the reaction is known. The conversion of oxygen carrier, or the degree of oxidation, was defined as:

$$X_{OC} = \frac{n_{O_2,in} \cdot b \cdot X_{O_2}}{n_{OC,reduced \ in}} \quad (65)$$

In the fuel reactor things are more complicated due to the larger number of reactions and different solids. Before the reaction with oxygen carrier occurs both pyrolysis and gasification of the coal takes place. The pyrolysis is considered to be fast and occur directly when the fuel enters the fuel reactor. For how the pyrolysis is modelled please see section 5.6. The gasification reactions that then takes place while the fixed carbon reacts with the steam and carbon dioxide can be seen in section 4.4.2. The reaction kinetics of coal for the gasification may according to (Abad, Gayán et al., 2013) when fluidized with steam be expressed as:

$$\frac{1}{m_c} \cdot \left[\frac{dm_c}{dt} \right]_{H_2O} = \frac{1}{1 - X_C} \cdot \left[\frac{dX_C}{dt} \right]_{H_2O} = \frac{k_{H_2O} \cdot P_{H_2O}}{1 + K_{H_2O} \cdot P_{H_2O} + K_{H_2} \cdot P_{H_2}} \quad (66)$$

and gasification with carbon dioxide (Adánez et al., 1985) as:

$$\frac{1}{m_c} \cdot \left[\frac{dm_c}{dt} \right]_{CO_2} = \frac{1}{1 - X_C} \cdot \left[\frac{dX_C}{dt} \right]_{CO_2} = \frac{k_{CO_2} \cdot P_{CO_2}}{1 + K_{CO_2} \cdot P_{CO_2} + K_{CO} \cdot P_{CO}} \quad (67)$$

For kinetic values see Table 6 below. The kinetic coefficients are temperature dependent and are assumed to be of Arrhenius type as described by equation (57).

Table 6: Kinetic parameters for coal char gasification (Abad, Gayán et al., 2013).

H ₂ O		CO ₂		Units
k _{0,H₂O}	52.6	k _{0,CO₂}	4530	s ⁻¹ atm ⁻¹
E _{a,H₂O}	95.1	E _{a,H₂O}	160.1	kJ/mol
K _{0,H₂O}	2.81·10 ⁻⁶	K _{0,CO₂}	3.28·10 ⁻⁷	atm ⁻¹
ΔH _{H₂O}	-135.1	ΔH _{CO₂}	-158.5	kJ/mol
K _{0,H₂}	8.10·10 ⁻⁹	K _{0,CO}	1.84·10 ⁻⁶	atm ⁻¹
ΔH _{H₂}	-218.5	ΔH _{CO}	-157.6	kJ/mol

The gasification kinetics of the biomass with steam can be calculated with the following expression from (Nikoo & Mahinpey, 2008):

$$\left[\frac{dX_C}{dt} \right]_{H_2O} = k_{Bio} \cdot e^{\frac{-E_{SG}}{T}} \cdot p_{H_2O}^n \cdot (1 - X_C)^{2/3} \quad (68)$$

Where $E_{SG}=19\,544\text{ K}$ and $k_{bio}=6474.7/\text{satm}$.

Simultaneously with the gasification reactions the reduction reactions of H_2 , CO and CH_4 occurs. The reaction rates for these three reactions can be expressed with equation (55). The molar rate change of a specie will occur due to either the gasification reactions, the oxidization reactions or both. A molar change due to the oxidization can be written as:

$$dn_{OC,i,j} = \left[\frac{dX_{OC}}{dt} \right]_{i,j} \cdot R_O \cdot m_{inv,j} \cdot (1 - y_{koks,j}) / M_O \quad (69)$$

Where index i represents either specie of hydrogen, carbon monoxide or methane that reacts with the oxygen carrier and j in which of the dense or lean zone the reaction occur. y_{koks} is a mass ratio of solids of char and oxygen carrier. A molar change due to a gasification reaction can be expressed in the same manner:

$$dn_{Gas,i,j} = \left[\frac{dX_{gas}}{dt} \right]_{i,j} \cdot char \cdot m_{inv,g} \cdot y_{koks,j} / M_C \quad (70)$$

Where index i represents either gasification reaction with steam or carbon dioxide and j in which of the dense or lean zone the reaction occur. $char$ is a mass ratio of char and ash from the solid fuel.

The reduction kinetics when using ilmenite as oxygen carrier can be seen in Table 7 below (Abad, Gayán et al., 2013).

Table 7: Kinetic parameters for ilmenite.

	H ₂	CO	CH ₄	O ₂	Units
ρ_m	13590	13590	13590	31100	mol/m ³
r_g	$1.25 \cdot 10^{-6}$	$1.25 \cdot 10^{-6}$	$1.25 \cdot 10^{-6}$	$1.20 \cdot 10^{-6}$	m
\bar{b}	1.45	1.45	5.78	4	-
k_{s0}	$6.2 \cdot 10^{-2}$	$1.0 \cdot 10^{-1}$	9.8	$1.9 \cdot 10^{-3}$	mol ¹⁻ⁿ m ³ⁿ⁻² s ⁻¹
E	65.0	80.7	135.2	25.5	KJ/mol
n	1	0.8	1	1	-

The kinetics for the iron ore (Research Fund for Coal & Steel, 2013) are yet not fully known but the reaction constants can be set as for the ilmenite but with a factor of two as a first approximation from a recommendation by Alberto Abad, see Table 8.

Table 8: Kinetic parameters for Iron ore.

	H ₂	CO	CH ₄	O ₂	Units
ρ_m	9303.7	9303.7	9303.7	9303.7	mol/m ³
r_g	$9.16 \cdot 10^{-7}$	$9.16 \cdot 10^{-7}$	$9.16 \cdot 10^{-7}$	$9.16 \cdot 10^{-7}$	m
\bar{b}	1.45	1.45	5.78	4	-
k_{s0}	$12.4 \cdot 10^{-2}$	$2.0 \cdot 10^{-1}$	19.6	$3.8 \cdot 10^{-3}$	mol ¹⁻ⁿ m ³ⁿ⁻² s ⁻¹
E	65.0	80.7	135.2	25.5	KJ/mol
n	1	0.8	1	1	-

The molar change of each specie can then be expressed as the reaction rate times the mass inventory of oxygen carrier.

$$\Delta n_i = -m_j \cdot \sum \nu_i \cdot \left[\frac{dX_j}{dt} \right]_i \quad (71)$$

The molar change of each specie in the fuel reactor can be expressed from these molar rates as, from equation (71):

$$\left\{ \begin{array}{l} dn_{C_j} = dn_{Gas, H_2O, j} + dn_{Gas, CO_2, j} \\ dn_{H_2, j} = dn_{OC, H_2, j} - 1.1 \cdot dn_{Gas, H_2O, j} \\ dn_{CO, j} = dn_{OC, CO, j} - 0.9 \cdot dn_{Gas, H_2O, j} - 2 \cdot dn_{Gas, CO_2, j} \\ dn_{CH_4, j} = 0.25 \cdot dn_{OC, CH_4, j} \\ dn_{H_2O, j} = dn_{OC, H_2, j} + 0.5 \cdot dn_{OC, CH_4, j} - 1.1 \cdot dn_{Gas, H_2O, j} \\ dn_{CO_2, j} = dn_{OC, CO, j} + 0.25 \cdot dn_{OC, CH_4, j} + 0.1 \cdot dn_{Gas, H_2O, j} - dn_{Gas, CO_2, j} \\ dn_{N_2, j} = 0 \\ dn_{OC} = dn_{OC, H_2, j} + dn_{OC, CO, j} + dn_{OC, CH_4, j} \end{array} \right. \quad (72)$$

These molar changes are calculated for each specie in each of the two reactor zones, where the output values from the dense zone is set as input values to the lean

zone. For the stoichiometric coefficients see equations (8)-(13), (15)-(17), (19) and (22).

However, due to the comparable large coal and biomass particles to the oxygen carriers, there might be a scenario where the solid fuel particles stay in the bed and are not entrained. This would result in a very small or even negligible loss of char from the fuel reactor. It was therefore decided to use two approaches for the planned test campaigns. A first approach was to consider a total gasification of the char particles and a second approach where the gasification is modelled as described above with the rest of the reactor model.

5.5.4 Results evaluation

To evaluate the performance of the chemical looping pilot plant some useful parameters are the carbon dioxide capture efficiency and oxygen demand. The carbon dioxide capture efficiency is the fraction of oxygen used for oxidation of the oxygen carrier and the total amount of consumed oxygen in the air reactor (Markström et al., 2013).

$$\eta_{OO} = \frac{0.21 - \chi_{O_2} - \chi_{CO_2}}{0.21 - \chi_{O_2} - 0.21\chi_{CO_2}} \quad (73)$$

Where χ_i is the molar fraction. Since there most probably will not be a total gas conversion in the fuel reactor a fraction of the oxygen lacking to achieve total gas conversion can be calculated. This fraction is the oxygen demand and is calculated from the fuel reactor outlet molar fractions (Markström et al., 2013).

$$\Omega_{OD} = \frac{0.5\chi_{CO} + 2\chi_{CH_4} + 0.5\chi_{H_2}}{\Phi (\chi_{CO_2} + \chi_{CO} + \chi_{CH_4})} \quad (74)$$

Φ is the fraction of the required moles of oxygen to fully convert the fuel and the moles of carbon in the fuel. The excess of air ratio to the fuel reactor should be considered to achieve an efficient process. It has been recommended by Mattisson (2013) to be in the range of 1.1-1.3. A higher excess air ratio is possible to set but this will result in a less efficient process and heat losses.

$$\lambda = \frac{0.21 \cdot (1 - x_{O_2,ex})}{0.21 - x_{O_2,ex}} \quad (75)$$

5.6 Pyrolysis model

What volatiles, and in what portion, that will be the products after the pyrolysis has to be estimated in some way. A model to calculate the products after pyrolysis of the coal was developed by (Matthesius et al., 1987). The model was developed to get approximated values for a certain number of products. The products considered were *Char*, *Ash*, CH_4 , C_2H_6 , CO , CO , *Tar*, H_2 , H_2O , NH_3 , and H_2S and are calculated

by the usage of information from the proximate and ultimate analyses of the coal. The model can be written in a multiplication of matrices as the following expression:

$$\sum_{j=1}^{10} A_{ij} \cdot m_j = B_i \quad (76)$$

The model is hence a set of 10 equations where the first five are representing balances for the elements present in any of the products. Each of the ten columns in matrix A is representing the mass fraction for a product into its elements. The vector m is the mass fraction of each product and the desired outcome from the model. B is also a vector which consists of the data from the ultimate and proximate analyses as well as experimentally achieved expressions for the portions of CH_4 , C_2H_6 , CO and CO_2 . The values in the model are considered for coals from the northern hemisphere and could therefore be considered useful for the Taldinsky coal.

$$\begin{bmatrix} 0.9632 & 0.75 & 0.8 & 0.4286 & 0.2727 & 0.8342 & 0 & 0 & 0 & 0 \\ 0.0059 & 0.25 & 0.2 & 0 & 0 & 0.0679 & 1 & 0.1111 & 0.1765 & 0.0588 \\ 0.0036 & 0 & 0 & 0.5714 & 0.7273 & 0.0652 & 0 & 0.8889 & 0 & 0 \\ 0.0129 & 0 & 0 & 0 & 0 & 0.0197 & 0 & 0 & 0.8235 & 0 \\ 0.0144 & 0 & 0 & 0 & 0 & 0.0130 & 0 & 0 & 0 & 0.9412 \\ 1 & 0 & 0 & 0 & 0 & 0 & 0 & 0 & 0 & 0 \\ 0 & 1 & 0 & 0 & 0 & 0 & 0 & 0 & 0 & 0 \\ 0 & 0 & 1 & 0 & 0 & 0 & 0 & 0 & 0 & 0 \\ 0 & 0 & 0 & 1 & 0 & 0 & 0 & 0 & 0 & 0 \\ 0 & 0 & 0 & 0 & 1 & 0 & 0 & 0 & 0 & 0 \end{bmatrix} \cdot \begin{bmatrix} Char \\ CH_4 \\ C_2H_6 \\ CO \\ CO_2 \\ Tar \\ H_2 \\ H_2O \\ NH_3 \\ H_2S \end{bmatrix} = \begin{bmatrix} C \\ H \\ O \\ N \\ S \\ 1 - VM \\ 0.82 \cdot H \\ 0.15 \cdot H \\ 0.59 \cdot O \\ 0.31 \cdot O \end{bmatrix} \quad (77)$$

However, it is not expected to exist any hydrocarbons of higher order than methane. That is the ethane and tar are assumed to react and produce a combination of the remaining products. Abad, Adánez et al. (2013) assumes that all higher hydrocarbons and tars are reformed by the fluidizing gas of either steam or carbon dioxide to produce methane and carbon monoxide. Two other changes from the model by Matthesius are that the coke is assumed to be pure carbon and SO_2 is produced rather than H_2S . Assuming that the tars from coal and biomass are alike the model could also be used for biomass as fuel. The final pyrolysis products composition from the Taldinsky coal and the torrefied biomass can be seen in Table 9 below:

Table 9: Solid fuel products after pyrolysis.

Component	Coal	Biomass
C	46.28	24.4
CH ₄	7.51	10.2
C ₂ H ₆	0.00	0.00
CO	25.17	44.9
CO ₂	2.74	10.2
Tar	0.00	0.00
H ₂	3.90	4.35
H ₂ O	3.32	5.23
N ₂	1.81	0.07
SO ₂	0.60	0.06
Ash	8.67	0.60

The final model with the mentioned changes for the pyrolysis products can be seen in appendix B.3.

5.7 Model Validation

To validate the model experimental data from a 100kW CLC unit at Chalmers technical university was used. The experimental data was collected and reported by Markström et al. (2013) and drift parameters as well as results were gathered for the validation. Drift parameters for running of the simulations are gathered from what can be found in the report including temperatures, pressure drops and mass flows at the two reactors. It is desirable to perform the comparison at stable experimental points since the simulation results are for a steady state scenario. Therefore some certain experimental points are chosen for the comparison and validation of the model. A total of 18 operational points are chosen from the five operational periods ranging from VI to X and the drift parameters for these points can be seen in Table 10 below. The nitrogen flow to the fuel reactor is set as a fixed value of 6 kg/h while the steam flow is varied for each operational point. The mass flow of oxygen carrier between the reactors is calculated from the pressure drop in the air reactor riser by Markström et al. (2013). If not known, the temperature is set as an average value and the reactor pressure drop is set for each operational point. The conversion of the oxygen carrier in the air reactor is considered to be 100 %.

Table 10: Operational points for the 100kW chemical looping pilot plant at Chalmers University of Technology.

	N ₂ [kg/h]	CO ₂ [kg/h]	H ₂ O [kg/h]	m _{OC} [kg/h]	m _{coal} [kg/h]	T _{FR} [C]	ΔP [bar]	Air [kg/h]
VI-1	6	0	31.5	900	6.3	942.5	0.13	143
VI-2	6	0	37.5	900	6.3	942.5	0.13	143
VI-3	6	0	37.5	900	6.3	942.5	0.13	157.3
VII-4	6	0	37.5	2700	12.6	957	0.22	178.8
VII-5	6	0	27.5	2520	12.6	959	0.21	178.8
VII-6	6	0	27.5	2520	12.6	969	0.20	178.8
VII-7	6	0	32.5	3300	12.6	976	0.16	178.8
VII-8	6	0	27.5	2220	12.6	969	0.19	178.8
VII-9	6	0	37.5	2100	12.6	963	0.19	178.8
VIII-1	6	0	27.5	1758	12.6	967	0.20	161
IX-1	6	0	27.5	1380	12.6	960	0.16	143
IX-2	6	0	27.5	1800	12.6	960	0.19	161
IX-3	6	0	27.5	2400	12.6	960	0.20	178.8
IX-4	6	0	27.5	2400	12.6	965	0.20	178.8
IX-5	0	6	27.5	2400	12.6	965	0.20	178.8
IX-6	6	0	27.5	2400	12.6	965	0.20	178.8
IX-7	6	0	28.5	2400	12.6	965	0.18	178.8
IX-8	6	0	29.5	2400	12.6	965	0.18	178.8

The coal used in the test campaign was a Colombian coal called *El Cerrejón* and the proximate and ultimate analyses together with the pyrolysis products can be seen in Table 11 (Markström et al., 2013), (Abad, Adánez et al., 2013).

Table 11: Proximate and ultimate analyses together with the pyrolysis products for the El Cerrejón coal.

Analysis	Component	Portion [% wt]	Pyrolysis product	Portion [% wt]
Proximate	Ash _{dry}	9.98	C	48.2
	Volatile matter _{dry}	34.1	CH ₄	7.60
	Fixed carbon _{dry}	55.9	C ₂ H ₆	0.00
	Moisture	13.8	CO	25.9
Ultimate	Ash _{dry}	9.98	CO ₂	1.40
	Carbon _{dry}	75.9	Tar	0.00
	Hydrogen _{dry}	5.34	H ₂	3.60
	Nitrogen _{dry}	1.51	H ₂ O	2.40
	Oxygen _{dry}	6.61	N ₂	1.60
	Chlorine _{dry}	0.00	SO ₂	0.70
	Sulfur _{dry}	0.70	Ash	8.60

The validation of the model is performed by comparison between the experimental findings and the simulation results. Outlet dry concentrations from the fuel reactor as well as oxygen demand and carbon dioxide capture efficiency are compared.

Some design parameters for running the simulations are not known and therefore has to be chosen. The ratio between solids of char and oxygen carrier in the fuel reactor has shown to give a large influence on the char gasification conversion, but this parameter is not known. Abad, Adánez et al. (2013) also validates a fuel reactor model to these experimental findings and claims that an average char conversion of 63 % in operational periods VII and VIII. With this as an aim a fixed solids ratio in the fuel reactor was set to 13 % char since the simulated conversion then came close to 63 %, see Figure 43 in appendix A. Another unknown parameter is the solid fraction in the dense zone. From Kunii & Levenspiel (1991) this parameter is considered to adapt a value between 0.16 and 0.22 and it was found that the upper value resulted in more accurate predictions, see Figure 45.

The validation results can be seen and compared in Figures 10 and 11. The experimental findings are represented as points in the graphs without any combining line. The simulation results from the elaborated model is represented as points with dashed lines. The model simulation results from Abad, Adánez et al. (2013) are represented as points with dotted lines. From the elaborated model it can be seen that methane is underestimated and the carbon monoxide a bit overestimated. The α -parameter for the gasification reaction in equation (22) as well as the portion between carbon monoxide and methane production in the cracking of the tar in the pyrolysis model have a direct effect on the dry gas concentrations. It might be that these parameters should be adjusted to achieve a better estimation, see Figures 46 and 47 in appendix A. However, the model was considered to estimate the chemical looping combustion plant in a satisfactory way.

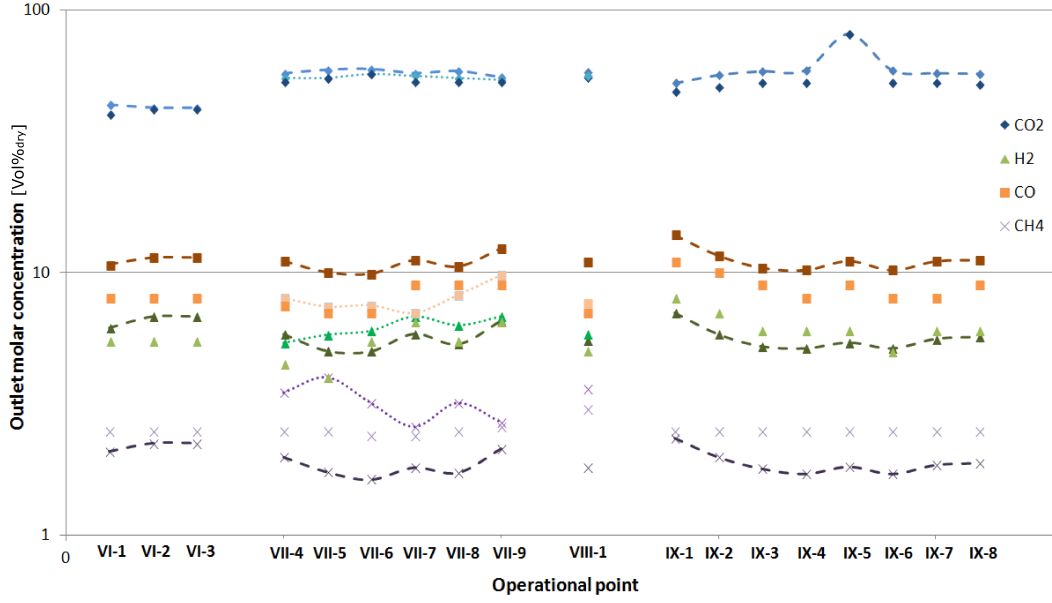


Figure 10: Comparison between experimental data (points), simulation results (dashed) and Abads model (dotted) for the dry gas composition out from the fuel reactor.

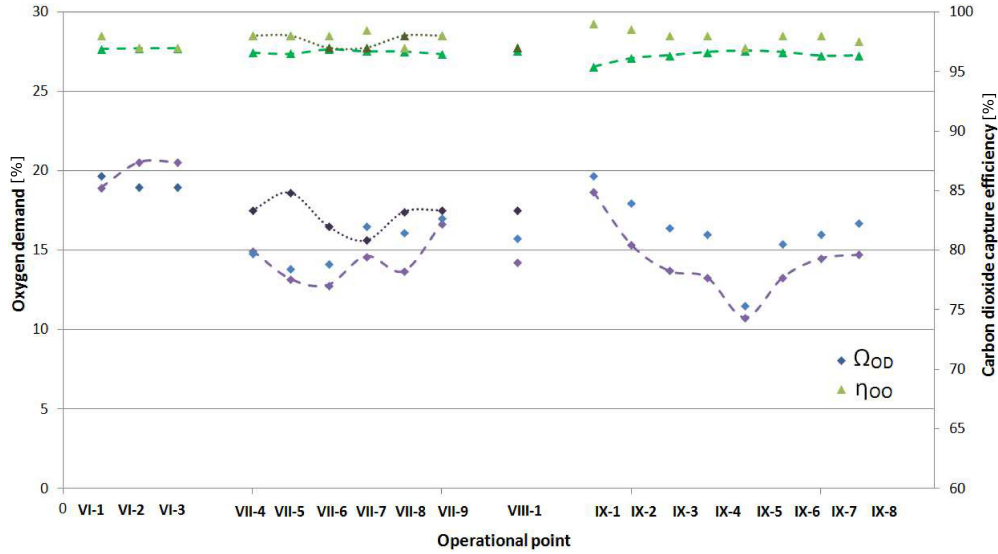


Figure 11: Comparison between experimental data (points), simulation results (dashed) and Abads model (dotted) for the CO₂ capture efficiency (η_{OO}) and the oxygen demand (Ω_{OD}).

Comparing the 100 kW unit at Chalmers University of Technology with the 1 MW_{th} pilot plant at Technische Universität Darmstadt both plants are similar to each other with both reactors acting as circulating fluidized bed reactors. However, one of the greater differences has been the reactor pressure drops. At the 100 kW plant pressure drops of 220 mbar could be measure while no such high pressure drop has been noted at the 1 MW_{th} plant.

6 Results and discussion

The elaborated model was used to simulate the three planned test campaigns considering necessary flows and expected outcomes. Since there are a number of different parameters that are unknown sensitivity analyses were performed to study how the process results would react and change. As a boundary condition the fuel reactor temperature was set to be a constant value with a set heat loss of 10 kW. The air feed temperature was set to a fixed value of 125 °C even though it can be varied in the process.

6.1 Fuel reactor entrainment

To secure the mass circulation of the oxygen carrier to be large enough it is important to have a large enough mass entrainment from the reactors. As mentioned in section 5.4 the volumetric flow to the air reactor can be set to a lot larger at the air reactor than at the fuel reactor. A first sensitive analysis was therefore performed where the steam flow to the fuel reactor was varied for all three planned test campaigns. The entrainment is calculated using equation (30) for an estimation of the saturated mass flux out from the reaction. It was found that using a maximum steam inlet of 400 kg/h resulted in an entrainment of more than 8000 kg/h of ilmenite and 9000 kg/h of iron ore, see Figure 12.

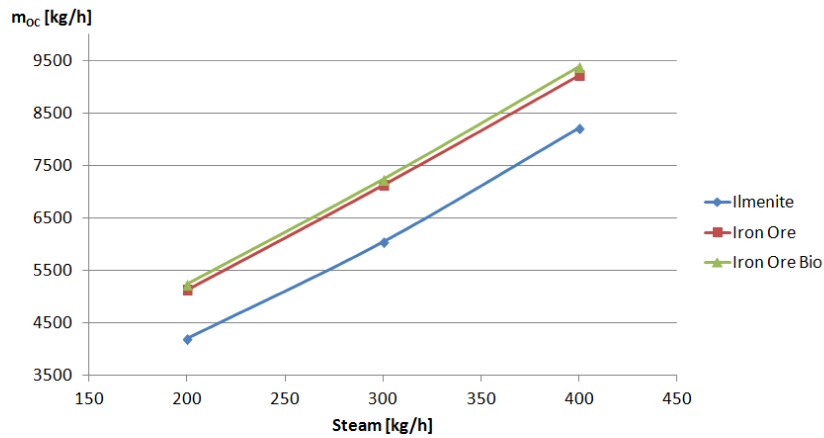


Figure 12: Sensitive analysis of the mass entrainment in the fuel reactor for a variation of the steam feed.

The estimated entrainment is highly dependent of the steam flow since a higher mass flow means a larger volumetric flow and also a higher gas velocity. The higher velocity results in a larger acting drag force on the particles and a larger mass entrainment. Large circulation mass flows will be necessary to keep the fuel reactor temperature and a steam flow of 400 kg/h and 400 °C is therefore chosen for further simulations.

6.2 Ilmenite as oxygen carrier

High fuel gas conversions are the desired result from the fuel reactor and it is therefore of great interest to investigate how sensitive the conversions are to parameter changes. The reactor heat demands and the circulating mass flow of oxygen carrier are also of great interest for the same parameter variations. If not specified or varied, the fuel reactor temperature is set to 970 °C and the air reactor temperature to 1050 °C.

Starting with the planned test campaign considering the ilmenite with coal a first sensitive analysis was performed where the pressure drop in both the reactors were changed simultaneously in a range of 60 to 100 mbar. The pressure interval set was chosen as what can be reasonable steady states for the reactor system. A clear trend where the gaseous fuel conversions are increased with the increased pressure drop could be seen. This can be explained since a higher pressure drop in the reactor is directly proportional to a higher solid mass inventory, that is the amount of reactant is increased with the pressure drop. The required heat removal from the air reactor was also increased with the increased pressure drop due to an increased conversion of the oxygen carrier and from this more released heat. The required mass circulation of oxygen carrier was instead decreased with an increased pressure drop due to the larger heat release in the fuel reactor with the higher gas conversions, see Figure 13.

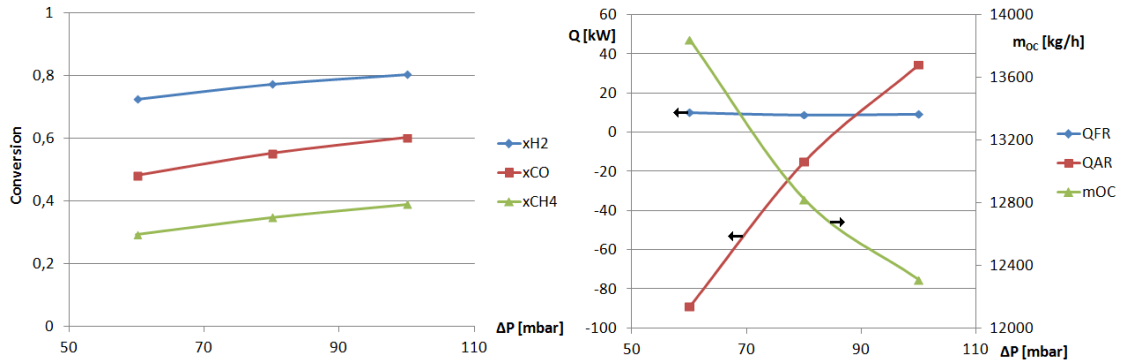


Figure 13: Gas conversions in the fuel reactor (left) and the reactor heat demands together with the required circulating mass of oxygen carrier for ilmenite (right), varying the reactor pressure drops.

A sensitive analysis of the fuel reactor temperature was performed where it was varied from 950 to 990 °C while keeping the air reactor temperature constant. From the fuel reactor temperature sensitive analysis a trend could be seen where the gaseous fuel conversions were increased with the fuel reactor temperature. This trend was expected as can be explained by the Arrhenius expression for the reaction constant from equation (57). To fulfil the boundary condition of a 10 kW heat loss from the fuel reactor a larger circulation mass of oxygen carrier is required from the hot air reactor. Together with the increased mass circulation of oxygen carrier the required heat removal from the air reactor is increased due to a larger bulk of

cold material from the fuel reactor, see Figure 14. For all fuel reactor temperature sensitive analyses the reactor pressure drops are set to 80 mbar.

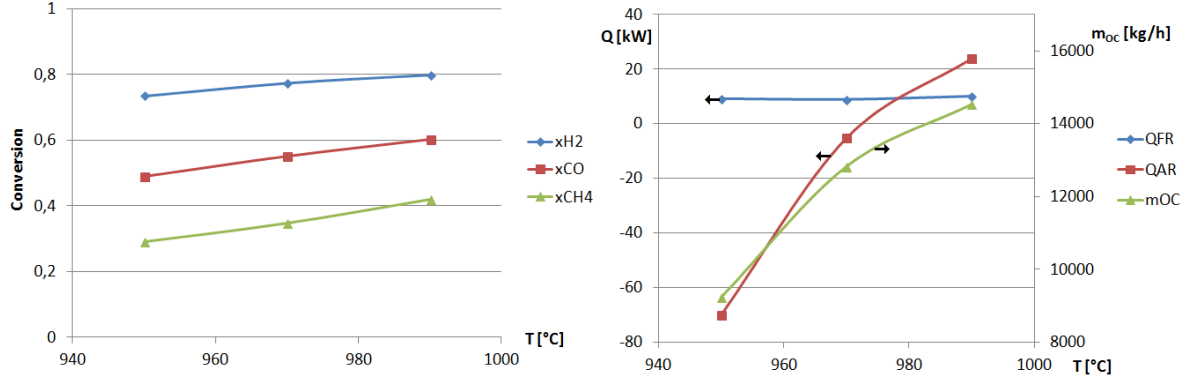


Figure 14: Gas conversions in the fuel reactor (left) and the reactor heat demands together with the required circulating mass of oxygen carrier for ilmenite (right), varying the fuel reactor temperature.

Another approach to the large coal particles used in the planned test campaigns is to also consider the modelling of the char gasification as mentioned under section 5.5. A comparison between the two approaches was made while varying the reactor pressure drop was performed. The char conversion is increased with the pressure drop while the gaseous conversions are more or less constant. However, the increased char conversion means an increased total conversion, see Figure 15.

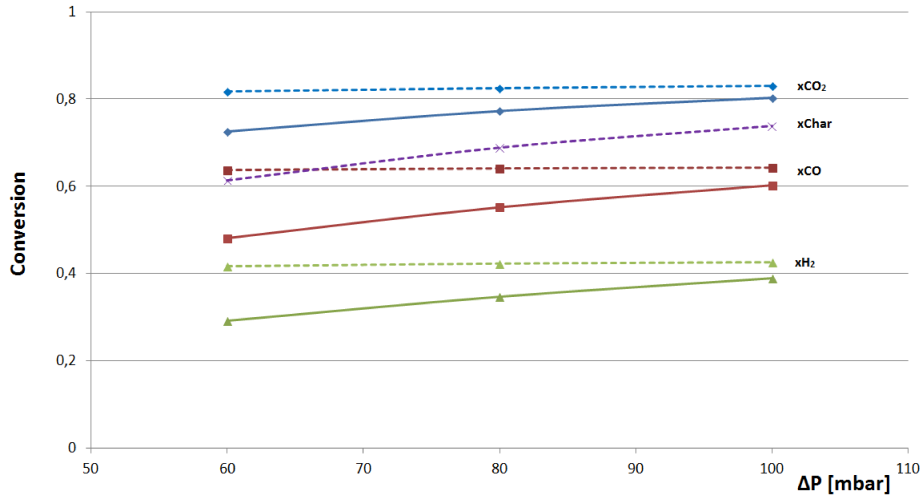


Figure 15: Comparison of the gaseous conversions of two char gasification approaches. Gasification of 100 % (solid curves) and a modelled char gasification (dashed curves).

The char particles that are not gasified in the fuel reactor is transported to the air reactor where they are oxidized causing the high energy removal as can be seen in the left graph of Figure 16. A lower char gasification causes a decreased

amount of endothermic reactions keeping the temperature up in the fuel reactor and the required mass circulation of oxygen carrier is lower compared to the perfect gasification scenario.

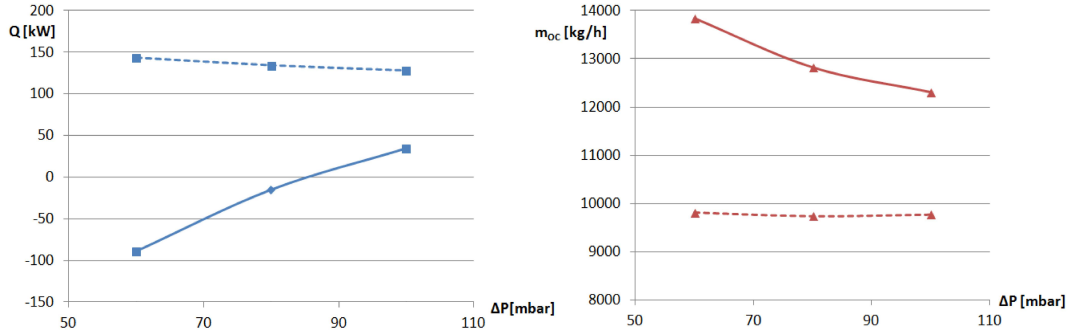


Figure 16: Comparison of the air reactor heat demands (left) and the required mass circulation of oxygen carrier (right) of two char gasification approaches. Gasification of 100 % (solid curves) and a modelled char gasification (dashed curves).

A higher reactor pressure drop is desirable to achieve high gas conversions as well as oxygen carrier conversions and a lower required mass circulation of oxygen carrier. A higher fuel reactor temperature also results in higher gas conversions but the required mass circulation of oxygen carrier is increased.

More pressure drop and fuel reactor temperature sensitive analyses have been performed for the ilmenite and coal test campaign. It was shown that the higher the pressure drop the higher the gaseous fuel conversions could be expected. See Figures 25, 26, 35-40 and 42 in appendix A. However, a higher pressure drop in the reactors than about 100 mbar have been shown to be hard to reach since there is a risk of filling parts of the reactor system with particles.

6.3 Comparison of ilmenite and iron ore as oxygen carriers

The same trends while changing the parameters of pressure drop and fuel reactor temperature as above for the other two planned test campaigns of iron ore with coal and iron ore with coal and biomass could be seen, see figures 27 - 34 in appendix A. A comparison between ilmenite and iron ore is shown below instead. The simulation results showed that slightly higher conversions can be expected when using iron ore compared to ilmenite, see Figure 17. Even though the oxygen transport capacity is lower for the iron ore, the kinetics are more beneficial and the conversions can therefore be expected to be higher.

However, the simulation results also showed that a smaller mass circulation of oxygen carrier was required when using iron ore since more heat seems to be released, see Figure 18. Comparing the sensitivity of the mass circulation flow of oxygen carrier of ilmenite and iron ore, the iron ore is more sensitive, that is a larger amount gives higher conversions, see figures 35 - 37 and 41 in appendix A. The simulation

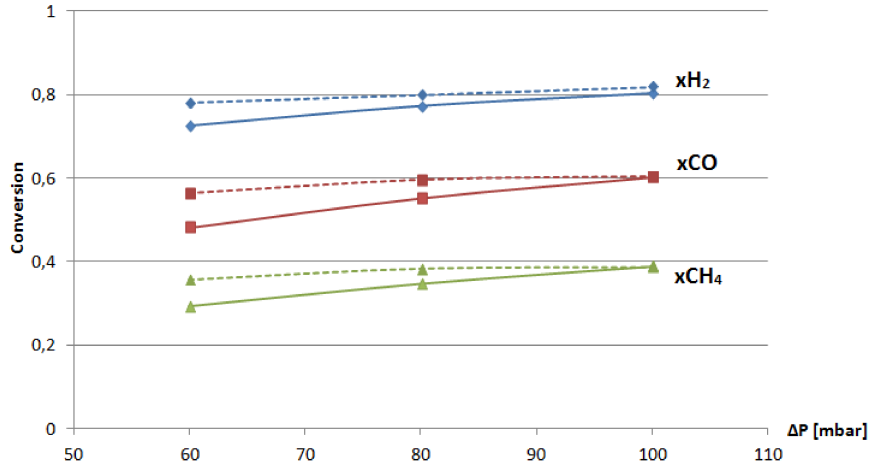


Figure 17: Comparison of the gaseous fuel conversions using ilmenite (solid curves) and iron ore (dashed curves) varying the pressure drop.

results showed that the heat removal could be expected to be higher from the air reactor when using iron ore.

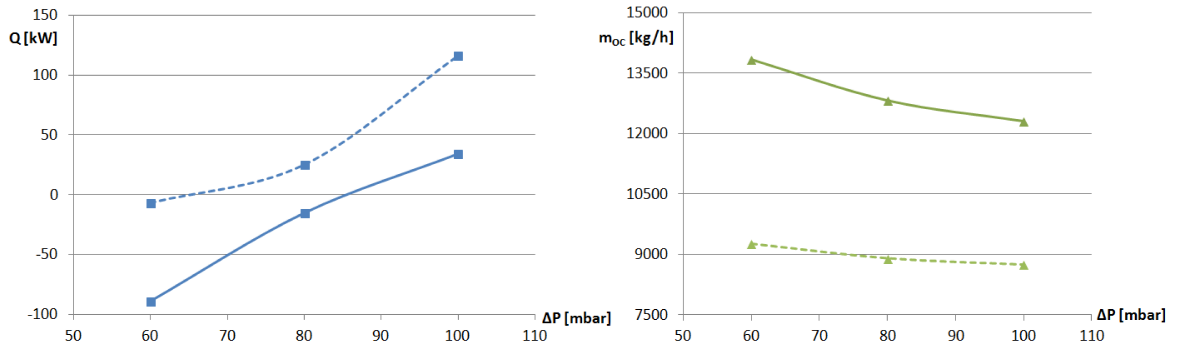


Figure 18: Comparison of the air reactor heat demands (left) and required mass circulation of oxygen carrier (right) using ilmenite (solid curves) and iron ore (dashed curves) varying the pressure drop.

As can be seen in Figure 18 there is a change in mass circulation of both oxygen carriers with the pressure drops. This might explain why there is a larger difference in gas conversions at lower pressure drops, see Figure 17. As discussed above a larger mass flow of iron ore has a greater influence than a larger mass flow of ilmenite on the conversions. That is, when using iron ore the gas conversions are increased with the pressure drop but reduced with the lowered mass circulation of oxygen carrier. When using ilmenite the gas conversion is more sensitive to the increased pressure drop rather than the reduced mass circulation of oxygen carrier.

The same trend was seen when comparing the gas conversion effect while varying the fuel reactor temperature. The difference in conversions is higher for a higher temperature due to the effect of a higher mass circulation flow, that as mentioned has a higher effect on the conversion using iron ore than ilmenite, see Figure 19.

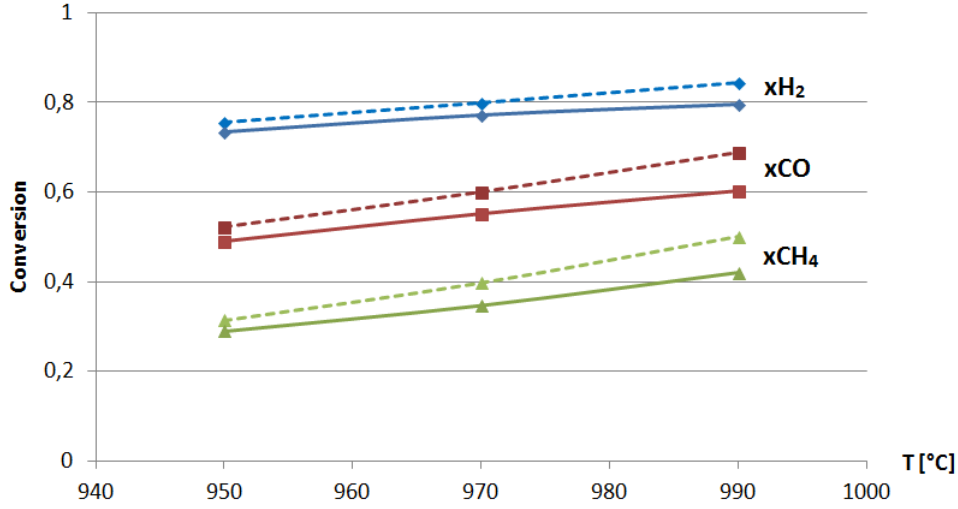


Figure 19: Comparison of the gaseous fuel conversions using ilmenite (solid curves) and iron ore (dashed curves), varying the fuel reactor temperature.

The simulations showed that while using iron ore higher gas conversions can be expected and at the same time a lower required mass circulation of oxygen carrier. This lower mass circulation is also an appreciated property of the iron ore since it is easier to achieve this entrainment in the fuel reactor. It can also be noted that allowing an increased fuel reactor temperature would have a larger effect when using iron ore.

6.4 Comparison of coal and coal with biomass as fuels

As can be seen in Table 9 and in section 5.5 the biggest differences between the coal and biomass are the gasification kinetics and the portion of volatile matters. While assuming a perfect gasification the differences are small since biomass only represents 10 % of the total heat release. Therefore it is more reasonable to consider a comparison while not assuming perfect gasification but modelling it. With a variation of the pressure drop the gas conversions for both cases seems to decrease with the pressure drop. However, the char conversions were increased with the pressure drop giving a total higher conversion with the increased pressure drop. The different gasification kinetics for the coal and biomass are visible in the difference of the char conversion where it is shown that adding biomass will result in an overall lower char conversion, see Figure 20.

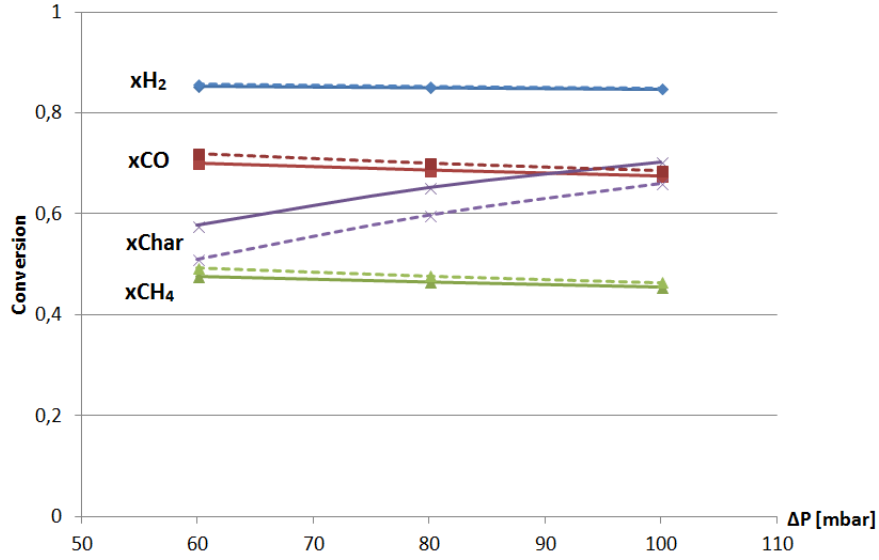


Figure 20: Comparison of the gaseous fuel conversions using coal (solid curves) and coal with biomass (dashed curves).

Due to the lower char conversion when adding the biomass more char particles will pass on to the air reactor and the required heat removal will be larger when adding biomass. Lower char conversion results in a smaller number of endothermic reactions and a smaller amount of circulating mass of oxygen carrier is required when adding biomass to the fuel, see Figure 21.

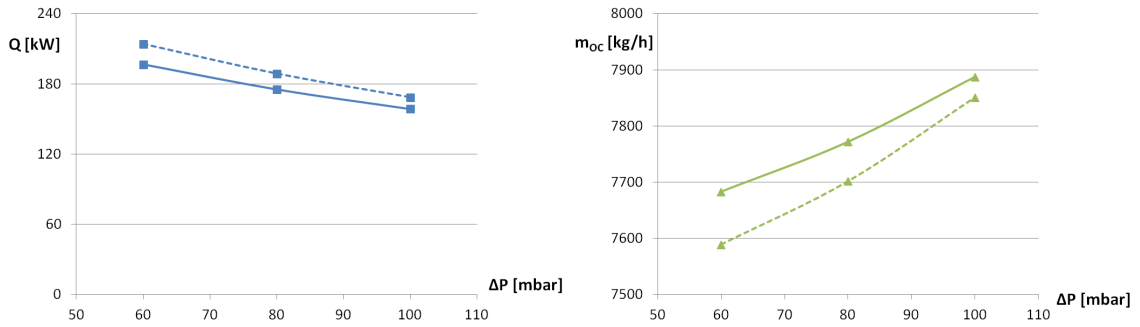


Figure 21: Comparison of the air reactor heat demands (left) and required mass circulation of oxygen carrier (right) using coal (solid curves) and coal with biomass (dashed curves) varying the pressure drop.

Variation of the fuel reactor temperature showed the same gas conversion trends of increasing gas conversions while increasing the fuel reactor temperature. The char conversion can be expected to be a bit lower when adding biomass to the fuel reactor, see Figure 22.

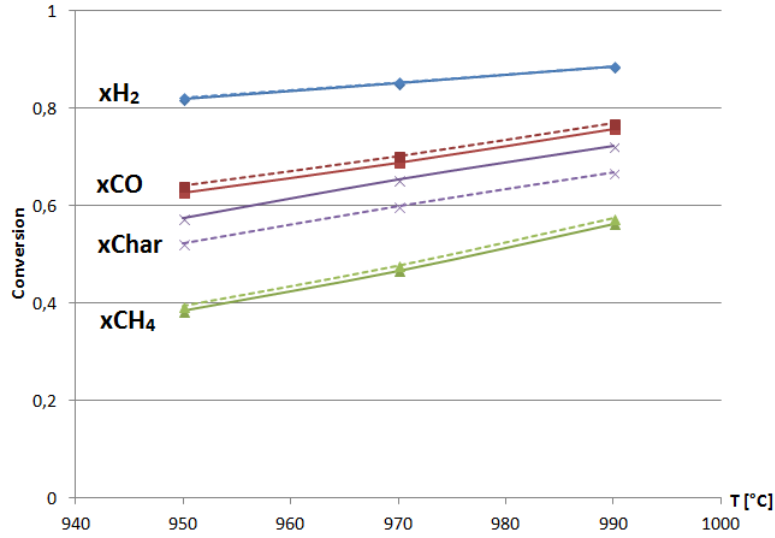


Figure 22: Comparison of the gaseous fuel conversions using coal(solid curves) and coal with biomass (dashed curves) varying the fuel reactor temperature.

Due to the material difference between the biomass and coal an overall lower gasification, that is char conversion, can be expected when biomass is introduced to the reactor. The gaseous fuel conversions are however almost the same for both cases.

6.5 Excess of air

As a recommendation from (Mattisson, 2013) the excess air ratio should be kept in an interval of 1.1-1.3 and a sensitive analysis was therefore performed where the air feed was varied. The gaseous conversions showed almost no change for the varied air feed while the heat demand for the air reactor was affected directly, see Figure 23.

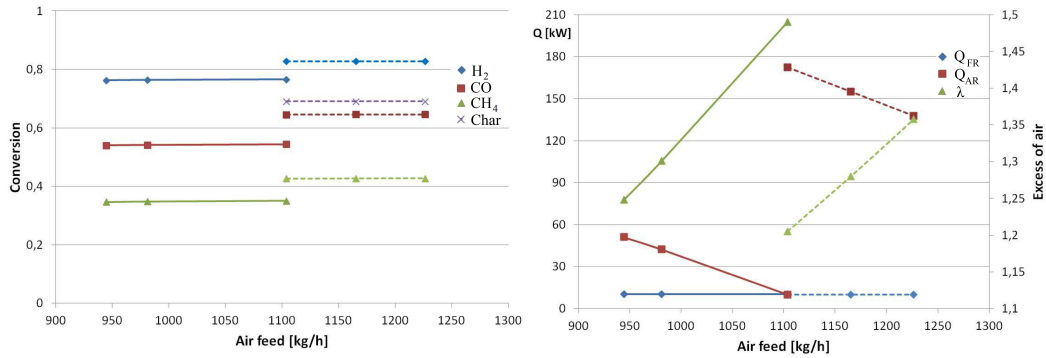


Figure 23: How the char and gas conversions are affected by a air feed variation (left) and how the air heat demand and excess air ratio varies with the air feed (right) using ilmenite. Graphs for assuming total char conversion (solid curves) and modelling of the char gasification (dashed curves).

The same trends were also found when using iron ore with coal and iron ore with coal and biomass. From these findings the air feed was set to match an excess air ratio within the given interval and the gas conversions, heat demands, required mass circulation of oxygen carrier, oxygen demands and carbon dioxide capture efficiencies were calculated. These were set as recommendations and the simulations were performed for both the scenario of a total gasification and a modelled gasification.

6.6 Planned test campaigns recommendations

From the sensitive analyses above a recommendation for each test campaign and gasification scenario could be considered. A pressure drop of about 80 mbar in both reactors can be expected in the plant. All scenarios were calculated for a fuel feed of 1 MW_{th} and the fuel reactor outlet concentrations and demands were calculated from this keeping the fuel reactor temperature at 970 °C with a heat loss of 10 kW and an air reactor temperature at 1050 °C. The air feed temperature was set to 125 °C but could be changed and would then directly affect the required heat removal from the air reactor. The steam flow to the fuel reactor was set to 400 kg/h to achieve a good mass entrainment of oxygen carrier and the air feed to the air reactor was set to achieve a excess air ratio of about 1.25, see Table 12.

Table 12: Recommendation for the three planned test campaigns with perfect char gasification (1) and modelled char gasification (2).

Parameter		Ilmenite & coal		Iron ore & coal		Iron ore & coal, biomass	
		1	2	1	2	1	2
Coal feed	[kg/h]	143.9	143.9	143.9	143.9	129.5	129.5
Biomass feed	[kg/h]	0	0	0	0	18.6	18.6
Air to air reactor	[kg/h]	945	1165	981	1227	989	1236
Steam to fuel reactor	[kg/h]	400	400	400	400	400	400
Circulating mass of oxygen carrier	[kg/h]	11423	9728	8989	7771	9045	7701
Reactor pressure drop	[mbar]	80	80	80	80	80	80
Air reactor inventory	[kg]	196	196	196	196	196	196
Fuel reactor inventory	[kg]	87	87	87	87	87	87
CO ₂	[Vol% _{dry}]	43.6	53.0	48.7	57.2	49.6	58.5
H ₂	[Vol% _{dry}]	21.5	16.6	18.3	14.8	18.5	14.4
CO	[Vol% _{dry}]	29.5	23.7	27.0	21.3	26.4	20.1
CH ₄	[Vol% _{dry}]	4.49	5.37	4.40	5.31	4.58	5.79
Q _{AR}	[kW]	51.1	155.0	92.0	175.2	90.7	188.7
Q _{FR}	[kW]	10.2	9.90	9.90	10.2	9.88	9.79
λ		1.25	1.28	1.22	1.29	1.22	1.29
Oxygen to POC	[kg/h]	129.7	85.4	115.8	74.7	117.5	72.6
Ω _{OD}		0.34	0.32	0.39	0.30	0.33	0.28
η _{OO}		1.0	0.75	1.0	0.73	1.0	0.70

6.7 Particle distribution

Calculations for how the pressure drop varies with the reactor height was also possible to perform. For a pressure drop of 80 mbar and a steam flow of 400 kg/h the pressure drop with the height was calculated from equations (32) and (40) for the fuel reactor and the result can be seen in Figure 24. The characteristic curve for the pressure drop with the height also shows the solid concentration with the reactor height. With the low pressure drop in the reactor the dense zone is small and almost non-existing as can be seen from Figure 24 since the pressure drop seems to change exponentially with the whole reactor height.

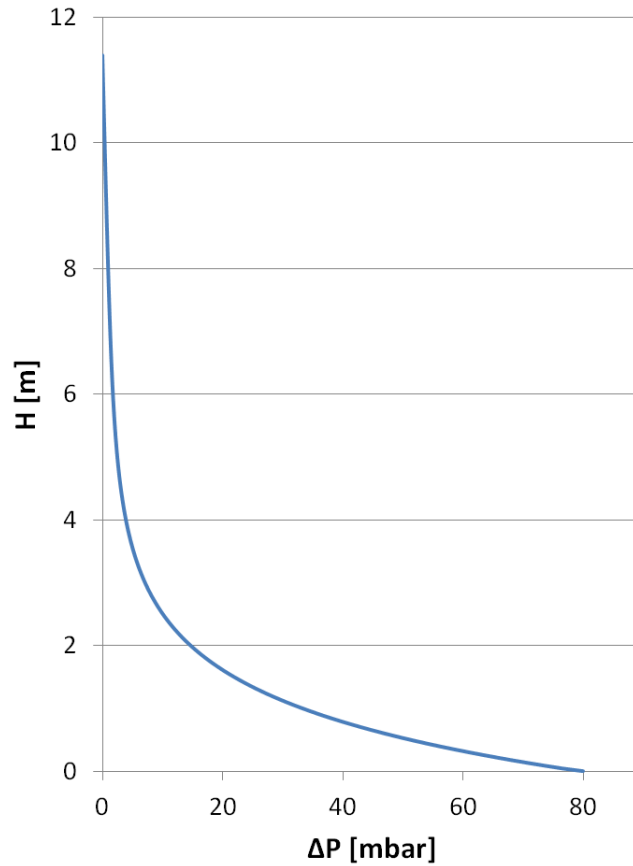


Figure 24: How the pressure changes with the reactor height.

An increased pressure drop, that is mass inventory in the reactor, would show on a more distinct dense zone and a linear pressure drop with the height indicating the dense zone. However, Figure 24 shows that the model can calculate for the particle distribution with the reactor height.

7 Conclusions

A model of the 1 MW_{th} chemical looping pilot plant has been elaborated that considers both the hydrodynamics and the chemical reactions in the two fluidized bed reactors. The model has been validated with experimental data with good results and simulations have been performed for three planned test campaigns. Also a model for the pyrolysis products composition has been elaborated and implemented. Simulations have been performed with ilmenite and iron ore as oxygen carriers and coal and biomass as fuels and the results were used to give recommendations and expected outcomes for running the plant.

It was shown during the sensitive analyses that a higher pressure drop in the reactors is beneficial for high conversions of gases as well as of solids. It was also shown that a higher fuel reactor temperature is beneficial for the gas conversions but a larger mass circulation is required to keep the fuel reactor temperature.

Higher fuel conversions can be expected while using iron ore compared to ilmenite and a required mass circulation of oxygen carrier is about 9.0 ton/h and 11.5 ton/h for iron ore and ilmenite respectively. It was also shown that a higher fuel reactor temperature would have a greater influence on the gas conversions for iron ore than for ilmenite. When adding biomass to the fuel feed the char gasification dropped with a few percentage points while the gaseous conversions were more or less unaffected.

A fuel feed of about 150 kg/h is the maximum feed value for the chemical looping pilot plant at Technische Universität Darmstadt. The total mass flows were calculated to 143.9 kg/h of pure coal and 148.1 kg/h for coal with biomass and a heating value of 1 MW_{th} is possible for the solid fuels in the planned test campaigns.

A high steam flow to the fuel reactor showed to be necessary to achieve the required mass entrainment from the fuel reactor and was therefore recommended to 400 kg/h. The gas flow to the air reactor was set to achieve a good excess air ratio and was recommended within an interval of about 950-1200 kg/h depending on degree of char gasification in the fuel reactor.

8 Further work

The elaborated model for the 1 MW_{th} chemical looping plant at Technische Universität Darmstadt is working for ilmenite and iron ore as oxygen carriers. It is possible to use coal or biomass or a mixture as fuel to the fuel reactor. Although some suggestions are mentioned in this section where the model can be improved and what further work that may be performed.

8.1 Validation work

The model used in this work has been validated to the experimental data gathered by Markström et al. (2013). However, these experimental findings were found for the 100 kW chemical looping plant at Chalmers technical university. It is therefore necessary to continue the validation work by comparison of future results from the 1 MW_{th} pilot plant after the planned test campaigns.

Some design parameters are unknown and should be investigated further, such as the decay constant or solid void fraction at the wall. These parameters are hard to measure and could likely be changed to better fit the simulation results to experimental data. Even better would be to study and determine these parameters in detail by experiments.

8.2 Model update

The kinetic parameters for the iron ore are yet not fully known and the ones used in this work are only approximated values based on a recommendation from Alberto Abad. It is therefore important to exchange these kinetics in the future when determined values are present.

The pyrolysis model used for the biomass pyrolysis is built on the same model for the coal pyrolysis. Even though different proximate and ultimate analysis are used it would be good to compare the simulated pyrolysis products with other models.

It is of course also important to always update the model when new data are available.

8.3 Large coal particles

The coal and biomass particles considered in this work for the 1 MW_{th} pilot plant have had a large diameter. This will cause the char particles to not be fluidized or entrained from the fluidization gas. One option was therefore to use a first reaction step where the steam gasification occurred to a total or fractional extent. Another option was to use the two reactors but setting a large ratio of char to oxygen carrier particles in the bottom bed zone. However, it is not known how the coal particles act in the fuel reactor. Due to the heat, gas flows and particle-particle contact, the char particles might brake to smaller pieces and an entrainment of char might occur anyway. Another effect of the large coal particles might be that the pyrolysis step

will not occur immediately as assumed in this work. It is therefore important to study what will happen with the coal and char particles in the fuel reactor and if necessary change the model.

References

- Abad, A., Adánez, J., Cuadrat, A., García-Labiano, F., Gayán, P. & de Diego, L. F. (2011, February). Kinetics of redox reactions of ilmenite for chemical-looping combustion. *Chemical Engineering Science*, 66(4), 689–702.
- Abad, A., Adánez, J., de Diego, L. F., Gayán, P., García-Labiano, F. & Lyngfelt, A. (2013, November). Fuel reactor model validation: Assessment of the key parameters affecting the chemical-looping combustion of coal. *International Journal of Greenhouse Gas Control*, 19, 541–551.
- Abad, A., García-Labiano, F., Diego, L. F. D., Gayán, P. & Adánez, J. (2007). Reduction Kinetics of Cu-, Ni-, and Fe-Based Oxygen Carriers Using Syngas ($\text{CO} + \text{H}_2$) for Chemical-Looping Combustion. *American Chemical Society*(6), 1843–1853.
- Abad, A., Gayán, P., de Diego, L. F., García-Labiano, F. & Adánez, J. (2013, January). Fuel reactor modelling in chemical-looping combustion of coal: 1. model formulation. *Chemical Engineering Science*, 87, 277–293.
- Abanades, J. C., Anthony, E. J., Lu, D. Y., Salvador, C. & Alvarez, D. (2004, July). Capture of CO_2 from combustion gases in a fluidized bed of CaO . *AIChE Journal*, 50(7), 1614–1622.
- Adánez, J., Miranda, J. L. & Gavilán, J. M. (1985). Kinetics of a lignite-char gasification by CO_2 . , 64, 801–804.
- Britannica, E. (2014). *Greenhouse effect*. Retrieved from <http://www.britannica.com.proxy.lib.chalmers.se/EBchecked/topic/245233/greenhouse-effect>
- Cho, P., Mattisson, T. & Lyngfelt, A. (2004, June). Comparison of iron-, nickel-, copper- and manganese-based oxygen carriers for chemical-looping combustion. *Fuel*, 83(9), 1215–1225.
- Cuadrat, A., Abad, A., García-Labiano, F., Gayán, P., de Diego, L. & Adánez, J. (2012, July). Relevance of the coal rank on the performance of the in situ gasification chemical-looping combustion. *Chemical Engineering Journal*, 195-196, 91–102.
- Cuadrat, A., Abad, A., Gayán, P., de Diego, L. F., García-Labiano, F. & Adánez, J. (2012, July). Theoretical approach on the CLC performance with solid fuels: Optimizing the solids inventory. *Fuel*, 97, 536–551.
- Global CCS Institute. (2014). *Sleipner CO_2 Injection*. Retrieved from sleipner%20co2-injection@www.globalccsinstitute.com

- IEA. (2012). *World Energy Outlook 2012* (First Edi ed.; R. Priddle, Ed.). Paris: OECD Publishing.
- Intergovernmental Panel on Climate Change. (2005). *CARBON DIOXIDE CAPTURE* (Tech. Rep.).
- Kaushal, P., Abedi, J. & Mahinpey, N. (2010, December). A comprehensive mathematical model for biomass gasification in a bubbling fluidized bed reactor. *Fuel*, 89(12), 3650–3661.
- Kunii, D. & Levenspiel, O. (1991). *Fluidization Engineering* (Second Edi ed.; H. Brenner, Ed.). Newton: Butterworth-Heinmann.
- Kuo, P.-C., Wu, W. & Chen, W.-H. (2014, January). Gasification performances of raw and torrefied biomass in a downdraft fixed bed gasifier using thermodynamic analysis. *Fuel*, 117, 1231–1241.
- Lasheras, A., Ströhle, J., Galloy, A. & Eppele, B. (2011, July). Carbonate looping process simulation using a 1D fluidized bed model for the carbonator. *International Journal of Greenhouse Gas Control*, 5(4), 686–693.
- Lee, J., Kim, Y., Lee, W. & Kim, S. (1998, June). Coal-gasification kinetics derived from pyrolysis in a fluidized-bed reactor. *Energy*, 23(6), 475–488.
- Leion, H., Lyngfelt, A., Johansson, M., Jerndal, E. & Mattisson, T. (2008, September). The use of ilmenite as an oxygen carrier in chemical-looping combustion. *Chemical Engineering Research and Design*, 86(9), 1017–1026.
- Leion, H., Mattisson, T. & Lyngfelt, A. (2009, January). Using chemical-looping with oxygen uncoupling (CLOU) for combustion of six different solid fuels. *Energy Procedia*, 1, 447–453.
- Linderholm, C., Lyngfelt, A., Cuadrat, A. & Jerndal, E. (2012, December). Chemical-looping combustion of solid fuels – Operation in a 10kW unit with two fuels, above-bed and in-bed fuel feed and two oxygen carriers, manganese ore and ilmenite. *Fuel*, 102, 808–822.
- Lyngfelt, A. (2014, January). Chemical-looping combustion of solid fuels – Status of development. *Applied Energy*, 113, 1869–1873.
- Markström, P., Linderholm, C. & Lyngfelt, A. (2013). Chemical-looping combustion of solid fuels – Design and operation of a 100 kW unit with bituminous coal. *International Journal of Greenhouse Gas Control*, 15, 150–162.
- Matthesius, G. A., Morris, R. M. & Desai, M. J. (1987). Prediction of the volatile matter in coal from ultimate and proximate analyses. , 87(6), 157–161.

- Mattisson, T. (2013). Materials for Chemical-Looping with Oxygen Uncoupling. *ISRN Chemical Engineering*, 2013(1), 1–19.
- Mayer, F., Bidwe, A. R., Schopf, A., Taheri, K., Zieba, M. & Scheffknecht, G. (2012). Comparison of a new micaceous iron oxide and ilmenite with respect to syngas conversion in a BFB reactor and adaptation of a 10 kWth DFB system for CLC to solid fuels. In (pp. 26–28).
- Mendiara, T., Abad, a., de Diego, L., García-Labiano, F., Gayán, P. & Adánez, J. (2013, November). Biomass combustion in a CLC system using an iron ore as an oxygen carrier. *International Journal of Greenhouse Gas Control*, 19, 322–330.
- Nicola, S. (2013). *Merkel Takes Germany From Nuclear Energy to Green*. Retrieved from <http://www.businessweek.com/articles/2013-11-14/2014-outlook-germanys-green-energy-switch>
- Nikoo, M. B. & Mahinpey, N. (2008, December). Simulation of biomass gasification in fluidized bed reactor using ASPEN PLUS. *Biomass and Bioenergy*, 32(12), 1245–1254.
- Orth, M. (2013, June). Report on optimized 1 MWth test rig testing. *ECLAIR report*, Technische Universität Darmstadt.
- Research Fund for Coal & Steel. (2013). *Report on performance of OC materials for coal CLC*.
- Song, T., Shen, T., Shen, L., Xiao, J., Gu, H. & Zhang, S. (2013, February). Evaluation of hematite oxygen carrier in chemical-looping combustion of coal. *Fuel*, 104, 244–252.
- Speight, J. G. (2005). *Handbook of coal analysis* (First Edi ed.; H. Brenner, Ed.). Hoboken: Wiley-Interscience.
- Ströhle, J., Orth, M. & Eppe, B. (2013, January). Design and operation of a 1MWth chemical looping plant. *Applied Energy*, 113, 1490–1495.
- Thon, A., Kramp, M., Hartge, E.-u., Heinrich, S. & Werther, J. (2012). Operational experience with a coupled fluidized bed system for chemical looping combustion of solid fuels. In (pp. 26–28).
- Tong, A., Bayham, S., Kathe, M. V., Zeng, L., Luo, S. & Fan, L.-S. (2014, January). Iron-based syngas chemical looping process and coal-direct chemical looping process development at Ohio State University. *Applied Energy*, 113, 1836–1845.
- Wedemeier, T. (2012). User’s Guide to the Carbonate Looping ASPEN PLUS Model.

- Welty, J. R., Wicks, C. E., Wilson, R. E. & Rorrer, G. L. (2008). *Fundamentals of Momentum, Heat, and Mass Transfer* (Fifth Edition; P. McFadden, Ed.). Hoboken: John Wiley & Sons, Inc.
- World Nuclear Association. (2011). *Comparison of Lifecycle Greenhouse Gas Emissions of Various Electricity Generation Sources* (Tech. Rep.).
- Xiao, R., Chen, L., Saha, C., Zhang, S. & Bhattacharya, S. (2012, September). Pressurized chemical-looping combustion of coal using an iron ore as oxygen carrier in a pilot-scale unit. *International Journal of Greenhouse Gas Control*, 10, 363–373.
- Zafar, Q., Abad, A., Mattisson, T., Gevert, B. & Strand, M. (2007, December). Reduction and oxidation kinetics of $\text{Mn}_3\text{O}_4/\text{Mg-ZrO}_2$ oxygen carrier particles for chemical-looping combustion. *Chemical Engineering Science*, 62(23), 6556–6567.

A Extra results

Simulation results using ilmenite as oxygen carrier with coal and modelling of the char gasification can be seen in Figures 25 and 26.

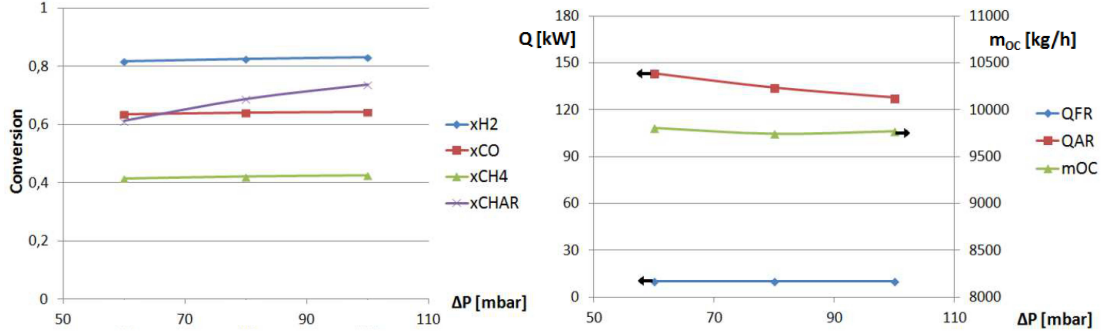


Figure 25: The gas and char conversions (left) and the reactor heat demands and required mass circulation of oxygen carrier (right), varying the pressure drop for ilmenite.

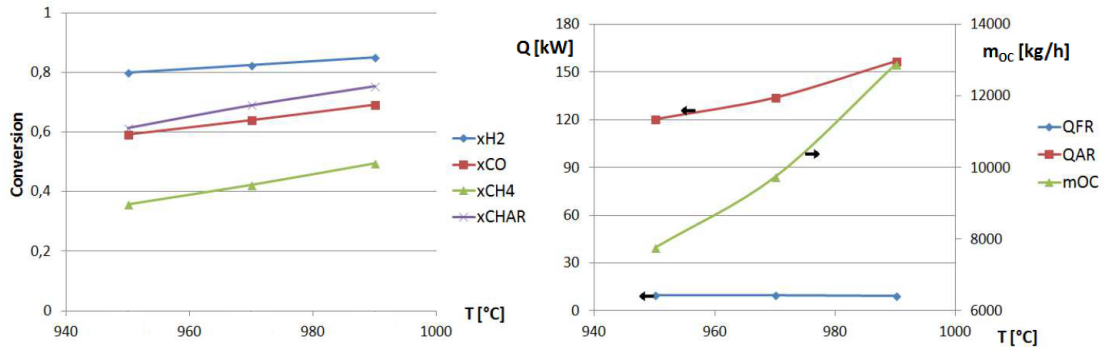


Figure 26: The gas and char conversions (left) and the reactor heat demands and required mass circulation of oxygen carrier (right), varying the fuel reactor temperature for ilmenite.

Simulation results using iron ore as oxygen carrier with coal and assuming total char gasification can be seen in Figures 27 and 28.

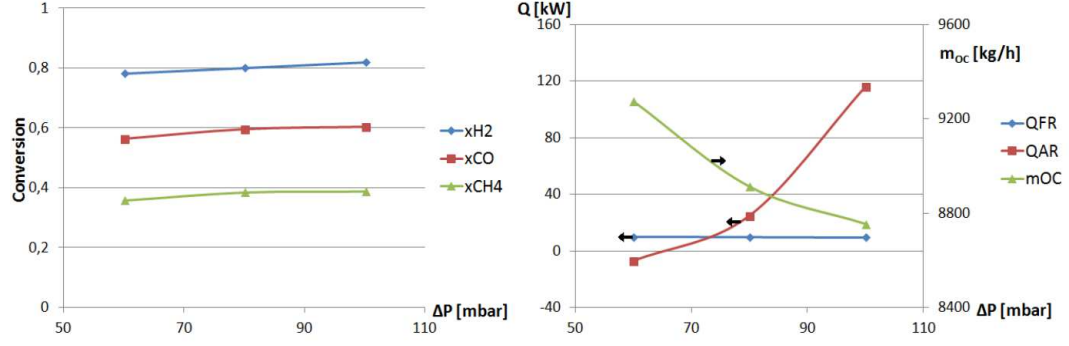


Figure 27: The gas conversions (left) and the reactor heat demands and required mass circulation of oxygen carrier (right), varying the pressure drop for iron ore.

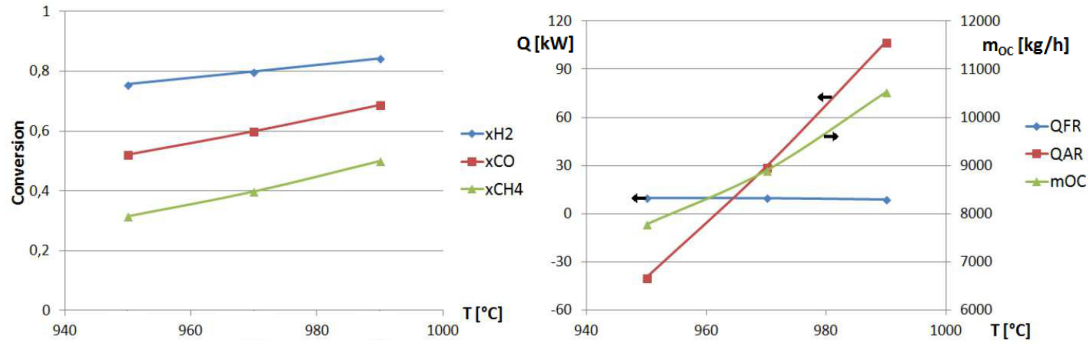


Figure 28: The gas conversions (left) and the reactor heat demands and required mass circulation of oxygen carrier (right), varying the fuel reactor temperature for iron ore.

Simulation results using iron ore as oxygen carrier with coal and biomass and assuming total char gasification can be seen in Figures 29 and 30.

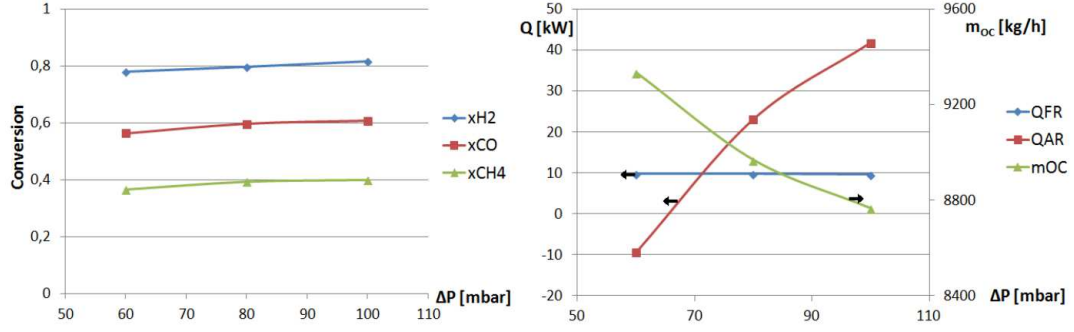


Figure 29: The gas conversions (left) and the reactor heat demands and required mass circulation of oxygen carrier (right), varying the pressure drop for iron ore and biomass.

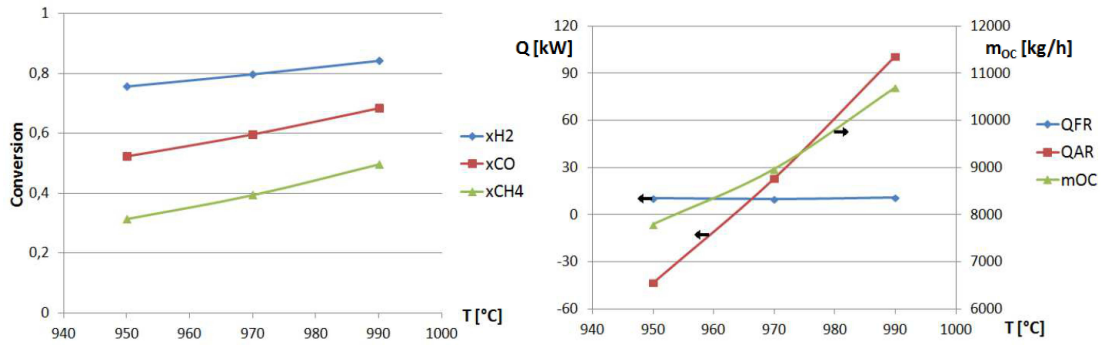


Figure 30: The gas conversions (left) and the reactor heat demands and required mass circulation of oxygen carrier (right), varying the fuel reactor temperature for iron ore and biomass.

Simulation results using iron ore as oxygen carrier with coal and biomass and modelling of the char gasification can be seen in Figures 31 and 32.

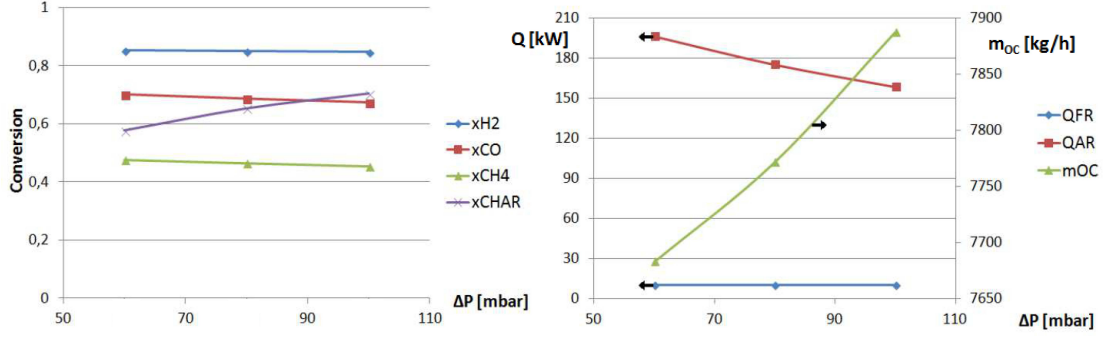


Figure 31: The gas and char conversions (left) and the reactor heat demands and required mass circulation of oxygen carrier (right), varying the pressure drop for iron ore.

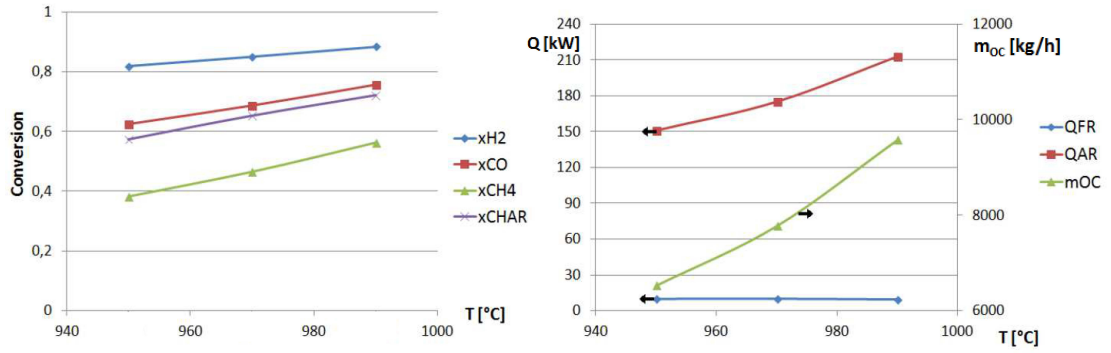


Figure 32: The gas and char conversions (left) and the reactor heat demands and required mass circulation of oxygen carrier (right), varying the fuel reactor temperature for iron ore.

Simulation results using iron ore as oxygen carrier with coal and biomass and modelling of the char gasification can be seen in Figures 33 and 34.

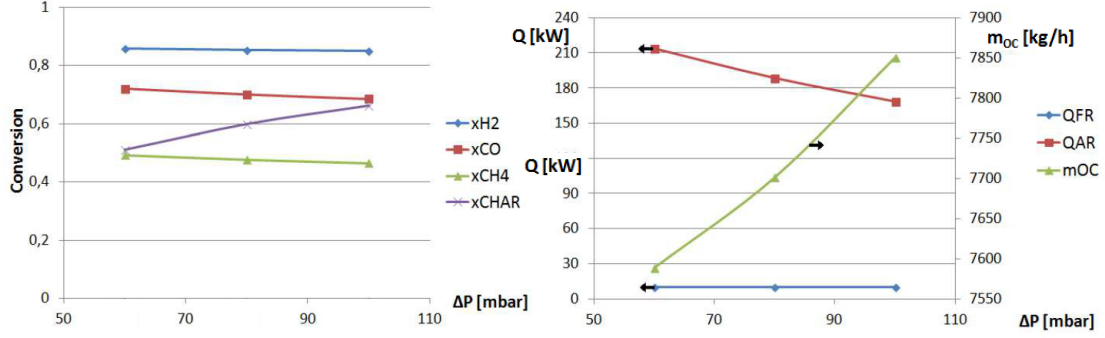


Figure 33: The gas and char conversions (left) and the reactor heat demands and required mass circulation of oxygen carrier (right), varying the pressure drop for iron ore with biomass.

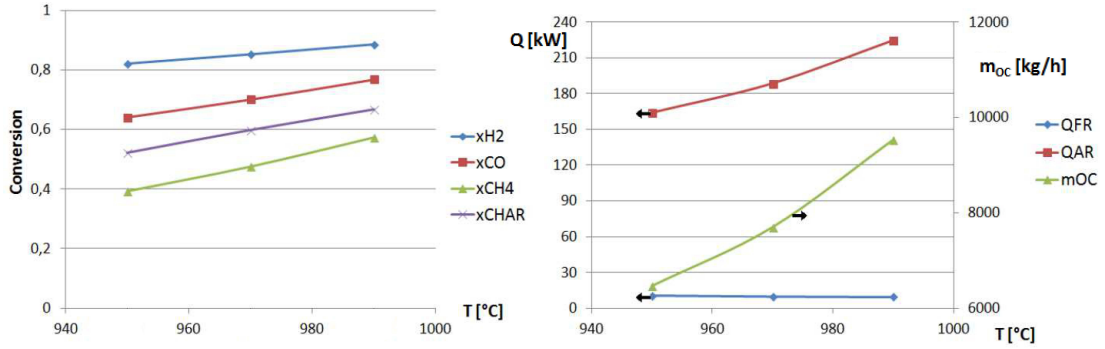


Figure 34: The gas and char conversions (left) and the reactor heat demands and required mass circulation of oxygen carrier (right), varying the fuel reactor temperature for iron ore with biomass.

Simulation results using ilmenite ore as oxygen carrier with coal and assuming a total char gasification. To better show the pressure and temperature dependence of the gaseous and oxygen carrier conversions the fuel reactor temperature is allowed to vary. The fuel feed, circulating mass flow of oxygen carrier, pressure drops, fuel reactor temperature and steam feed are varied. The left column of graphs shows the gas conversions of hydrogen, carbon monoxide and methane. The middle column of graphs shows the oxygen carrier conversion in both reactors. The right column of graphs shows the reactor heat demands. See Figures 35 - 40.

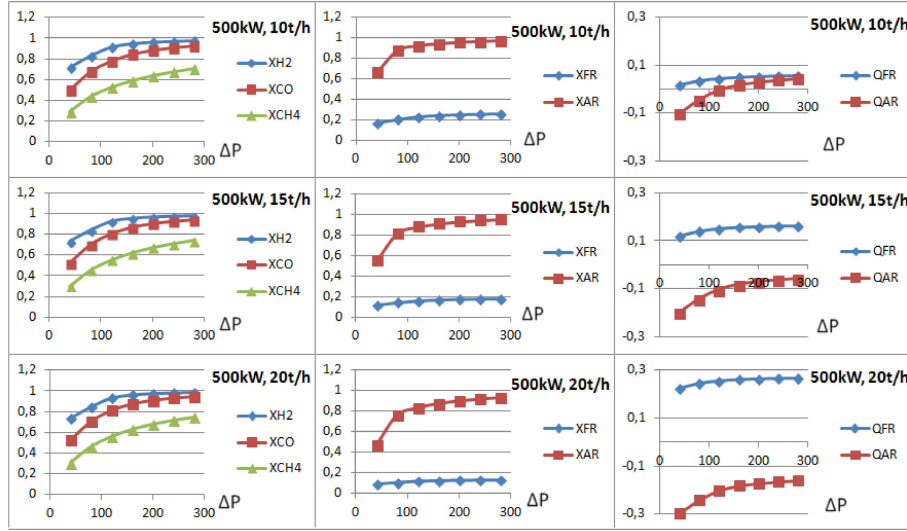


Figure 35: A 500kW feed of coal and a circulating mass flow of 10, 15 and 20 ton/h of ilmenite while varying the pressure drops in the two reactors.

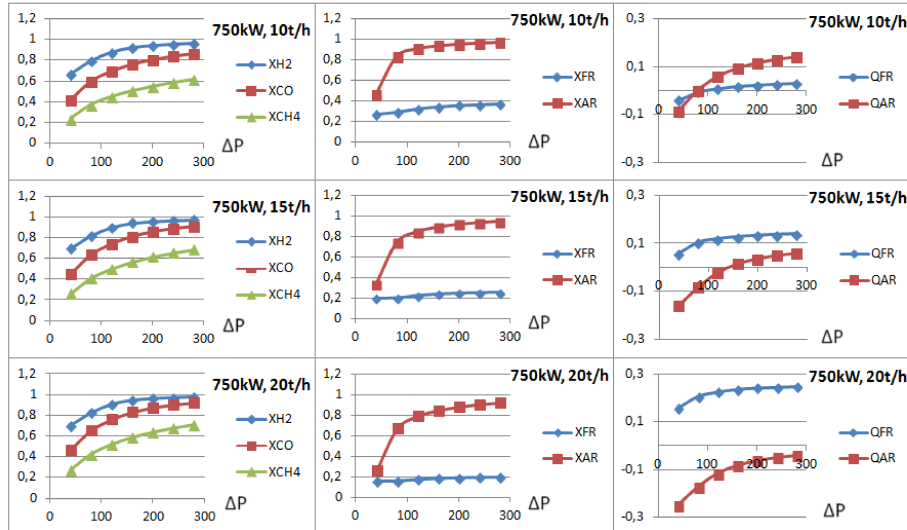


Figure 36: A 750kW feed of coal and a circulating mass flow of 10, 15 and 20 ton/h of ilmenite while varying the pressure drops in the two reactors.

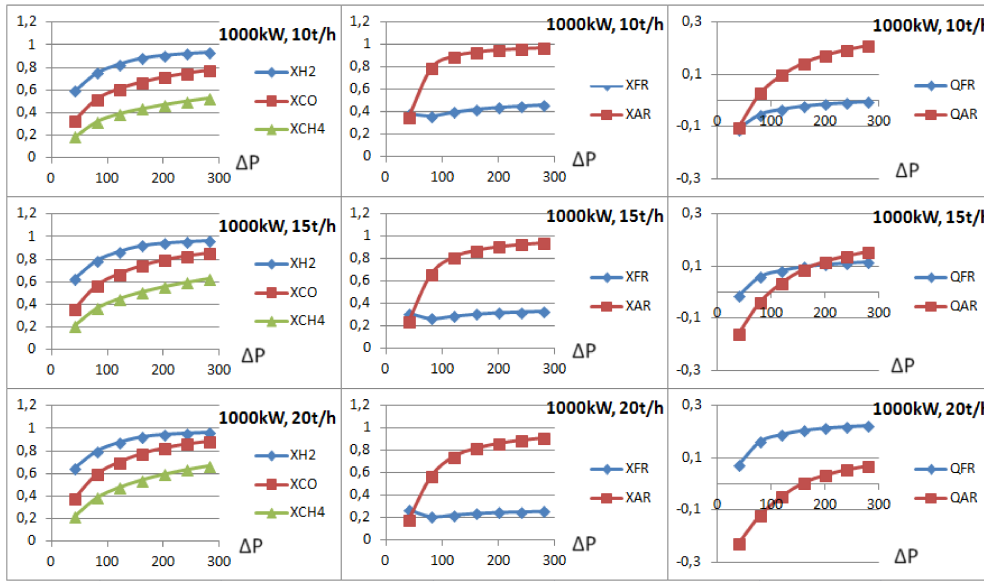


Figure 37: A 1000 kW feed of coal and a circulating mass flow of 10, 15 and 20 ton/h of ilmenite while varying the pressure drops in the two reactors.

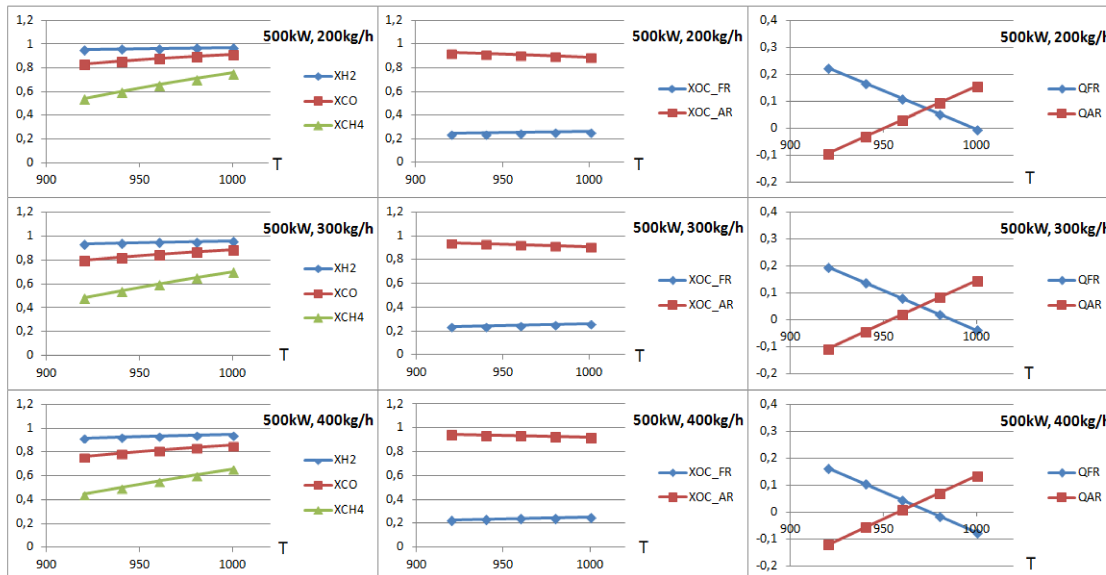


Figure 38: A 500 kW feed of coal, a circulating mass flow of 10 ton/h of ilmenite and a pressure drop of 140 mbar. The temperature in the fuel reactor is varied for a steam feed off 200, 300 and 400 kg/h.

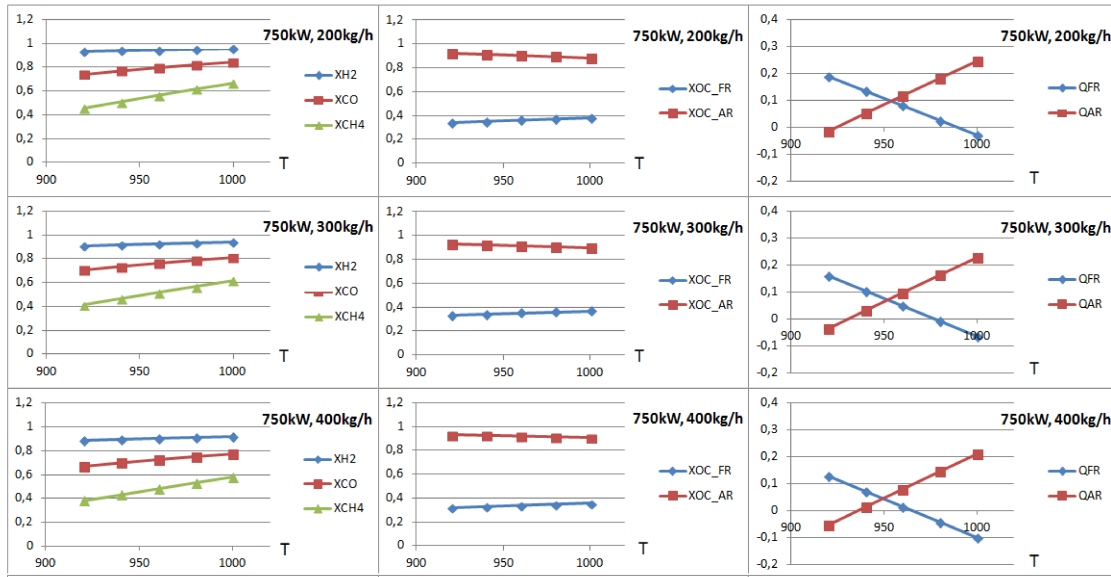


Figure 39: A 750 kW feed of coal, a circulating mass flow of 10 ton/h of ilmenite and a pressure drop of 140 mbar. The temperature in the fuel reactor is varied for a steam feed off 200, 300 and 400 kg/h.

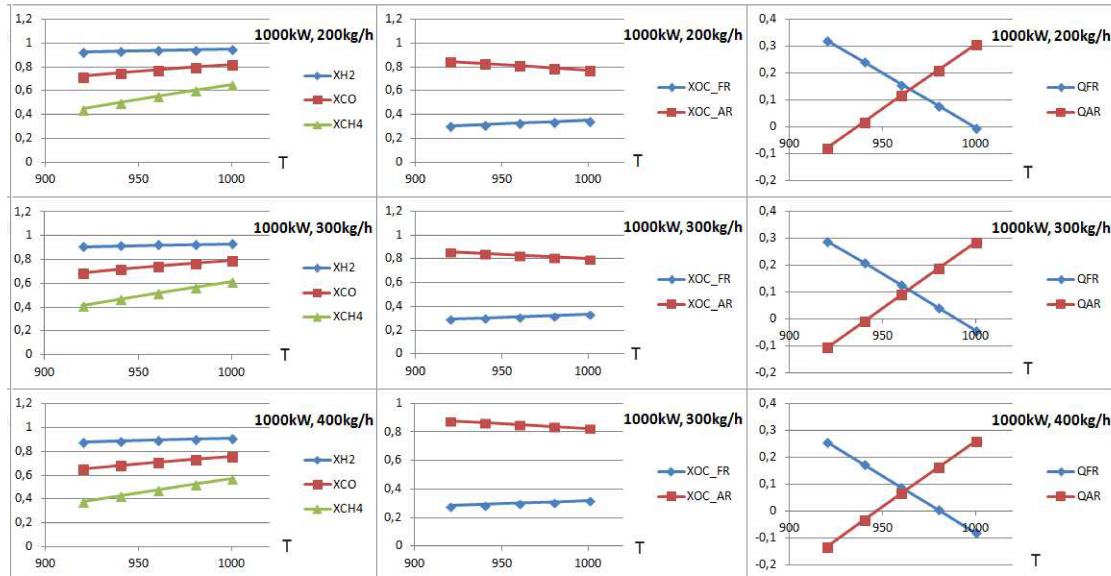


Figure 40: A 1000 kW feed of coal, a circulating mass flow of 15 ton/h of ilmenite and a pressure drop of 140 mbar. The temperature in the fuel reactor is varied for a steam feed off 200, 300 and 400 kg/h.

Simulation results using iron ore as oxygen carrier with coal and assuming a total char gasification. To better show the pressure dependence of the gaseous and oxygen carrier conversions the fuel reactor temperature is allowed to vary. The fuel feed, circulating mass flow of oxygen carrier and pressure drops. The left column of graphs shows the gas conversions of hydrogen, carbon monoxide and methane. The middle column of graphs shows the oxygen carrier conversion in both reactors. The right column of graphs shows the reactor heat demands. See Figure 41.

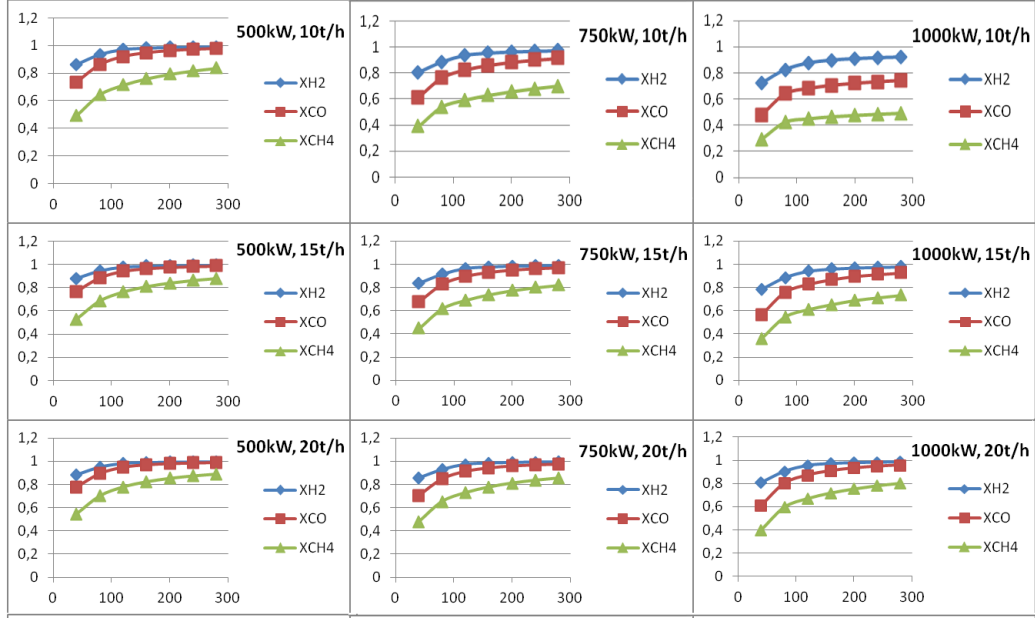


Figure 41: Coal feeds of 500, 750 and 1000 kW and a circulating mass flow of 10, 15 and 20 ton/h of iron ore while varying the pressure drops in the two reactors.

Simulation results using ilmenite as oxygen carrier with coal and modelling for the char gasification. To better show the pressure dependence of the gaseous and oxygen carrier conversions the fuel reactor temperature is allowed to vary. The fuel feed, circulating mass flow of oxygen carrier and pressure drops. The left column of graphs shows the gas conversions of hydrogen, carbon monoxide and methane. The middle column of graphs shows the oxygen carrier conversion in both reactors. The right column of graphs shows the reactor heat demands. See Figure 42.

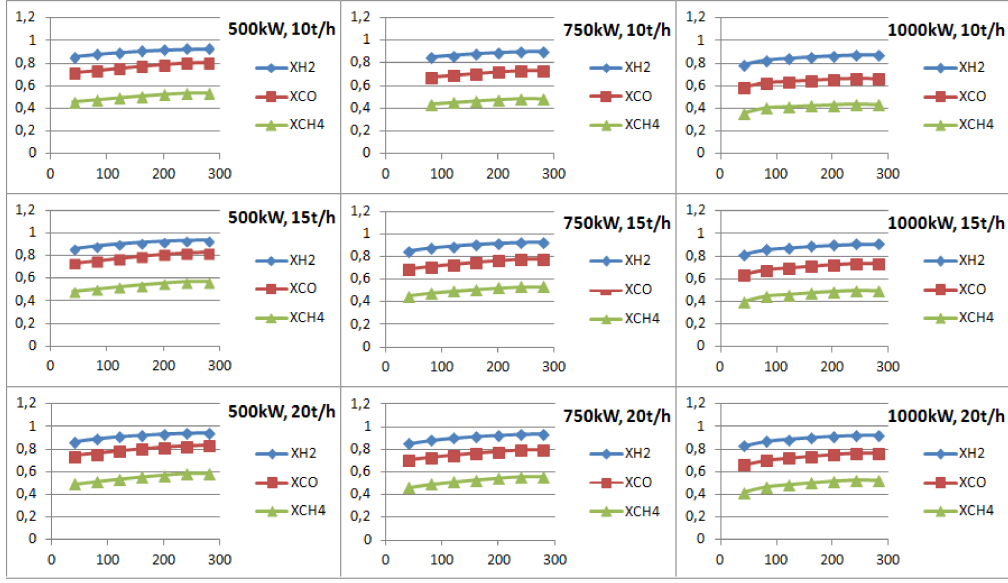


Figure 42: Coal feeds of 500, 750 and 1000 kW and a circulating mass flow of 10, 15 and 20 ton/h of ilmenite while varying the pressure drops in the two reactors.

Sensitive analyses were performed on different model parameters at the 100 kW unit at Chalmers Technical University. For the following sensitive analyses operational point VII-8 in Table 10 was chosen arbitrarily. The left graph shows the gas and char conversion, the middle graph the fuel reactor outlet dry gas concentrations and the right graph the oxygen demand and carbon dioxide capture efficiency, see Figures 43 - 47.

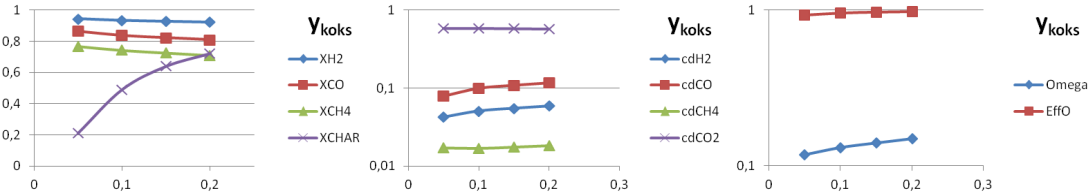


Figure 43: Variation of the ratio of solid particles of char and oxygen carrier, y_{koks} , in the fuel reactor.

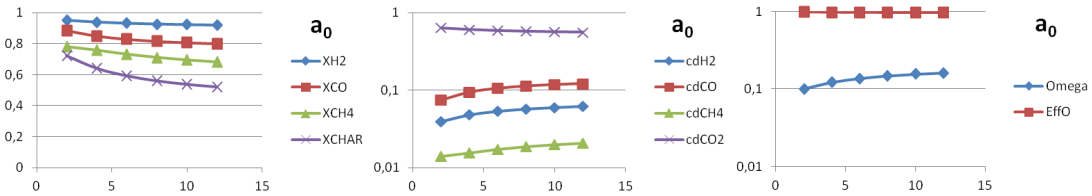


Figure 44: Variation of the decay constant, a_0 , in the fuel reactor.

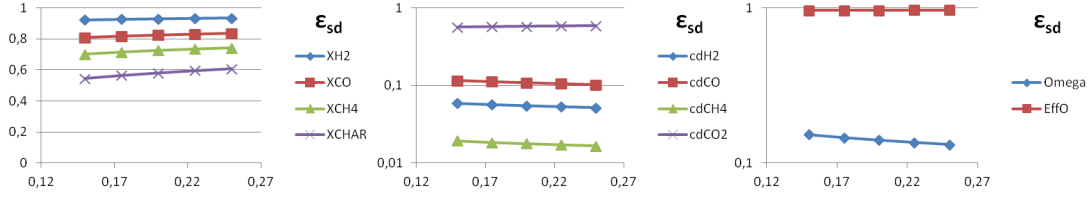


Figure 45: Variation of the solids concentration in the bottom bed zone, ϵ_{sd} , in the fuel reactor.

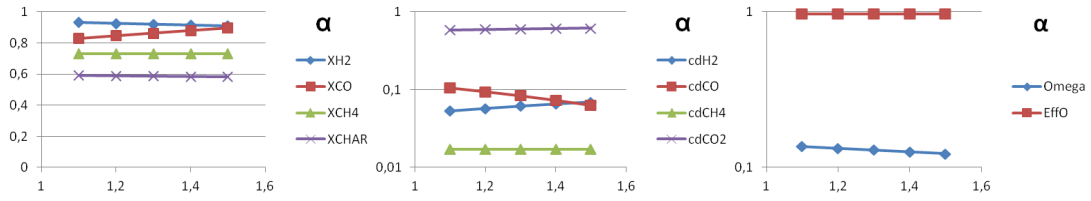


Figure 46: Variation of the stoichiometric coefficient, α , in the gasification reaction, see reaction 22.

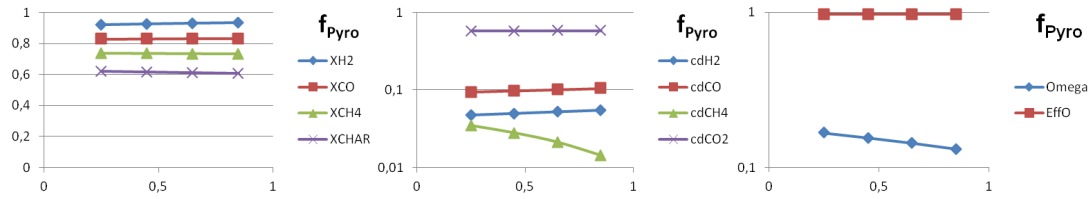


Figure 47: Variation of the tar pyrolysis fraction for the produced amount of CO and CH₄, see section B.3.

B Fortran code

Both the fluidized bed reactors were modelled and implemented to Aspen Plus using Fortran code and Excel. All rows and executed equations are listed below. Rows beginning with a capital C are comments and are not executed. The code for the air and fuel reactor is written as Fortran code while the pyrolysis model is calculated using Excel, however in this appendix it is written in Matlab format.

The first option of oxygen carrier properties is for iron ore and the second option for ilmenite.

B.1 Air reactor

C Counter for the number of iterations for changing the size of z_alpha
Counter=0

C Inlet flow of oxygen carrier [kmol/h]
zILMIN=ILMIN1+ILMIN2+ILMIN3+ILMIN4
zRUTIN=RUTIN1+RUTIN2+RUTIN3+RUTIN4
zHEMIN=HEMIN1+HEMIN2+HEMIN3+HEMIN4
zMAGIN=MAGIN1+MAGIN2+MAGIN3+MAGIN4

C Solid molar flow inlet [mol/s]
z_nILMin=zILMIN/3.6
z_nRUTin=zRUTIN/3.6
z_nHEMin=zHEMIN/3.6
z_nMAGin=zMAGIN/3.6
z_nTOTin=z_nILMin+z_nRUTin+z_nHEMin+z_nMAGin

C Oxygen molar flow inlet [mol/s]
z_nO2in=OXYIN/3.6

C Average reactor pressure [Pa]
P=1.1e5

C Average gas temperature [K]
TEMP=T+273

C Universal gas constant [J/mol*K]
R=8.3145

C Molar inlet oxygen fraction in air [mol O2 / mol air]
yO2=MOLFRAC

C Molar inlet oxygen concentration [mol O2 / m3 air]
 $CO2in=yO2*P/(R*TEMP)$

C PARTICLE DISTRIBUTION

C Reactor diameter [m]
dt=0.59
pi=3.141593

C Reactor area [m²]
 $At=pi*(dt*dt)/4$

C Pressure drop [Pa]
deltap=8000

C Reactor height [m]
Ht=7.80

C Specific air gas constant [J/kg K]
Rair=287

C Air density [kg/m3]
 $\rho_{og}=P/(Rair*TEMP)$

C True density of activated oxygen carrier[kg/m3]
rhoIlm=4462
C rhoIlm=4250

C Oxygen carrier particle porosity
por=0.333
C por=0.127

C Apparent density of porous oxygen carrier particle [kg/m3]
 $\rho_{os}=\rho_{oIlm}*(1-por)$

C Initial oxygen transport capacity (%)
Roc0=0.025
C Roc0=0.033

C Oxygen transport capacity (%)
Roc=0.025
C Roc=0.040

C Particle size diameter [m]

dp=127e-6

C Superficial speed [m/s]
u0=z_nO2in/(At*CO2in)

C Decay constant for vertical solid distribution
au0=6
a=au0/u0
aprima=6.62

C Mean solid volume fraction in the lower dense zone
esd=0.12

C Mean void fraction in the vicinity of wall
ew=0.4

C Reference air viscosity @291.15K [Pas]
z_mu0=0.00001827

C Reference Temperature [K]
T0=291.15

C Sutherland air constant [K]
C=120

C Viscosity at temperature T (Sutherland formula) [Pas]
z_mu=z_mu0*(T0+C)/(TEMP+C)*(TEMP/T0)**(1.5)

C Universal gravity constant[m/s²]
g=9.81

C Dimensionsless particle diameter
dpstar=dp*((rhog*(rhos-rhog)*g)/z_mu**2)**(0.33333)

C Dimensionsless terminal velocity
utstar=(18/dpstar**2+0.5191/dpstar**0.5)**-1

C Terminal velocity
ut=utstar*(z_mu*(rhos-rhog)*g/rhog**2)**(0.33333)

C Slip velocity
ur=1.6*ut

C Saturated solids flux

$$G_{ssat} = 23.7 \cdot \rho_{hog} \cdot u_0 \cdot \exp(-5.4 \cdot u_t / u_0)$$

C Saturated carrying capacity of a gas

$$e_{sat} = G_{ssat} / ((u_0 - u_t) \cdot \rho_{hos})$$

C SOLID DISTRIBUTION

C Solid inventory in reactor [kg]

$$z_{ms} = 0.85 \cdot \Delta t_p \cdot A_t / 9.81$$

C Lean zone height (initial value for iteration) [m]

$$H_l = 4$$

$$err_0 = 1$$

$$CONST = ((z_{ms} \cdot a) / (\rho_{hos} \cdot A_t) - esd + esat - H_t \cdot esd \cdot a) / (esd - esat)$$

C Newton-Raphson method iteration

do while (abs(err0) .GT. 1e-4)

$$X_0 = H_l \cdot a$$

$$F = -CONST \cdot \exp(-X_0) - X_0$$

$$DF = \exp(-X_0) - 1$$

$$X_1 = X_0 - F / DF$$

$$err_0 = X_1 - X_0$$

$$H_l = X_1 / a$$

end do

C Dense zone height [m]

if (H_l .GT. H_t) then

$$H_l = H_t$$

end if

$$H_d = H_t - H_l$$

C Solid fraction at reactor exit

$$e_{se} = esat + (esd - esat) \cdot \exp(-a \cdot H_l)$$

C Average solid volume fraction in lean zone

$$e_s = esat + (esd - e_{se}) / (a \cdot H_l)$$

C Core area in dense zone

$$\Delta t_{ad} = (e_w - esd) / (e_w - esat)$$

C Average core area in lean zone

$$\Delta t_{al} = (e_w - e_s) / (e_w - esat)$$

C Solid mass flow density at reactor exit [kg/m2s]
Gs=rhos*(u0-ur)*ese

C Solid inventory at dense zone [kg]
z_msd=Hd*At*esd*rhos

C Solid inventory at lean zone [kg]
z_msl=Hl*At*es*rhos
IF (Hl .EQ. Ht) THEN
z_msl=z_ms
es=z_msl/(Hl*At*rhos)
deltad=(ew-esd)/(ew-esat)
deltal=(ew-es)/(ew-esat)
END IF

C OXIDATION REACTION
C OXYGEN CARRIER OXIDATION CONSTANTS
C Stoichiometric ratio of the oxidation
b=4

C Me Molar Density [mol/m3]
rhom=27911/3
C rhom=13890

C Gas exchange coefficient between core and wall zone [1/s]
zKcw=0.3

C Grain radius for Changing Grain Size Model [m]
rg=9.16E-7
C rg=1.25E-6

C Preexponential factor for chemical reaction constant [1/s]
zks0=1.9e-3

C Activation energy [J/mol]
E=25500

C Chemical reaction constant (Arrhenius) [1/s]
zks=zks0*exp(-E/(R*TEMP))

C Iron ore molecular weight (g/mol)
PIIm=164
C PIIm=152

C Oxygen molecular weight (g/mol)
PMo2=32

C Solid inventory in reactor (mol)
 $z_nTOT = z_ms * 1000 / PIlm$

C Reactor volume (m3)
 $Vr = At * Ht$

C GAS-SOLID REACTION
C Initial conversion for iteration
 $Xs0 = 0.9$
 $Xs = Xs0$
 $err1 = 1$
 $z_iter = 0$
do while (abs(err1) .GT. 1e-4)
 $z_iter = z_iter + 1$

C Oxidation kinetic constant (1/s)
 $zKr = (3 * zks * Roc0 * (1 - Xs) ** 0.66666) / (rg * Roc)$

C DENSE PHASE
C Fraction of solids in the core of the reactor
 $gammac = 0.01$

C Fraction of solids in the wall region of the reactor
 $gammaw = 0.15$

C Overall gas interchange coeff. between bubble and
emulsion phase (1/s)
 $zKbe = 11$

C Overall rate for fast fluidization (1/s)
 $zKff = gammac * zKr + 1 / ((1 / zKbe) + (1 / (gammaw * zKr)))$

C Grace constants
 $C1 = 27.2$
 $C2 = 0.0408$

C Arquimedes number
 $Ar = (dp ** 3 * rhog * (rhos - rhog) * g) / (z_mu ** 2)$

C Minimum fluidization velocity (m/s)

$$umf=(z_{\mu}*((C1^{**2}+C2*Ar)^{**0.5}-C1))/(rho_g*dp)$$

C Bubble diameter (m)

$$db=(0.853*(1+0.272*(u0-umf))^{**}(0.3333)*(1+0.0684*Hd)^{**1.21})/100$$

C Rise velocity of a bubble with respect to the emulsion phase (m/s)

$$ubr=0.711*(g*db)^{**0.5}$$

C Velocity of a bubble rising through a bed (m/s)

$$ub=u0-umf+ubr$$

C Bubble fraction in fluidized bed

$$\delta a=u0/ub$$

C Gas conversion in the dense zone

$$y1=\exp(zK_{ff}*\delta t_{ad}*Hd/u0)$$

C Dense zone exit concentration (mol/m3)

$$CO2d=CO2in/y1$$

C Dense zone conversion

$$XO2d=1-CO2d/CO2in$$

C LEAN PHASE

C Sphericity

$$sph=0.9$$

C Minimum fluidization void fraction

$$emf=0.586*sph^{**}(-0.72)*Ar^{**}(-0.029)*(rho_g/rho_s)^{**0.021}$$

C Bed void fraction

$$oneminef=(1-\delta t_{al})*(1-emf)$$

C Bed yield

$$effbed=(\gamma_{mac}+1/((zK_r/zK_{be})+(1/\gamma_{maw})))*\delta t_{ad}/oneminef$$

C Gas conversion in the lean zone

$$y2=\exp((oneminef*zK_r/(u0*a))*((1-\exp(-a*Hl))-(1-effbed) \\ \& *(1-\exp(-(a+a_{prima})*Hl))/(1+a_{prima}/a)))$$

C Reactor exit concentration (mol/m3)

$$CO2ex=CO2d/y2$$

```
C GENERAL BALANCE
C Oxygen conversion
XO2ex=1-CO2ex/CO2in

C Inlet conversion
Xsin=(z_nHEMin)/z_nTOTin

C New conversion
Xsnew=(b*z_nO2in*XO2ex/(z_nTOTin))+Xsin

IF (Xsnew .GT. 0.99) THEN
  Xsnew=0.99
END IF

err1=Xs-Xsnew
Xsold=Xs
z_alpha=0.1

IF (Counter .GT. 100) THEN
  z_alpha=0.01
END IF

IF (Counter .GT. 1000) THEN
  z_alpha=0.001
END IF

Xs=z_alpha*Xsnew+(1-z_alpha)*Xsold
Counter=Counter+1
CONV=XO2ex
Oreac=b*OXYIN*CONV
MAGOUT=zMAGIN-Oreac
C ILMOUT=zILMIN-Oreac end do

C Reaction conversions
IF (MAGOUT .GT. 0) THEN
  CONV1=XO2ex
END IF
C IF (ILMOUT .GT. 0) THEN
C CONV1=XO2ex
C END IF

IF (MAGOUT .EQ. 0) THEN
```

```
CONV1=zMAGIN/(b*OXYIN)-0.01
MAGOUT=0
END IF
C IF (ILMOUT .EQ. 0) THEN
C CONV1=zILMIN/(b*OXYIN)-0.01
C ILMOUT=0
C END IF
```

```
IF (MAGOUT .LT. 0) THEN
CONV1=zMAGIN/(b*OXYIN)-0.01
MAGOUT=0
END IF
C IF (ILMOUT .LT. 0) THEN
C CONV1=zILMIN/(b*OXYIN)-0.01
C ILMOUT=0
C END IF
```

```
XOCAR=1-MAGOUT/(MAGIN1+MAGIN2+MAGIN3+MAGIN4)
C XOCAR=1-ILMOUT/(ILMIN1+ILMIN2+ILMIN3+ILMIN4)
```

```
C Excess of air
AIREX=0.21*(1-O2EX/N2EX)/(0.21-O2EX/N2EX)
```

B.2 Fuel reactor

C NATURAL CONSTANTS

counter=1

C Acceleration due to gravity [m/s²]

g=9.81

C General gas constant [J/kmolK]

R=8314

C Mass of oxygen carrier

zm_OCi= FE3O4IN+FE3O4IN2+FE2O3IN+FE2O3IN2

C zm_OCi= FETIO3IN+FETIO3I2+FE2O3IN+FE2O3IN2+TIO2IN+TIO2IN2

C 2. REACTOR CHARACTERISTICS

C Temperature [K]

T=970+273

C Pressure drop[Pa]

delta_p = 8000

C Reactor diameter [m]

d_r= 0.4

C Cross sectional area [m²]

A= 3.14159*(d_r**2) / 4

C Reactor volume [m³]

Hr=11.4

V=A*Hr

C Solids inventory [kg]

zm_inv=delta_p * A / g*0.85

y_koksd = 0.95

y_koksl = 0.03

zm_invOC=zm_inv

char=0.85

C Pressure [Pa]

p = PBAR* 1e5

C Gas inventory [mol]

zn_ges = p * V /(R*T)

C KINETIC PROPERTIES OF OXYGEN CARRIER

C Molar densities [mol/m³]

rhoCH4 = 9635

rhoCO = 9635

rhoH2 = 9635

C rhoCH4 = 13890

C rhoCO = 13890

C rhoH2 = 13890

C Grain radius [m]

rgCH4 = 9.16E-7

rgCO = 9.16E-7

rgH2 = 9.16E-7

C rgCH4 = 1.25E-6

C rgCO = 1.25E-6

C rgH2 = 1.25E-6

C Stoichiometric reduction coefficient

bCH4 = 5.78

bCO = 1.45

bH2 = 1.45

C Reaction order

znCH4 = 1

znCOexp = 0.8

znH2 = 1

C Constant rate of relations [mol⁽¹⁻ⁿ⁾ * m⁽³ⁿ⁻²⁾ * s⁽⁻¹⁾]

zkCH40 = 9.8*2

zkCO0 = 1.0E-1*2

zkH20 = 6.2E-2*2

C zkCH40 = 9.8

C zkCO0 = 1.0E-1

C zkH20 = 6.2E-2

ECH4 = 135.9

ECO = 80.7

EH2 = 65.0

zkCH4 = zkCH40*exp((-ECH4*1E+6)/(R*T))

zkCO = zkCO0*exp((-ECO*1E+6)/(R*T))

zkH2 = zkH20*exp((-EH2*1E+6)/(R*T))

C Oxygen transport capacity

R_O=0.025
C R_O=0.033

C Kinetic parameters for coal gasification

C H2O
zk10=52.6
zk20=2.81E-6
zk30=8.1E-9
Ek1=95.1
Ek2=-135.1
Ek3=-218.5
zk1=zk10*exp((-Ek1*1E+6)/(R*T))/1.01325
zk2=zk20*exp((-Ek2*1E+6)/(R*T))/1.01325
zk3=zk30*exp((-Ek3*1E+6)/(R*T))/1.01325

C CO2

zks40=4.53E3
zk50=3.28E-7
zk60=1.84E-6
Ek4=160.1
Ek5=-158.5
Ek6=-157.6
zk4=zk40*exp((-Ek4*1E+6)/(R*T))/1.01325
zk5=zk50*exp((-Ek5*1E+6)/(R*T))/1.01325
zk6=zk60*exp((-Ek6*1E+6)/(R*T))/1.01325

C Kinetic parameters for biomass gasification

zksg=6474.7
Esg=19544

C Input streams

zmOi = (FE2O3IN+FE2O3IN2) * R_O
C zmOi = (FE2O3IN+FE2O3IN2+TIO2IN+TIO2IN2)*R_O
znOi = zmOi / 16
znCi = (CIN+CIN2+CINC) / 12
znCic=(CINC+CIN2/2)/12
znCib=(CIN+CIN2/2)/12
znCH4i = CH4IN+CH4INC
znCOi = COIN+COINC
znH2i = H2IN+H2INC
znCO2i = CO2IN+CO2INC
znH2Oi = H2OIN+H2OINC+STEAMIN
znN2i = N2IN+N2INC

znIN=znCH4i+znCOi+znH2i+znCO2i+znH2Oi+znN2i

C START VALUES

C Conversions

X_O = 0.7

X_Cc= 0.5

X_Cb=0.5

C Gas portions

c_CH4d = 1e-6

c_COd = 1e-6

c_H2d = 1e-6

c_CO2d = 1e-6

c_H2Od = 1e-6

c_N2d = 1e-6

c_CH4l = 1e-6

c_COl = 1e-6

c_H2l = 1e-6

c_CO2l = 1e-6

c_H2Ol = 1e-6

c_N2l = 1e-6

C Molar flows at dense zone

zmH2Od=znH2Oi*18

zmCO2d=znCO2i*44

zmH2d=znH2i*2

zmCOd=znCOi*28

zmCH4d=znCH4i*16

zmN2d=znN2i*28

C Molar flows at lean zone

zmH2Ol=znH2Oi*18

zmCO2l=znCO2i*44

zmH2l=znH2i*2

zmCOl=znCOi*28

zmCH4l=znCH4i*16

zmN2l=znN2i*28

C Reactor zones volumes

Vd=0.2*V

Vl=V-Vd


```
zn_gesd=zn_ges*Vd/V  
zn_gesl=zn_ges*Vl/V
```

```
C Reactor zones conversions
```

```
X_Od=0.5  
X_Ol=0.5  
X_Cd=0.5  
X_Cl=0.5  
X_Cdb=0.5  
X_Clb=0.5
```

```
C Total error erges=1
```

```
C Iteration starts
```

```
DO WHILE (erges .GT. 0.011)
```

```
C Partial pressures
```

```
pCH4d = c_CH4d * R * T / (1e5 * Vd)  
pH2Od = c_H2Od * R * T / (1e5 * Vd)  
pH2d = c_H2d * R * T / (1e5 * Vd)  
pCO2d = c_CO2d * R * T / (1e5 * Vd)  
pCOd = c_COd * R * T / (1e5 * Vd)  
pN2d = c_N2d * R * T / (1e5 * Vd)
```

```
pCH4l = c_CH4l * R * T / (1e5 * Vl)  
pH2Ol = c_H2Ol * R * T / (1e5 * Vl)  
pH2l = c_H2l * R * T / (1e5 * Vl)  
pCO2l = c_CO2l * R * T / (1e5 * Vl)  
pCOL = c_COL * R * T / (1e5 * Vl)  
pN2l = c_N2l * R * T / (1e5 * Vl)
```

```
C Total mass of gas inside of reactor
```

```
zm_gasd=zn_gesd/PBAR*(pCH4d*16+pH2Od*18+pH2d*2+pCO2d*44+  
&pCOd*28+pN2d*28)  
zm_gasl=zn_gesl/PBAR*(pCH4l*16+pH2Ol*18+pH2l*2+pCO2l*44+pCOL*28+  
&pN2l*28)  
zm_gas=zm_gasd+zm_gasl
```

```
C Total mass flow of gas inside of the reactor
```

```
zmf_gasd=(zmH2Od+zmCO2d+zmH2d+zmCOd+zmCH4d+zmN2d)/3600  
zmf_gasl=(zmH2Ol+zmCO2l+zmH2l+zmCOL+zmCH4l+zmN2l)/3600  
zmf_avg=(zmf_gasd+zmf_gasl)/2
```

```
C Passing gas velocity through reactor
```

```
t_gas=zm_gas/zmf_avg  
v_gas=Hr/t_gas  
u0=v_gas
```

```
C Gas density in reactor [kg/m³]  
rhog=zm_gas/V
```

```
C Gas viscosities @ approx 950C [Pa·s]  
zmuCH4=4.2017E-5  
zmuH2O=4.3015E-5  
zmuH2=2.3828E-5  
zmuCO2=4.6730E-5  
zmuCO=4.9566E-5  
zmuN2=4.6948E-5
```

```
zmud=(zmuCH4*pCH4d+zmuH2O*pH2Od+zmuH2*pH2d+  
&zmuCO2*pCO2d+zmuCO*pCOd+zmuN2*pN2d)/PBAR  
zmul=(zmuCH4*pCH4l+zmuH2O*pH2Ol+zmuH2*pH2l+zmuCO2*pCO2l+  
&zmuCO*pCOl+zmuN2*pN2l)/PBAR  
zmu=(zmud+zmul)/2
```

```
C Oxygen carrier data, true density and diameter  
rhoOCtru = 4462  
C rhoOCtru = 4250  
por = 0.333  
C por=0.127  
rhoOC=rhoOCtru*(1-por)  
dpOC = 127*1E-6  
sph = 0.9
```

```
C Char data, apparent density  
dpC = 3108*1E-6  
rhoChar = 1100*0.9+1300*0.1
```

```
C Terminal velocity  
dpstarOC=dpOC*((rhog*(rhoOC-rhog)*g)/(zmu**2))**(1./3.)  
utstarOC=(18/dpstarOC**2+(2.335-1.744*sph)/dpstarOC**0.5)**(-1)  
utOC=utstarOC*((zmu*(rhoOC-rhog)*g)/rhog**2)**(1./3.)  
  
dpstarC=dpC*((rhog*(rhoChar-rhog)*g)/(zmu**2))**(1./3.)  
utstarC=(18/dpstarC**2+(2.335-1.744*sph)/dpstarC**0.5)**(-1)  
utC=utstarC*((zmu*(rhoChar-rhog)*g)/rhog**2)**(1./3.)
```

```
C Saturated mass flux [kg/m2s]
Gstar=23.7*rhog*u0*exp(-5.4*utOC/u0)
estar=Gstar/((u0-utOC)*rhoOC)
GstarC=23.7*rhog*u0*exp(-5.4*utC/u0)
estarC=GstarC/((u0-utC)*rhoChar)

C Lean zone height for pure oxygen carrier [m]
HIOC=1
esd=0.22
es_sat=estar
ew=0.4
a0=6.0/u0
ur=1.6*utOC
err0=1
CONST=((zm_invOC*a0)/(rhoOC*A)-esd+es_sat-Hr*esd*a0)/(esd-es_sat)

C Newton-Raphson method iteration
DO WHILE (abs(err0) .GT. 1e-4)
X0=HIOC*a0
F=-CONST-exp(-X0)-X0
DF=exp(-X0)-1
X1=X0-F/DF
err0=X1-X0
HIOC=X1/a0
END DO

C Dense zone height for pure oxygen carrier [m]
IF (HIOC .GT. Hr) THEN
HIOC=Hr
END IF
HdOC=Hr-HIOC

C Lean zone height for pure char [m]
HIC=1
esd=0.22
es_saCt=estarC
ew=0.4
a0=6.0/u0
ur=1.6*utC
err0=1
CONST=((zm_invOC*a0)/(rhoChar*A)-esd+es_satC-Hr*esd*a0)/
&(esd-es_satC)
```

C Newton-Raphson method iteration

DO WHILE (abs(err0) .GT. 1e-4)

X0=HlC*a0

F=-CONST-exp(-X0)-X0

DF=exp(-X0)-1

X1=X0-F/DF

err0=X1-X0

HlC=X1/a0

END DO

C Dense zone height for pure char [m]

IF (HlC .GT. Hr) THEN

HlC=Hr

END IF

HdC=Hr-HlC

C Using both the oxygen carrier and the char to calculate final height

Hd=y_koksd*HdC+(1-y_koksd)*HdOC

Hl=Hr-Hd

C Solid fraction at reactor exit

ese=es_sat+(esd-es_sat)*exp(-a0*Hl)

C Average solid volume fraction in lean zone

esl=es_sat+(esd-ese)/(a0*Hl)

C Solid mass flow density at reactor exit [kg/m²·s]

Gs=rhoOC*(u0-ur)*ese

C Solid inventory at dense zone [kg]

z_msd=Hd*A*esd*rhoOC

C Solid inventory at lean zone [kg]

z_msl=Hl*A*esl*rhoOC

IF (Hl .EQ. Hr) THEN

z_msl=zm_invOC

es=z_msl/(Hl*A*rhoOC)

END IF

Vd=Hd/Hr*V

Vl=V-Vd

```

IF (Vd .EQ. 0) THEN
Vd=0.001*V
END IF

zn_gesd=zn_ges*Vd/V
zn_gesl=zn_ges*Vl/V

C BUBBLES
C Number of nozzles
Nnz=20
A00=A/Nnz
ug=u0
C Constants in Archimedes number
C1=27.2
C2=0.0408
z=Hd/2
Ar=(dpOC**3*rhog*(rhoOC-rhog)*g)/(zmu**2)
umf=(zmu*((C1**2+C2*Ar)**0.5-C1))/(rhog*dpOC)
fb=(0.26+0.70*2.7183**(-3300*dpOC))
gaf=fb*(z+4*sqrt(A0))**0.4
dbb=0.54*(ug-umf)**0.4*(z+4*sqrt(A00))**0.8*g**(-0.2)
ubr=0.71*sqrt(g*dbb)
uvis=1
errbub=1

DO WHILE (errbub .GT. 0.0001)
deltab=uvis/(uvis+ubr)
uvis2=gaf*(ug-umf*(1-deltab))
errbub=abs(uvis-uvis2)
uvis=uvis2
END DO

deltab=uvis/(uvis+ubr)
C Volume fraction free from bubbles
bubble=1-deltab

C Time for complete turnover [s]
tauCH4d = rhoCH4 * rgCH4 / (bCH4 * zkCH4*(c_CH4d*1000/Vd)**znCH4)
tauCOd = rhoCO * rgCO / (bCO * zkCO * (c_COd*1000/Vd)**znCOexp)
tauH2d = rhoH2 * rgH2 / (bH2 * zkH2 * (c_H2d*1000/Vd)**znH2)

tauCH4l = rhoCH4 * rgCH4 / (bCH4 * zkCH4*(c_CH4l*1000/Vl)**znCH4)
tauCOL = rhoCO * rgCO / (bCO * zkCO * (c_COL*1000/Vl)**znCOexp)

```

$$\text{tauH2l} = \text{rhoH2} * \text{rgH2} / (\text{bH2} * \text{zkH2} * (\text{c_H2l} * 1000 / \text{Vl}) ** \text{znH2})$$

C Gasification [1/s]

$$\text{dXCH2Od} = 1 * ((\text{zk1} * \text{pH2Od}) / (1 + \text{zk2} * \text{pH2Od} + \text{zk3} * \text{pH2d})) * (1 - \text{X_Cc}) * \text{bubble}$$

$$\text{dXCCO2d} = 1 * ((\text{zk4} * \text{pCO2d}) / (1 + \text{zk5} * \text{pCO2d} + \text{zk6} * \text{pCOd})) * (1 - \text{X_Cc}) * \text{bubble}$$

$$\text{dXCH2Odb} = \text{zksg} * \exp(-\text{Esg} / \text{T}) * \text{pH2Od} * (1 - \text{X_Cb}) ** (2. / 3.) * \text{bubble}$$

$$\text{dXCH2Ol} = 1 * ((\text{zk1} * \text{pH2Ol}) / (1 + \text{zk2} * \text{pH2Ol} + \text{zk3} * \text{pH2l})) * (1 - \text{X_Cc})$$

$$\text{dXCCO2l} = 1 * ((\text{zk4} * \text{pCO2l}) / (1 + \text{zk5} * \text{pCO2l} + \text{zk6} * \text{pCOl})) * (1 - \text{X_Cc})$$

$$\text{dXCH2Olb} = \text{zksg} * \exp(-\text{Esg} / \text{T}) * \text{pH2Ol} * (1 - \text{X_Cb}) ** (2. / 3.)$$

C in [1/s]

$$\text{dXCH4d} = (3 / \text{tauCH4d}) * (1 - \text{X_O}) ** (0.67) * \text{bubble}$$

$$\text{dXCOd} = (3 / \text{tauCOd}) * (1 - \text{X_O}) ** (0.67) * \text{bubble}$$

$$\text{dXH2d} = (3 / \text{tauH2d}) * (1 - \text{X_O}) ** (0.67) * \text{bubble}$$

$$\text{dXCH4l} = (3 / \text{tauCH4l}) * (1 - \text{X_O}) ** (0.67)$$

$$\text{dXCOl} = (3 / \text{tauCOl}) * (1 - \text{X_O}) ** (0.67)$$

$$\text{dXH2l} = (3 / \text{tauH2l}) * (1 - \text{X_O}) ** (0.67)$$

C Per hour [1/h]

$$\text{rH2Od} = \text{dXCH2Od} * 3600$$

$$\text{rH2Odb} = \text{dXCH2Odb} * 3600$$

$$\text{rCO2d} = \text{dXCCO2d} * 3600$$

$$\text{rCH4d} = \text{dXCH4d} * 3600 * \text{R_O}$$

$$\text{rCOd} = \text{dXCOd} * 3600 * \text{R_O}$$

$$\text{rH2d} = \text{dXH2d} * 3600 * \text{R_O}$$

$$\text{rH2Ol} = \text{dXCH2Ol} * 3600$$

$$\text{rH2Olb} = \text{dXCH2Olb} * 3600$$

$$\text{rCO2l} = \text{dXCCO2l} * 3600$$

$$\text{rCH4l} = \text{dXCH4l} * 3600 * \text{R_O}$$

$$\text{rCOl} = \text{dXCOl} * 3600 * \text{R_O}$$

$$\text{rH2l} = \text{dXH2l} * 3600 * \text{R_O}$$

C Mass change of char and oxygen carrier due to either reaction

$$\text{dmCO2d} = \text{rCO2d} * \text{char} * \text{y_koks d} * \text{z_msd}$$

$$\text{dmH2Od} = \text{rH2Od} * \text{char} * \text{y_koks d} * \text{z_msd}$$

$$\text{dmH2Odb} = \text{rH2Odb} * \text{char} * \text{y_koks d} * \text{z_msd}$$

$$\text{dmCO2l} = \text{rCO2l} * \text{char} * \text{y_koks l} * \text{z_msl}$$

dmH2Ol = rH2Ol * char * y_koksl * z_msl
dmH2Olb = rH2Olb * char * y_koksl * z_msl

dmCH4d = rCH4d * z_msd*(1-y_koksd)
dmCOd = rCOd * z_msd*(1-y_koksd)
dmH2d = rH2d * z_msd*(1-y_koksd)

dmCH4l = rCH4l * z_msl*(1-y_koksl)
dmCOl = rCOl * z_msl*(1-y_koksl)
dmH2l = rH2l * z_msl*(1-y_koksl)

C Molar change of char and oxygen carrier due to either reaction

dnCCO2d = dmCO2d / 12
dnCH2Od = dmH2Od / 12
dnCH2Odb = dmH2Odb / 12

dnCCO2l = dmCO2l / 12
dnCH2Ol = dmH2Ol / 12
dnCH2Olb = dmH2Olb / 12

dnCH4OCd = dmCH4d / 16
dnCOOCd = dmCOd / 16
dnH2OCd = dmH2d / 16

dnCH4OCl = dmCH4l / 16
dnCOOCl = dmCOl / 16
dnH2OCl = dmH2l / 16

C Stoichiometry

dnCd = dnCCO2d + dnCH2Od
dnCdb=dnCH2Odb
dnCH4d = 3./12. * dnCH4OCd
dnCOd = 3./3.*dnCOOCd - 0.9*dnCH2Od - 2*dnCCO2d - 0.9*dnCH2Odb
dnH2d = 3./3.*dnH2OCd - 1.1 * dnCH2Od - 1.1 * dnCH2Odb
dnH2Od = 3./3.*dnH2OCd + 3./6. * dnCH4OCd - 1.1 * dnCH2Od-
&1.1 * dnCH2Odb
dnCO2d = 3./3.*dnCOOCd + 3./12.*dnCH4OCd + 0.1*dnCH2Od - dnCCO2d+
&0.1*dnCH2Odb
dnOd = dnCH4OCd + dnCOOCd + dnH2OCd
dnN2d = 0

dnCl = dnCCO2l + dnCH2Ol
dnClb=dnCH2Olb

```
dnCH4l = 3./12. * dnCH4OCl
dnCOl = 3./3.*dnCOOCl - 0.9*dnCH2Ol - 2*dnCCO2l - 0.9*dnCH2Ol
dnH2l = 3./3.*dnH2OCl - 1.1 * dnCH2Ol - 1.1 * dnCH2Ol
dnH2Ol = 3./3.*dnH2OCl + 3./6. * dnCH4OCl - 1.1 * dnCH2Ol -
&1.1 * dnCH2Ol
dnCO2l = 3./3.*dnCOOCl+3./12.*dnCH4OCl+0.1*dnCH2Ol-dnCCO2l+
&0.1*dnCH2Ol
dnOl = dnCH4OCl + dnCOOCl + dnH2OCl
dnN2l = 0
```

C Output streams from the dense zone [kmol/h]

```
znCH4d = znCH4i - dnCH4d
znCOd = znCOi - dnCOd
znH2d = znH2i - dnH2d
znH2Od = znH2Oi + dnH2Od
znCO2d = znCO2i + dnCO2d
znOd = znOi - dnOd
znCd = znCic - dnCd
znCdb =znCib-dnCdb
znN2d = znN2i - dnN2d
```

```
IF (znOd .LT. 0) THEN
znOd = 1e-6
END IF
```

```
IF (znCd .LT. 0) THEN
znCd = 1e-6
END IF
```

```
IF (znCdb .LT. 0) THEN
znCdb = 1e-6
END IF
```

```
IF (znCOd .LT. 0) THEN
znCOd = 1e-6
END IF
```

```
IF (znCO2d .LT. 0) THEN
znCO2d = 1e-6
END IF
```

```
IF (znCH4d .LT. 0) THEN
znCH4d = 1e-6
```


END IF

IF (znH2d .LT. 0) THEN
znH2d = 1e-6
END IF

IF (znH2Od .LT. 0) THEN
znH2Od = 1e-6
END IF

IF (znN2d .LT. 0) THEN
znN2d = 1e-6
END IF

C Output streams from the lean zone [kmol/h]
znCH4l = znCH4d - dnCH4l
znCOl = znCOd - dnCOl
znH2l = znH2d - dnH2l
znH2Ol = znH2Od + dnH2Ol
znCO2l = znCO2d + dnCO2l
znOl = znOd - dnOl
znCl = znCd - dnCl
znClb=znCdb-dnClb
znN2l = znN2d - dnN2l

IF (znOl .LT. 0) THEN
znOl = 1e-6
END IF

IF (znCl .LT. 0) THEN
znCl = 1e-6
END IF

IF (znClb .LT. 0) THEN
znClb = 1e-6
END IF

IF (znCOl .LT. 0) THEN
znCOl = 1e-6
END IF

IF (znCO2l .LT. 0) THEN
znCO2l = 1e-6

END IF

IF (znCH4l .LT. 0) THEN
znCH4l = 1e-6
END IF

IF (znH2l .LT. 0) THEN
znH2l = 1e-6
END IF

IF (znH2Ol .LT. 0) THEN
znH2Ol = 1e-6
END IF

IF (znN2l .LT. 0) THEN
znN2l = 1e-6
END IF

C Total output streams
zn_d=znCOd+znH2d+znH2Od+znCO2d+znCH4d+znN2d
zn_l=znCOl+znH2l+znH2Ol+znCO2l+znCH4l+znN2l

C Conversion of solids
X_Odn=1-(znOd/znOi)
X_Cdn=1-(znCd/znCic)
X_Cdnb=1-(znCdb/znCib)

X_Oln=1-(znOl/znOd)
X_Cln=1-(znCl/znCd)
X_Clnb=1-(znClb/znCdb)

C Gas compositions
xCH4d = znCH4d / zn_d
xCOd = znCOd / zn_d
xH2d = znH2d / zn_d
xCO2d = znCO2d / zn_d
xH2Od = znH2Od / zn_d
xN2d = znN2d/zn_d

xCH4l = znCH4l / zn_l
xCOl = znCOl / zn_l
xH2l = znH2l / zn_l
xCO2l = znCO2l / zn_l

```
xH2O1 = znH2O1 / zn_1  
xN21 = znN21/zn_1
```

C Gas portions

```
cCH4nd = xCH4d * zn_gesd  
cCOnd = xCOd * zn_gesd  
cH2nd = xH2d * zn_gesd  
cCO2nd = xCO2d * zn_gesd  
cH2Ond = xH2Od * zn_gesd  
cN2nd = zn_gesd-(cCH4nd+cCOnd+cH2nd+cCO2nd+cH2Ond)
```

```
cCH4nl = xCH4l * zn_gesl  
cCOnl = xCOl * zn_gesl  
cH2nl = xH2l * zn_gesl  
cCO2nl = xCO2l * zn_gesl  
cH2Onl = xH2Ol * zn_gesl  
cN2nl = zn_gesl-(cCH4nl+cCOnl+cH2nl+cCO2nl+cH2Onl)
```

C Calculation of the error

```
er1 = abs(c_CH4d - cCH4nd)/ abs(c_CH4d+ 1E-12)  
er2 = abs(c_COd - cCOnd)/ abs(c_COd + 1E-12)  
er3 = abs(c_H2d - cH2nd)/ abs(c_H2d + 1E-12)  
er4 = abs(c_CO2d - cCO2nd)/ abs(c_CO2d + 1E-12)  
er5 = abs(c_H2Od - cH2Ond)/ abs(c_H2Od + 1E-12)  
er6 = abs(c_N2d - cN2nd) / abs(c_N2d + 1E-12)  
er7 = abs(X_Od - X_Odn) / abs(X_Od+1E-12)  
er8 = abs(X_Ol - X_Oln) / abs(X_Ol+1E-12)  
er9 = abs(X_Cd - X_Cdn) / abs(X_Cd+1E-12)  
er10 = abs(X_Cl - X_Cln) / abs(X_Cl+1E-12)  
er11 = abs(c_CH4l - cCH4nl)/ abs(c_CH4l + 1E-12)  
er12 = abs(c_COl - cCOnl)/ abs(c_COl + 1E-12)  
er13 = abs(c_H2l - cH2nl)/ abs(c_H2l + 1E-12)  
er14 = abs(c_CO2l - cCO2nl)/ abs(c_CO2l + 1E-12)  
er15 = abs(c_H2Ol - cH2Onl)/ abs(c_H2Ol + 1E-12)  
er16= abs(c_N2l - cN2nl) / abs(c_N2l + 1E-12)  
er17 = abs(X_Cdb - X_Cdnb) / abs(X_Cdb+1E-12)  
er18 = abs(X_Cdb - X_Cdnb) / abs(X_Cdb+1E-12)  
  
erges =er1+er2+er3+er4+er5+er6+er7+er8+er9+er10+er11+er12+  
&er13+er14+er15+er16+er17+er18
```

C Relaxation rate

```
w=0.01
```

C New values are calculated

$$c_CH4d = (1-w) * c_CH4d + w*cCH4nd$$

$$c_COd = (1-w) * c_COd + w*cCOnd$$

$$c_H2d = (1-w) * c_H2d + w*cH2nd$$

$$c_CO2d = (1-w) * c_CO2d + w*cCO2nd$$

$$c_H2Od = (1-w) * c_H2Od + w*cH2Ond$$

$$c_N2d = (1-w) * c_N2d + w*cN2nd$$

$$X_Od = (1-w)*X_Od+w*X_Odn$$

$$X_Ol = (1-w)*X_Ol+w*X_Oln$$

$$X_Cd = (1-w)*X_Cd+w*X_Cdn$$

$$X_Cl = (1-w)*X_Cl+w*X_Cln$$

$$X_Cdb = (1-w)*X_Cdb+w*X_Cdnb$$

$$X_Clb = (1-w)*X_Clb+w*X_Clnb$$

$$c_CH4l = (1-w) * c_CH4l + w*cCH4nl$$

$$c_COl = (1-w) * c_COl + w*cCONl$$

$$c_H2l = (1-w) * c_H2l + w*cH2nl$$

$$c_CO2l = (1-w) * c_CO2l + w*cCO2nl$$

$$c_H2Ol = (1-w) * c_H2Ol + w*cH2Onl$$

$$c_N2l = (1-w) * c_N2l + w*cN2nl$$

C Overall conversions of chars and oxygen carrier

$$X_O = X_Od+X_Ol*(1-X_Od)$$

$$X_Cc = X_Cd+X_Cl*(1-X_Cd)$$

$$X_Cb = X_Cdb+X_Clb*(1-X_Cdb)$$

counter=counter+1

C Mass flows

$$zmH2Od=znH2Od*18$$

$$zmCO2d=znCO2d*44$$

$$zmH2d=znH2d*2$$

$$zmCOd=znCOd*28$$

$$zmCH4d=znCH4d*16$$

$$zmN2d=znN2d*28$$

$$zmH2Ol=znH2Ol*18$$

$$zmCO2l=znCO2l*44$$

$$zmH2l=znH2l*2$$

$$zmCOl=znCOl*28$$

$$zmCH4l=znCH4l*16$$

zmN2l=znN2l*28

C Iteration ends END DO

C Mass flows

zmOo = znOl * 16

zmCo = (znCl+znClb) * 12

zmH2Oo = znH2Ol * 18

zmCO2o = znCO2l * 44

zmH2o = znH2l * 2

zmCOo = znCOl*28

zmCH4o = znCH4l*16

zmN2o = znN2l*28

zmH2Oi = znH2Oi * 18

zmCO2i = znCO2i * 44

zmH2i = znH2i * 2

zmCOi = znCOi*28

zmCH4i = znCH4i*16

zmN2i = znN2i*28

C Gas compositions out from reactor

gasout=znH2Ol+znCO2l+znH2l+znCOl+znCH4l+znN2l

cwH2O=znH2Ol/gasout*100

cwCO2=znCO2l/gasout*100

cwH2=znH2l/gasout*100

cwCO=znCOl/gasout*100

cwCH4=znCH4l/gasout*100

cwN2=znN2l/gasout*100

C Dry gas compositions out from reactor

gasdry=znCO2l+znH2l+znCOl+znCH4l+znN2l

cdCO2=znCO2l/gasdry

cdH2=znH2l/gasdry

cdCO=znCOl/gasdry

cdCH4=znCH4l/gasdry

cdN2=znN2l/gasdry

C Output values

COUt=zmCo

C Conversions of char particles, exported to FR-block as CONV

C CONVH2O=(dmH2Od+dmH2Ol+dmH2Odb+dmH2Olb)/(CIN+CIN2+CINC)

CCONVCO2=(dmCO2d+dmCO2l)/(CIN+CIN2+CINC-dmH2Od-dmH2Ol-
&dmH2Odb-dmH2Olb)

H2OOUT=zmH2Oo
CO2OUT=zmCO2o
H2OUT=zmH2o
COOUT=zmCOo
CH4OUT=zmCH4o
ASHOUT=ASHIN+ASHIN2+ASHINC
ZN2OUT=N2IN+N2INC
SOUT=SIN

C Conversions of gaseous fuels, exported to FR-block as CONV
H2CONV=1-znH2l/(znH2i+(CIN+CIN2+CINC)/12*CCONVH2O*1.1)
COCONV=1-znCOl/(znCOi+(CIN+CIN2+CINC)/12*CCONVH2O*0.9+
&(CIN+CIN2+CINC-dmH2Od-dmH2Ol-dmH2Odb-dmH2Olb)/12*CCONVCO2*2)
CH4CONV=1-znCH4l/znCH4i

C Char conversion
XCHAR=1-zmCo/(CIN+CIN2+CINC)

C Oxygen demand
eta=1.179
Omega=(0.5*cdCO+2*cdCH4+0.5*cdH2)/(eta*(cdCO2+cdCO+cdCH4))

C Carbon dioxide capture efficiency
AirO2i=AIRIN/(0.21*32+0.79*28)*0.21
AirN2=AIRIN/(0.21*32+0.79*28)*0.79
AirO2=(znOi-znOl)/2
AirO2o=AirO2i-AirO2-znCl
AirCO2o=CAIR
AirTot=AirO2o+AirCO2o+AirN2
AxO=AirO2o/AirTot
AxC=AirCO2o/AirTot
effO=(0.21-AxO-AxC)/(0.21-AxO-0.21*AxC)

B.3 Pyrolysis

Proximate analysis [Moist, Fixed Carbon, Volatile Matter, Ash]

Prox=[12.13; 46.28; 32.92; 8.67];

Ultimate analysis on a dry basis [C, H, O, N, S]:

Udry=[72.21; 5.45; 10.07; 2.06; 0.34];

Ultimate analysis on a dry and ash free basis:

Udaf=Udry/sum(Udry)

A=[1 0.75 0.8 0.4286 0.2727 0.8342 0 0 0 0;
0 0.25 0.2 0 0 0.0679 1 0.1111 0 0;
0 0 0 0.5714 0.7273 0.0652 0 0.8889 0 0.5;
0 0 0 0 0.0197 0 0 1 0;
0 0 0 0 0.0130 0 0 0 0.5;
1 0 0 0 0 0 0 0 0;
0 1 0 0 0 0 0 0 0;
0 0 1 0 0 0 0 0 0;
0 0 0 1 0 0 0 0 0;
0 0 0 0 1 0 0 0 0];

Ainv=inv(A);

B=[Udaf(1);
Udaf(2);
Udaf(3);
Udaf(4);
Udaf(5);
Prox(2)/(Prox(2)+Prox(3));
0.82*Udaf(2);
0.15*Udaf(2);
0.59*Udaf(3);
0.31*Udaf(3)];

X=Ainv*B;

mass=X*(100-Prox(1)-Prox(4));

moist=12.13/18;

molar=[12; 16; 30; 28; 44; 1; 2; 18; 28; 64];

```
mol=mass./molar;

Tar=[0.8342; 0.0679; 0.0652; 0.0197; 0.0130];

Cmol=mol(3)*2+mass(6)*Tar(1)/12;

Hmol=mol(3)*6+mass(6)*Tar(2)+mol(8)*2+moist*2;

Omol=mass(6)*Tar(3)/16+mol(8)+moist;

Nmol=mass(6)*Tar(4)/14;

Smol=mass(6)*Tar(5)/32

factor=0.76076303;

COmol=Cmol*factor;

CH4mol=Cmol*(1-factor);

SO2mol=Smol

H2Omol=Omol-COmol-SO2mol*2;

H2mol=(Hmol-CH4mol*4-H2Omol*2)/2;

N2mol=Nmol/2;

mC=mol(1)*12;

mCH4=(mol(2)+CH4mol)*16;

mC2H6=0;

mCO=(mol(4)+COmol)*28;

mCO2=mol(5)*44;

mTar=0;

mH2=(mol(7)+H2mol)*2;
```


mH2O=H2Omol*18;

mN2=(mol(9)+N2mol)*28;

mSO2=(mol(10)+SO2mol)*64;

mAsh=8.67;

massPyro=[mC; mCH4; mC2H6; mCO; mCO2; mTar; mH2; mH2O; mN2; mSO2;
mAsh]